MASTER COPY KEEP THIS COPY FOR REPRODUCTION PURPOSES

REPORT DOCUMENTATION PAGE

Form Approved
OMB No. 0704-0188

1. AGENCY USE ONLY (Leave blank)	2. REPORT DATE	3. REPORT TYPE AND DATES COVERED
	December, 1994	Final Report 1992-1994

4. TITLE AND SUBTITLE
Fiber Optic Raman and Micro Raman Measurements of Bonding Agents at Interface During the Curing Process

5. FUNDING NUMBERS
DAAL03-92-G-0316

6. AUTHOR(S)
M. L. Myrick, S. M. Angel

7. PERFORMING ORGANIZATION NAME(S) AND ADDRESS(ES)
University of South Carolina
Columbia, SC 29208

8. PERFORMING ORGANIZATION REPORT NUMBER

9. SPONSORING / MONITORING AGENCY NAME(S) AND ADDRESS(ES)
U.S. Army Research Office
P. O. Box 12211
Research Triangle Park, NC 27709-2211

10. SPONSORING / MONITORING AGENCY REPORT NUMBER
ARO 30450.5-MS-SIP

11. SUPPLEMENTARY NOTES
The views, opinions and/or findings contained in this report are those of the author(s) and should not be construed as an official Department of the Army position, policy, or decision, unless so designated by other documentation.

12a. DISTRIBUTION / AVAILABILITY STATEMENT
Approved for public release; distribution unlimited.

12b. DISTRIBUTION CODE

13. ABSTRACT (Maximum 200 words)

Curing of polymers has been studied with Raman, Surface-enhanced Raman, and Micro-Raman Spectroscopy. Ab initio calculations model compound and multivariate statistics were used to develop understanding of the cure kinetics of epoxies in bulk and interfacial processing.

14. SUBJECT TERMS
Raman, Epoxy, SERS, Principal Component, Micro Raman

15. NUMBER OF PAGES

16. PRICE CODE

17. SECURITY CLASSIFICATION OF REPORT	18. SECURITY CLASSIFICATION OF THIS PAGE	19. SECURITY CLASSIFICATION OF ABSTRACT	20. LIMITATION OF ABSTRACT
UNCLASSIFIED	UNCLASSIFIED	UNCLASSIFIED	UL

NSN 7540-01-280-5500

Standard Form 298 (Rev 2-89)
Prescribed by ANSI Std Z39-18
298-102

Fiber-Optic Raman and Micro-Raman Measurements of Bonding Agents at Interfaces During the Curing Process

FINAL REPORT

M.L. Myrick, Principal Investigator
S.L. Morgan, Co-Investigator

December 1994

U.S. ARMY RESEARCH OFFICE

GRANT # DAAL-03-92-G-0316

University of South Carolina
Columbia, SC 29208

APPROVED FOR PUBLIC RELEASE;
DISTRIBUTION UNLIMITED.

THE VIEWS, OPINIONS, AND/OR FINDINGS CONTAINED IN THIS REPORT ARE THOSE OF THE AUTHORS AND SHOULD NOT BE CONSTRUED AS AN OFFICIAL DEPARTMENT OF THE ARMY POSITION, POLICY OR DECISION, UNLESS SO DESIGNATED BY OTHER DOCUMENTATION.

1. FOREWORD

This project was funded as an ARO Young Investigator Project in 1992. Over its course, a number of important findings and developments were made, as detailed in the report below. As Principal Investigator for this program, I wanted to add a personal note to describe the impact this project has had on my research group, my students and the University of South Carolina.

This Polymer-Curing work has been more applied than most research done by graduate students in the Department of Chemistry, and it has benefited a good number of them; I have had the benefit of seeing students who were uncertain in the laboratory develop into strong experimental scientists who can confidently attack real-world problems, some of whom are the equal of the best scientists I have seen.

One former Post-Doc from this group has obtained an Assistant Professorship at a University since leaving us. Partly as a result of this project, my group was recently able to attract Dr. Karl Booksh (Ph.D., University of Washington, Seattle, 1994) as a Post-Doctoral Associate. Dr. Booksh is one of the top two or three chemical statisticians in the country (at least according to the National Science Foundation, who awarded him with an NSF Post-Doctoral Fellowship this year). With his credentials and Fellowship, Dr. Booksh could literally have gone anywhere -- he preferred to come to the University of South Carolina because we were doing applied chemistry here. Dr. Booksh is the first NSF Post-Doctoral Fellowship holder ever to work anywhere in the state of South Carolina, and we are priviledged to have him.

Support from the Army Research Office has enabled this group to establish a research base and facility among the best in our State, with a growing reputation for solving problems and interacting with Industry, other Universities and Government Laboratories. We give frequent tours of our laboratory to high school students and teachers from around South Carolina, and have mentored several high school and undergraduate students in research. Much of this interaction with the public in our state is made possible by support from the Army Research Office - otherwise there would be too few members of the group to handle these tasks without it becoming burdensome, and the facility and research would be a less desirable place to visit.

On behalf of myself, the Department, the University and the State of South Carolina, I truly appreciate the financial, technical, and personal support I have received from the Army Research Office, and from Dr. Edward Chen of that Agency.

2. TABLE OF CONTENTS

LIST OF APPENDIXES, ILLUSTRATIONS AND TABLES

4.A. STATEMENT OF THE PROBLEM STUDIED

The strength of a joint or processed composite depends to a great extent on the physical properties of interfaces and the bulk matrix. These physical properties depend on chemical composition and bonding, characteristics that are readily observable with vibrational spectroscopy. Raman scattering is uniquely applicable to this type of analysis.

We have proposed to investigate Raman scattering of epoxies and polyimides in interfacial regions using fiber optic spectroscopy. This will be complemented by micro-Raman measurements that will determine the spatial extent of the interface with 1 μm resolution and observe inhomogeneities in the curing process at high optical resolution. This project combines the efforts of two research groups: those of Professor Myrick (experimental measurements) and of Professor Morgan (statistical analysis).

4.B. SUMMARY OF THE MOST IMPORTANT RESULTS

Raman of Raw Matrix Components

A test polymer system was chosen for this project. This is the DER332/Jeffamine T-403 epoxy cure system, a two-component cure system.

For the epoxy, structures of the two components are shown below in Figure 1.

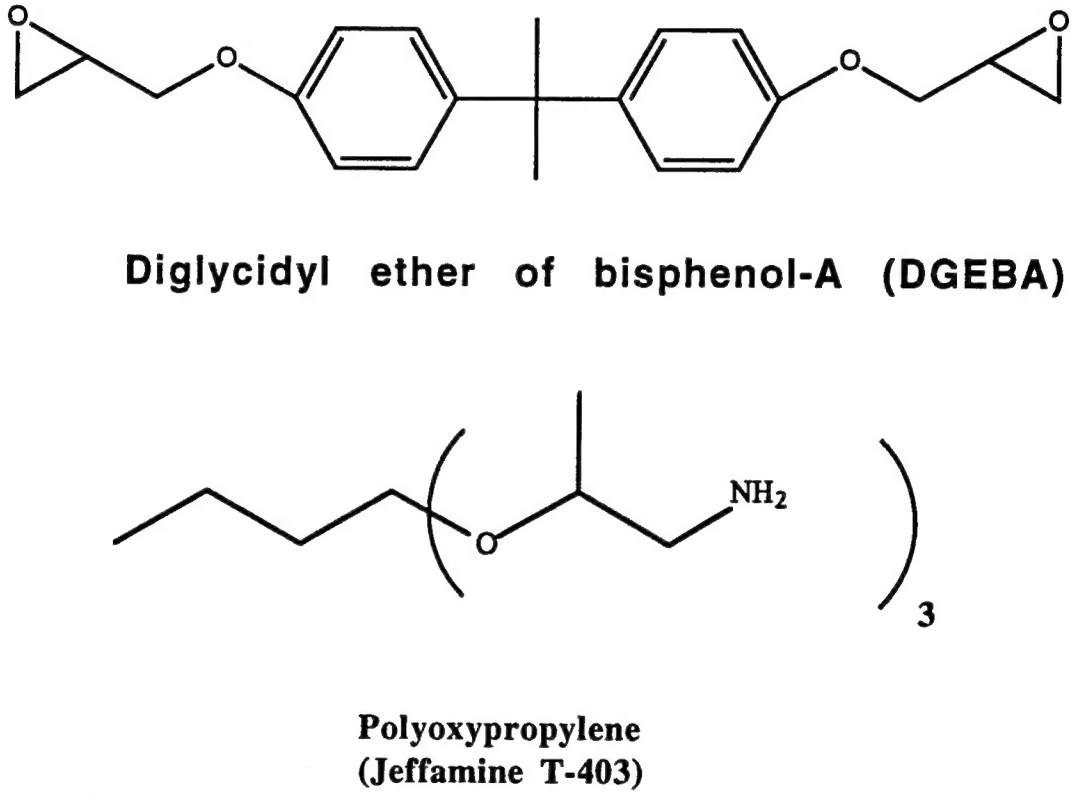

Figure 1: Chemical Structures of DER 332 and Jeffamine T-403

Figure 2 shows Raman spectra acquired for the epoxy resin (DGEBA), which dominates the spectra of the epoxy.

Assignment of Vibrations

Vibrational assignments for the epoxy resin of Figure 1 were obtained by studies of model compounds, ab initio calculations, and comparison with other literature. Table I gives rough assignments for the epoxy components.

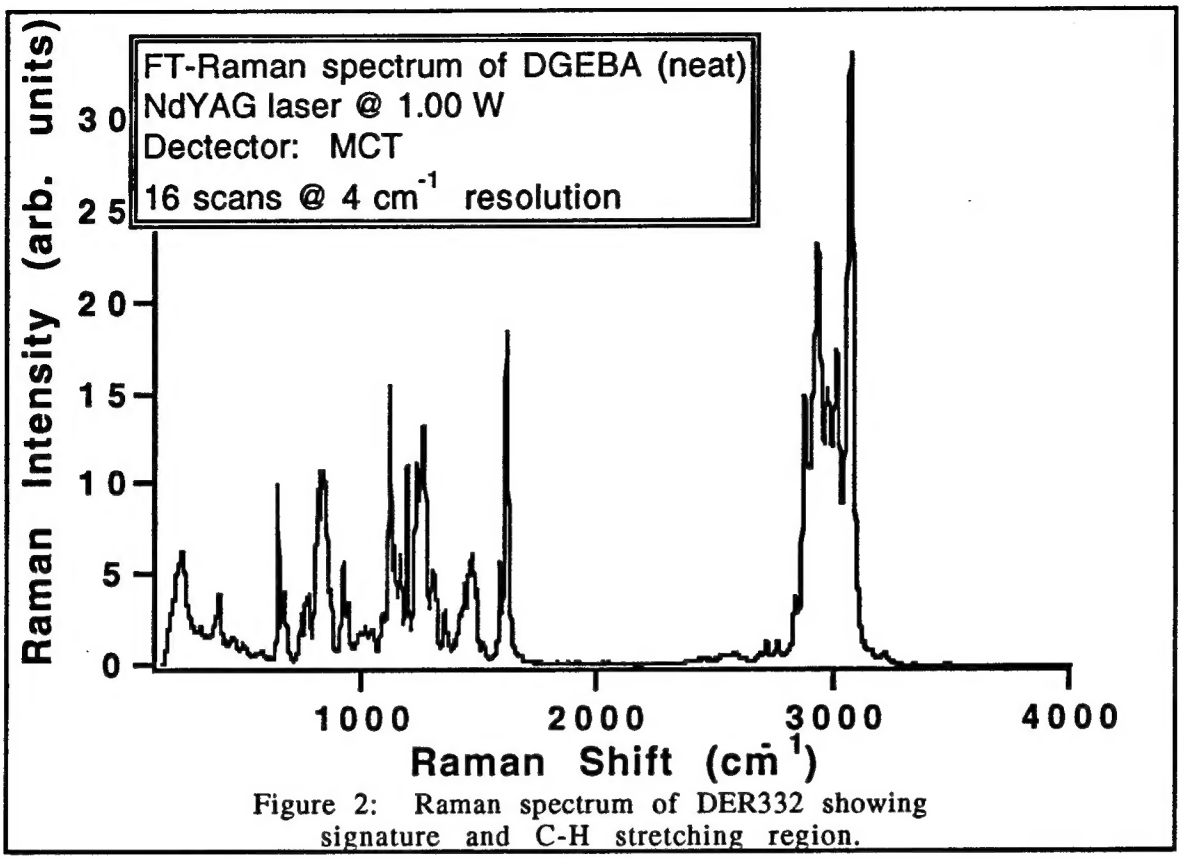

Figure 2: Raman spectrum of DER332 showing signature and C-H stretching region.

Model compounds studied are shown below in Figure 3.

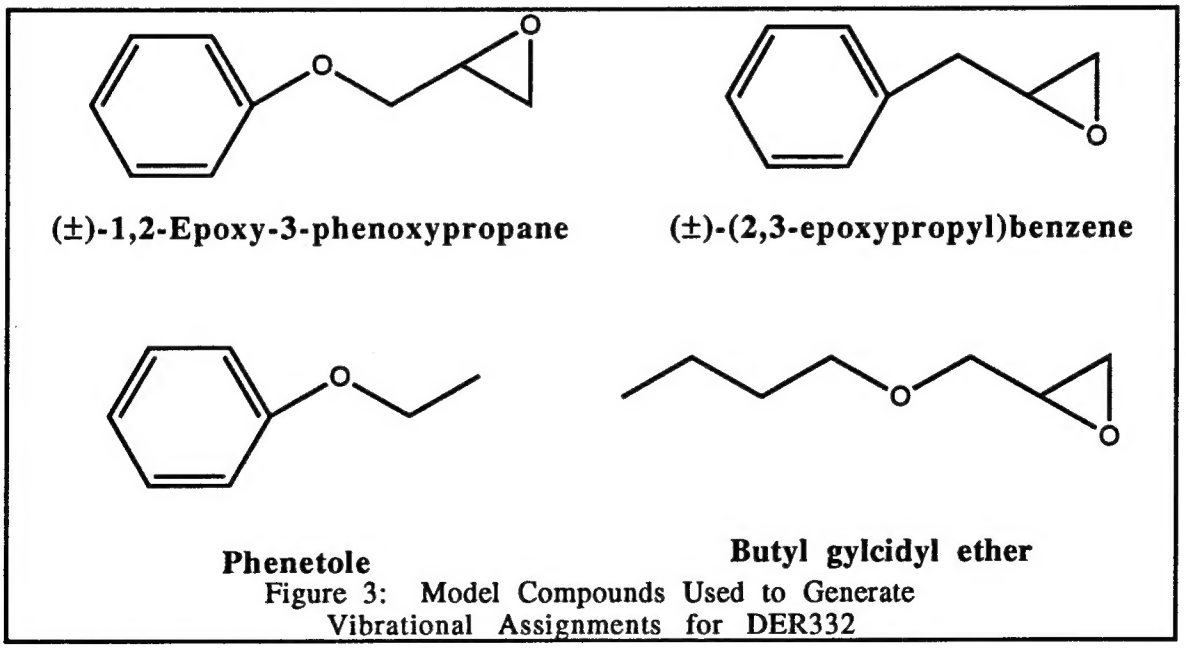

Figure 3: Model Compounds Used to Generate Vibrational Assignments for DER332

Table 1. Infrared and Raman band assignments for DGEBA. s = strong, m = medium, w = weak, vw = very weak, sh = shoulder, str = stretch, and def = deformation.

IR	Raman	Assignments
1298m	1272w	C-O str. (ether groups)[d]
1248s	----	C-O str. (ether groups) and C-C str.[a,d]
----	1232s	C-O str. and phenolic C_4-O_2 str.[a]
----	1211s	Epoxy group?
1184s	1186s	CH_3/gem-dimethyl def. and C_6-$C_{7/8}$ str.[a,d]
1157vw	1140vw	----
----	1113s	Aromatic C-H str. and in-plane def.[a-d]
1065vw	----	Phenolic C_4-O_2 str.[e]
1036s	----	Substituted aromatic[c,d,e]
1010sh	----	Substituted aromatic[c,d,e]
970w	----	----
916m	924sh	Epoxy group[a,d,e]
862sh	908m	Epoxy group[a,d,e]
806s	819s	Substituted aromatic[c,d,e]
772m	762m	C_3-C_2 skeletal[a]
----	736sh	C_3-C_2 skeletal[a]
----	667m	Aromatic C-H out-of-plane def.[b-e]
----	641s	Aromatic C-H out-of-plane def.[b-e]

[a]This paper. [b]Reference 1. [c]Reference 2. [d]Reference 3. [e]Reference 4.

Laboratory Measurements of Curing

The curing of the epoxy system has been studied using FT-Raman spectroscopy, Argon-ion-laser-excited Raman and Diode-laser-excited Raman. Figure 4 shows spectra of the epoxy cure system before and after curing performed with FT-Raman spectroscopy.

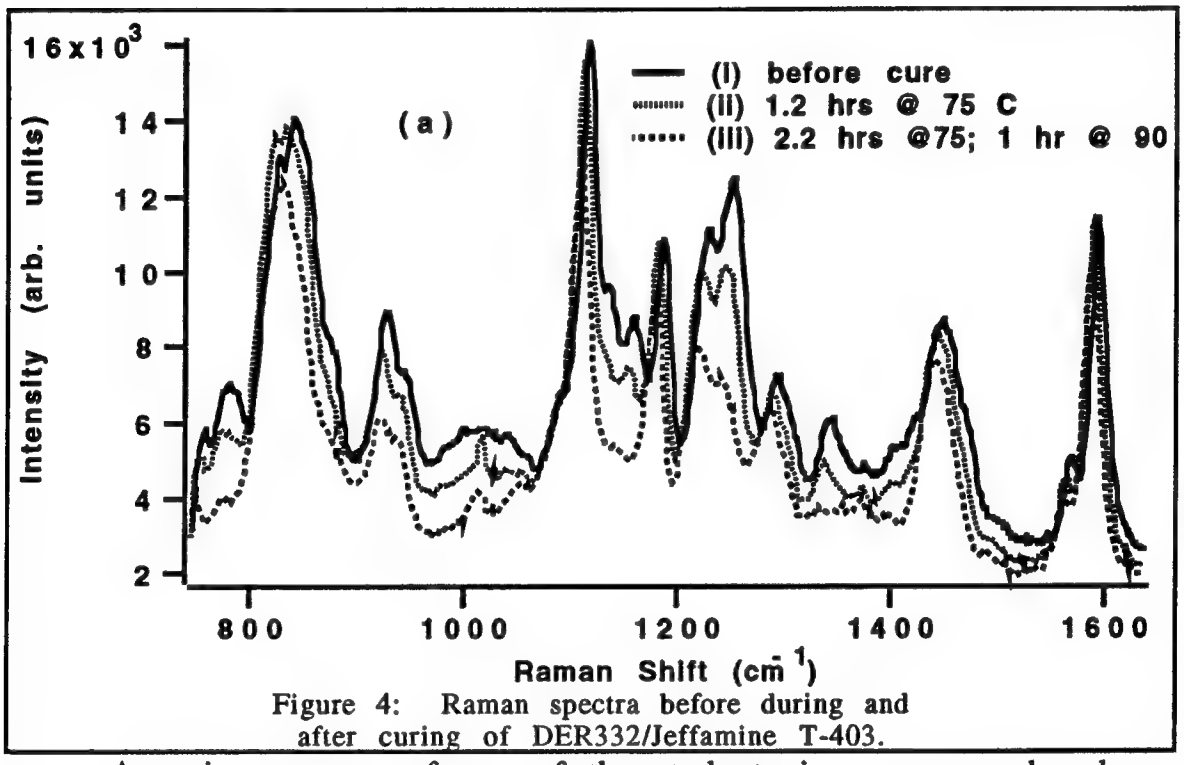

Figure 4: Raman spectra before during and after curing of DER332/Jeffamine T-403.

A major concern of one of the students in my group has been the transfer of heat during the curing process in thick-section parts, and the relation of heat transfer to curing kinetics. As a result, we have (with a collaborator in the USC Department of Chemical Engineering, Dr. Eric Markel) made measurements inside 1-inch cylindrical sections of polymer (for ease of comparison between experiment and predictions). Figure 5 shows the experimental setup for a multi-probe experiment in which five separate locations within a cylindrical polymer sample were interrogated. Local temperature at each of the five probe sites was monitored with a thermocouple situated at the fiber probe tips. Excitation for each probe was derived from an Argon ion laser which was beam-split into five beams and directed to the five separate excitation fibers. Returning scattered radiation was detected with a charge coupled device (CCD) array simultaneously

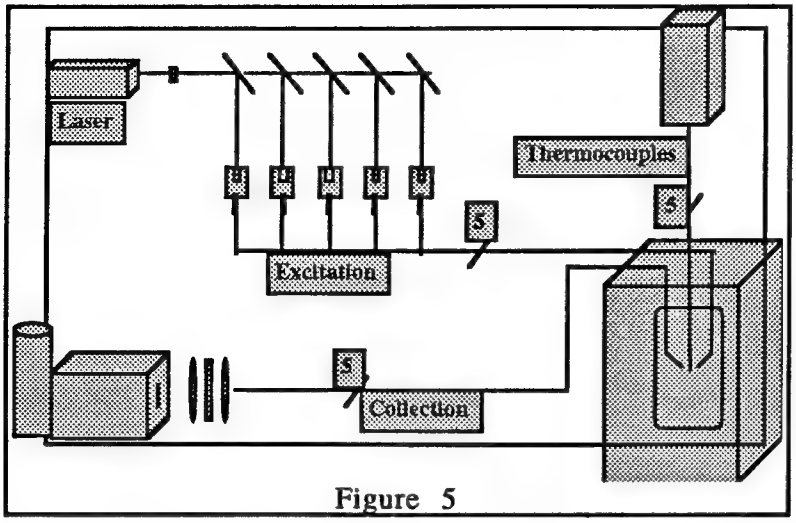

Figure 5

using five detection bins, and all spectra were analyzed using principal component analysis.

A sample result from these measurements is shown below in Figure 6, in which a set of Raman spectra from four locations (one of the five optical probes failed during the experiment shown in Figure 6) inside the thick polymer are reproduced.

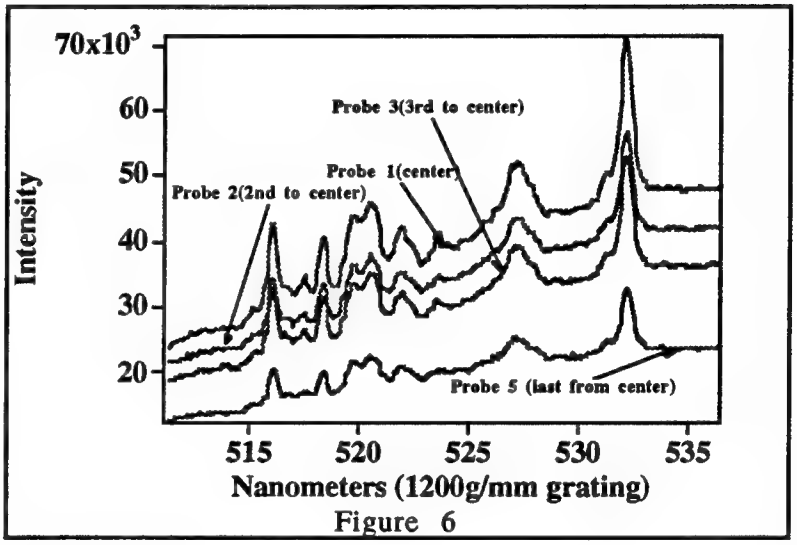

Figure 6

Spectra such as these are used to determine the percentage of curing in the polymer (via Principle Component Analysis, PCA) at each location in the sample as a function of time. Reaction rates determined from these measurements can be compared to theoretical reaction rates, with results that are in good agreement.

Theoretical rates are relatively simple to produce for simple geometric shapes of thick polymers. However, complex shapes and components manufactured with anisotropic elements (e.g., embedded graphite fibers) are substantially more difficult to model and may themselves be irreproducible, since most thick-section composite parts are prepared by hand. An experimental measurement of curing would be highly advantageous in these situations.

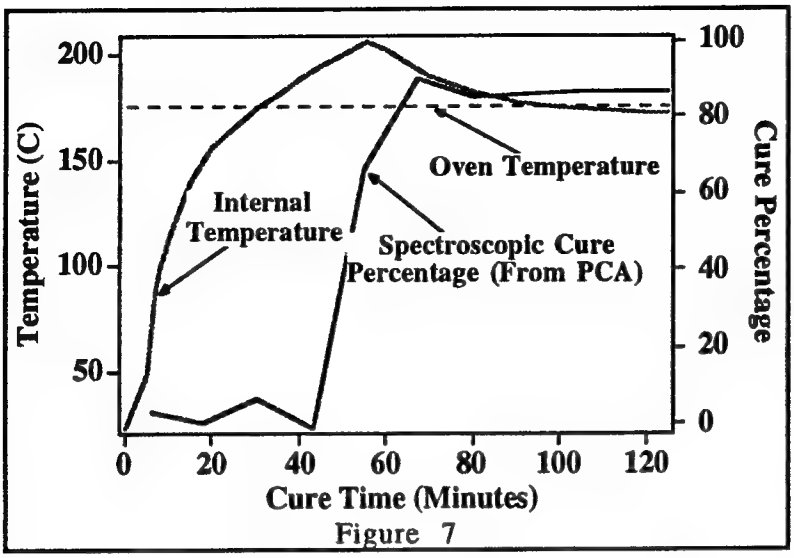

Figure 7

Figure 7 shows the result for a single point in the center of a 1"-thick polymer (a Ciba-Geigy polyimide). In this case, the oven temperature was set at 180 C, and the initial part temperature was 30 C. Following an in-duction period neces-sary for heat to begin to transfer to the center of the part, the internal temperature begins to climb. As the rate of polymerization increases (approximately exponentially) with temperature, heat is generated internally in the part and the temperature exceeds that of the oven by over 20 C. It is evident from study of Figure 7 that the internal heat which raises the temperature of the polymer center is not due to the curing of the polymer in the center. This is because the reaction of the center only proceeds slowly until the temperature is already elevated above the over temperature. At this point, the reaction proceeds very quickly to completion.

Cursory visual examination of parts prepared in this way show even curing of the exterior of the part, with brittle, deeply colored polymer in the very center which is presumably highly stressed. We believe that complex parts can be examined in this way during curing to control these runaway exotherms in a real-time situation.

Evanescent Thin-Film Measurements

The refractive index of the epoxy selected for this study exceeded the refractive indices of typical silica-core optical fibers. Consequently, evanescent spectroscopy of this polymer was not possible with these fibers. Figure 8 shows the refractive index of the DER332-Jeffamine T403 polymer as it changes during the curing process. In order to perform evanescent Raman, a core material with an index greater than the maximum index attained in the cure is necessary - an index greater than about 1.547 at the sodium D line. The indices of the typical silica fibers we utilized were all near 1.45-1.50 and could not be used. Some measurements were attempted with sapphire rod supports (refractive index > 1.6), but these were

experimentally difficult to undertake and it was not clear that a glass-polymer interface could be suitably mimicked in this way.

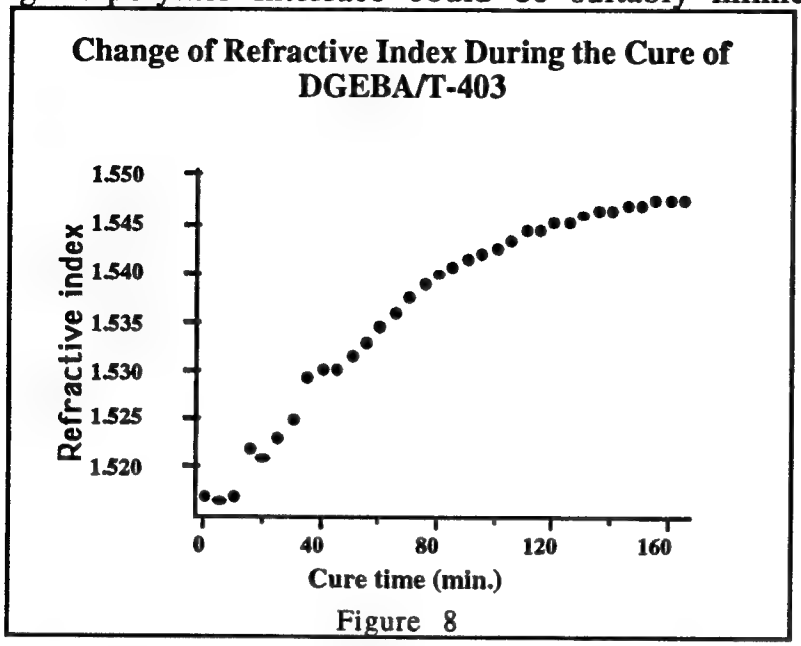

Figure 8

More recently, we have initiated a collaboration with scientists at NIST who are manufacturing high-index fibers for evanescent NIR spectroscopy. If joint research concerns on the NIST partners behalfs can be addressed, we expect to conduct research with these new fibers early in 1995.

Non-Evanescent Thin-Film Measurements

We developed a novel method for interrogating variable-thickness thin polymer films and studying them during the curing process. Figure 9 below shows the experimental layout for the technique.

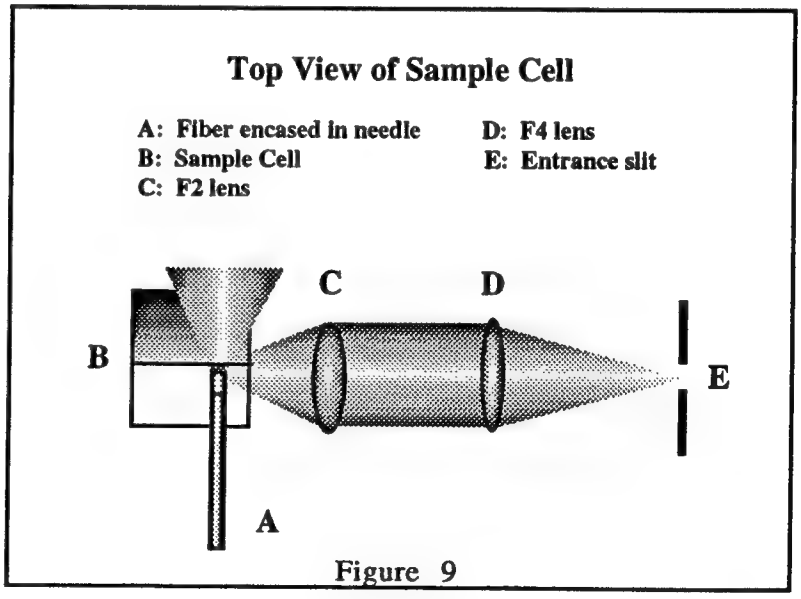

Figure 9

At the left of Figure 9, an optical fiber enters a vial containing the uncured liquid polymer. The fiber is driven by an ultramicrometer for positioning accuracy near 10 nanometers. The fiber is driven by the micrometer through the liquid polymer until it contacts a flat plate, and is then withdrawn to a specified position relative to the plate to interrogate the thin polymer film compressed between the fiber and plate. Laser excitation directed down the fiber excites only the polymer directly in front of the fiber. Scattered light is collected at 90 degrees into a spectrograph.

In an actual experiment, both the fiber and plate are micrometer-driven to ensure that the sample excited is directly in the focal plane of the spectrograph.

The sample thickness can be inferred from the withdrawal of the fiber (and the spacing produced between the fiber and plate thereby), or from the relative intensity of the Raman spectra arising from the sample. This latter estimation is based upon the magnification of the optics in the optical train, the effective width of the spectrograph slits, and the magnitude of the thin-film spectrum to the bulk measurement made by withdrawing the fiber and plate from the view of the spectrograph. (Consider, for example, that if the fiber and plate were in intimate contact -- zero sample thickness -- no spectrum of the sample would be produced at all). The advantages of this experimental setup are that variable sample thicknesses can be easily studied, and the plate can have any type of metallization or coating desired so that numerous interfaces can be studied.

Figure 10 shows an example of the polymer spectrum in bulk (the larger spectrum) and thin-film conditions.

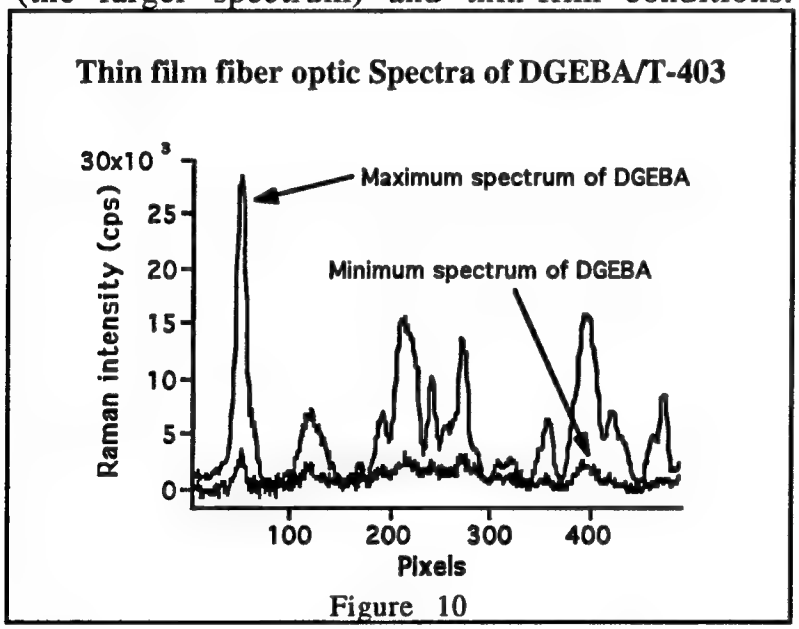

Figure 10

The thin-film (minimum) spectrum shown here corresponds to a sample thickness of approximately 2 micrometers. Using conventional peak-height or integrated peak intensity calculations, the signal-to-noise ratio of the weaker spectrum is near the minimum necessary for useful results. With no additional processing, a 2-μm-thick film is the effective minimum film thickness that can be studied using this method. Figure 11 shows results for the integrated band intensity of a cure-sensitive peak normalized to a cure-insensitive peak.

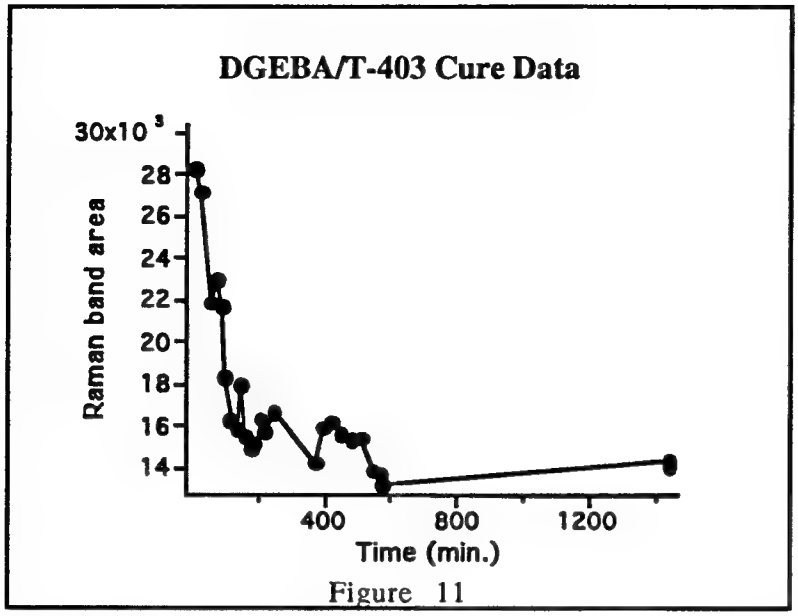

Figure 11

The noise in Figure 11 suggests the data are for a film at our effective minimum detection limit. In order to extend this method to sub-micrometer film thicknesses, multivariate statistical processing of the data can be used. Principal Component Analysis (PCA) is a form of pattern-recognition processing (see section on statistical analysis below) that permits improved signal-to-noise in spectroscopic measurements. Figure 12 shows the results of PCA cure analysis for the 2-micrometer-thick film of Figures 10 and 11.

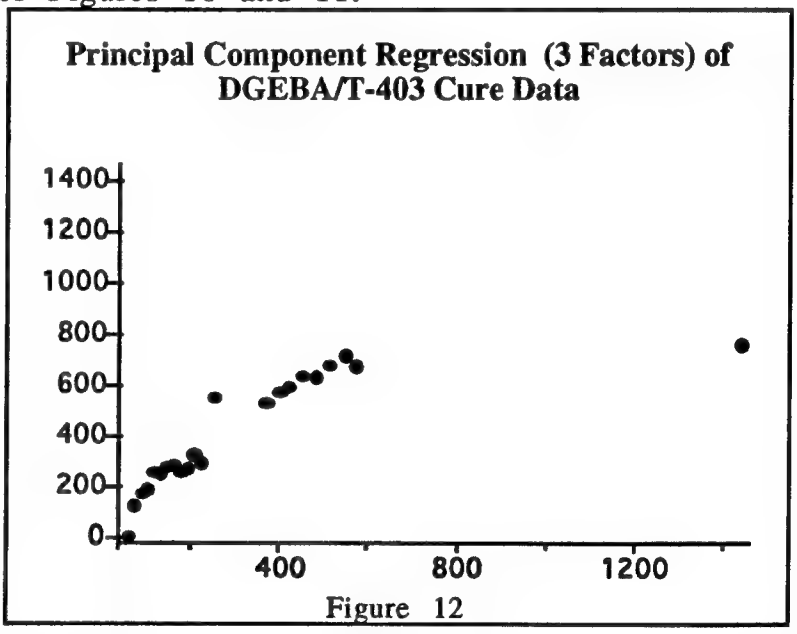

Figure 12

In Figure 12, the x-axis is time in minutes at room temperature, while the y-axis is a linear combination of spectral wavelengths in the Raman spectrum. These measurments are made at room temperature, and the curing of the polymer at room temperature is a slow process ending at about 75% cure when the glass transition temperature of the partially cured liquid exceeds room temperature and all reaction halts. As the figure shows, this occurs in the thin film at approximately 600 minutes into the cure. The signal-to-noise increase in data interpreted via Principal Component Analysis is substantial, permitting weaker signals to be distinguished from background, and extending the detection limits of this technique to films as thin as 100-200 nm.

Work is currently still in progress on comparing these interfacial curing data with bulk curing data.

Principal Component Analysis

The application of chemometric methods to spectra obtained by fiber-optic Raman spectroscopy addresses the interpretation of optical spectra to determine physical and chemical properties of the polymer.

Raman spectra obtained by fiber optic monitoring during the curing process represent mixtures of several components. Spectral subtraction or least squares fitting of reference spectra is not adequate to resolve mixture spectra when dealing with such "real" mixture problems. Unpredictable chemical changes in polymeric structure complicate spectral interpretation, and reference spectra of pure components are not usually available.

Instead of concentrating on individual features, principal component analysis (PCA) explores relationships between samples and derives a subset of linear combinations of the features that describe the largest proportion of variability.

Accounting for the variability in a data set requires a number of principal components (PC's) equal to the smaller of the number of features or the number of objects in the data set. PCA attempts to represent the higher dimensional data with a smaller set of features, or principal components (PC's). The first PC is the line that best fits the data, with the sum of squares of deviations of the data points from this linear combination of the original axes a minimum. The second and higher PC's are perpendicular to this axis and are ranked in decreasing order of correlation with the data. This decomposition of the data matrix is obtained by eigenvalue-eigenvector analysis, an efficient method which is based on the singular value decomposition [5]. The magnitude of the resulting eigenvalues is a measure of the variance explained by each eigenvector or PC. The number of "significant" eigenvalues indicates the number of real factors or components. Additionally, the PC model can be rotated to make the PC's easier to interpret in chemical terms.

A major purpose of PCA is dimensionality reduction: a plot of the data projected on the plane formed by the first two PC's permits relationships among the clusters of data points to be visualized in two dimensions. More important, however, is the ability to extract chemically meaningful principal components that represent components of the original mixture.

A variety of software packages for chemometric analysis of data have been used during this project. The limitation on any

software analysis tool is the maximum matrix size which the program (or computer platform on which it runs) can invert. The first software tool used here was SYSTAT, a UNIX-based statistical programming language. The limitations of SYSTAT prevented analysis of data matrices larger than 60 X 60 arrays of double-precision values.

A software package available from Infometrix, Inc. called Pirouette® was obtained which was capable of inverting substantially larger arrays - larger than 1000 X 60. Subsequently, the MATLAB programming language was added with new computational facilities to allow inversion of data matrices larger than 1000 X 500 arrays of double-precision numbers. For routine statistical exploration of data, Pirouette® proved convenient and powerful. MATLAB programs, however, were more versatile and provided additional tools for visualization.

To illustrate the effect that application of PCA can have on data analysis, consider Figure 13 below.

In this figure, thin-film measurements have been made as a function of micro-meter position. In other words, the sample pathlength is varied during this experiment, and the integrated area of an epoxy Raman peak is plotted vs. micrometer position to help determine the sample thickness. In this case, the optical fiber is advanced toward a wall, squeezing polymer out of the way until contact is made, then the fiber is withdrawn. From these data, sample thickness appears independent of direction (approach or withdrawing). Figure 14 below shows the results of PCA analysis of the same data shown in Figure 13.

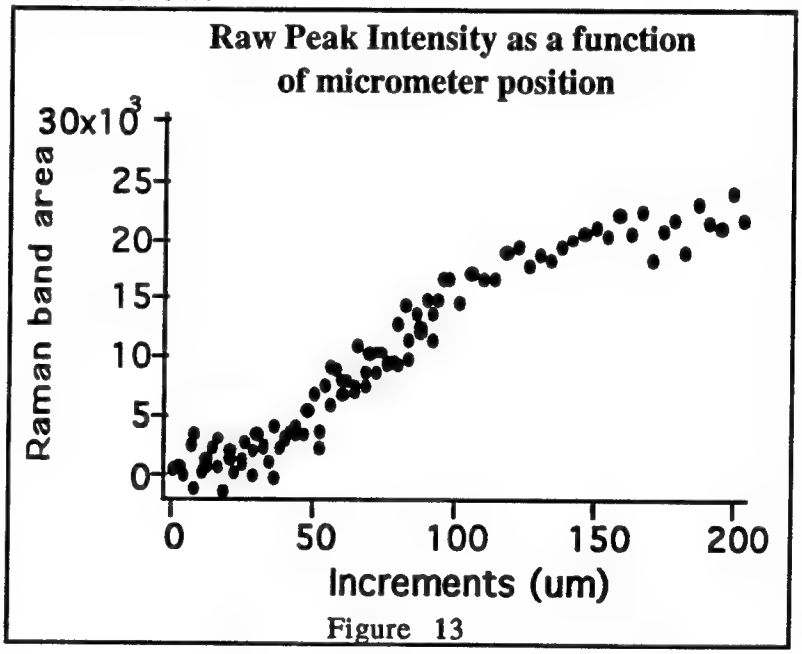

Figure 13

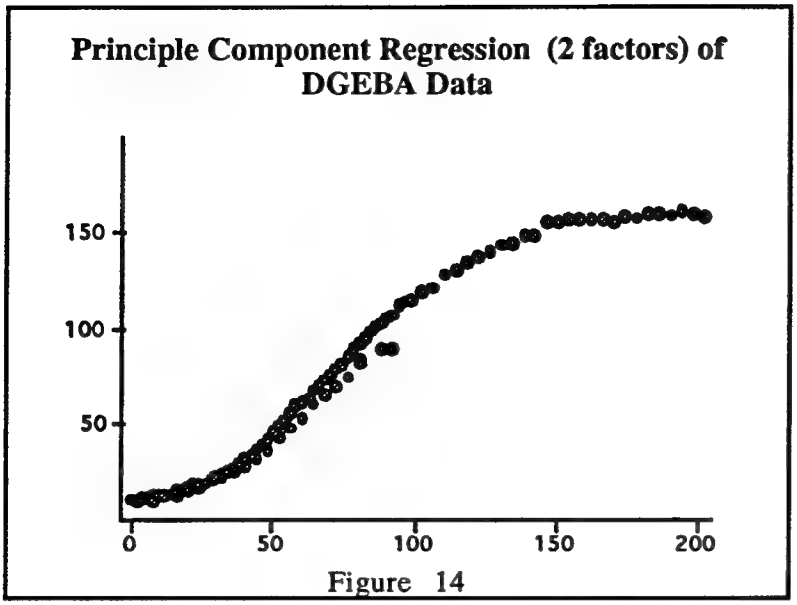

Figure 14

The substantial improvement in signal-to-noise introduced by the multivariate statistical analysis allows the analyst to view the subtle distinction between data points acquired with the micrometer driven in the forward versus reverse directions, caused by hysteresis of the mechanism.

The same multivariate statistics applied to individual spectra can be applied to spectral imaging data, as shown below.

Construction of a Micro-Raman System

One purpose of the grant to the University of South Carolina was to design, construct and utilize a micro-Raman system for studying interfacial zones in composites. Figure 15 below shows the overall layout of the system constructed in our laboratory.

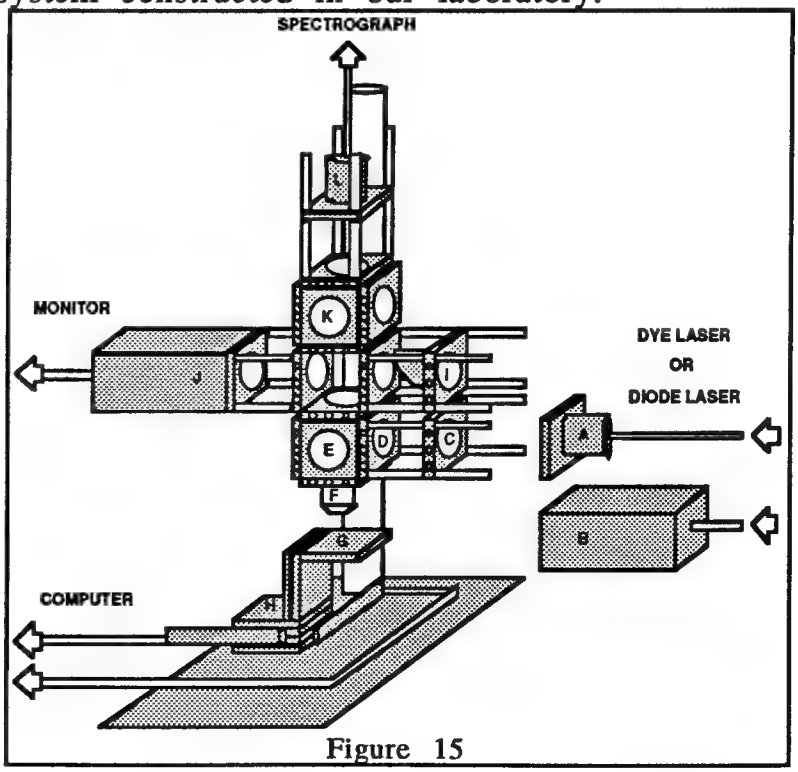

Figure 15

This system utilizes a versatile optical scheme which permits bright-field images to be acquired via a video frame-grabber system or a cooled CCD camera mounted to the left of the optical train. Removal of a sliding mirror permits a spectrum of the sample at the focal point of the microscope to be obtained. In this case, scattered light is focused onto an optical fiber at the top of the instrument, and this conducts the light to a

1/4-meter spectrograph and N_2(l)-cooled CCD array. Excitation for Raman or Fluorescence spectroscopies is derived from either an Argon-ion laser, a NIR dye laser, or a laser diode mounted directly to the microscope on the right of the optical train. The sample sits atop a stage with X-Y motorized positioners, and the entire data collection system is under computer control so that arrays of spectra can be acquired - a complete spectrum for each point in an image. The spatial resolution of the system using a 52X reflecting Schwartzchild objective is approximately diffraction limited -- 0.5 μm full width at half maximum using visible illumination for bright-field images. Used in the spectroscopic mode, the resolution is somewhat lower in the horizontal spatial domain. This is due to the viewing aperture defined by the 200-μm-core optical fiber, translating to approximately a 4-mm theoretical horizontal resolution for the 52X objective, and only 20-μm resolution using a 10X objective. Figure 16 below shows results for horizontal resolution obtained using three objectives in Raman spectroscopic mode.

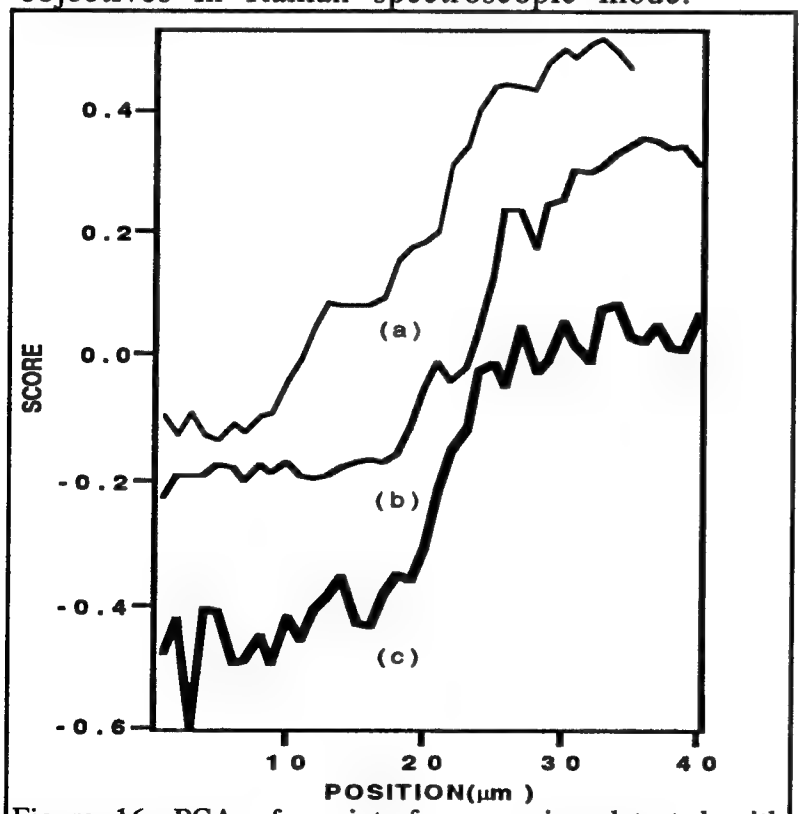

Figure 16: PCA of an interface crossing detected with Raman scattering using the USC microRaman with a (a) 10X objective, (b) 20X objective, and (c) 52X objective

These data were obtained by scanning across the polished interface between two polymers - Delrin and the DER332/T403 epoxy. The plots are projections on the first principal component from the PCA of the spectra, and the results are in almost perfect agreement with the ideal predictions based on geometric optics.

Vertical resolution is typically poor in most micro-Raman systems unless the confocal technique is used. In confocal microscopy, the sample is illuminated by a moving pinhole, with light collected through another pinhole located in the focal plane

of the returning light. Out-of-focus light is strongly selected against, resulting in improved depth resolution for "optical sectioning". The USC system is confocal in design: illumination is provided by a diode laser (effectively a point source), and detection is through a 200-μm-core optical fiber (effectively a 1/5-mm pinhole). A ray-tracing program was used to model the vertical resolving power of the microscope using the 52X Schwartzchild reflecting objective. The predicted vertical resolution of the microscope under optimal conditions was approximately 20 μm. Figure 17 below shows experimental data from a sectioning experiment in which the focal point of the microscope was scanned vertically through an epoxy-glass interface.

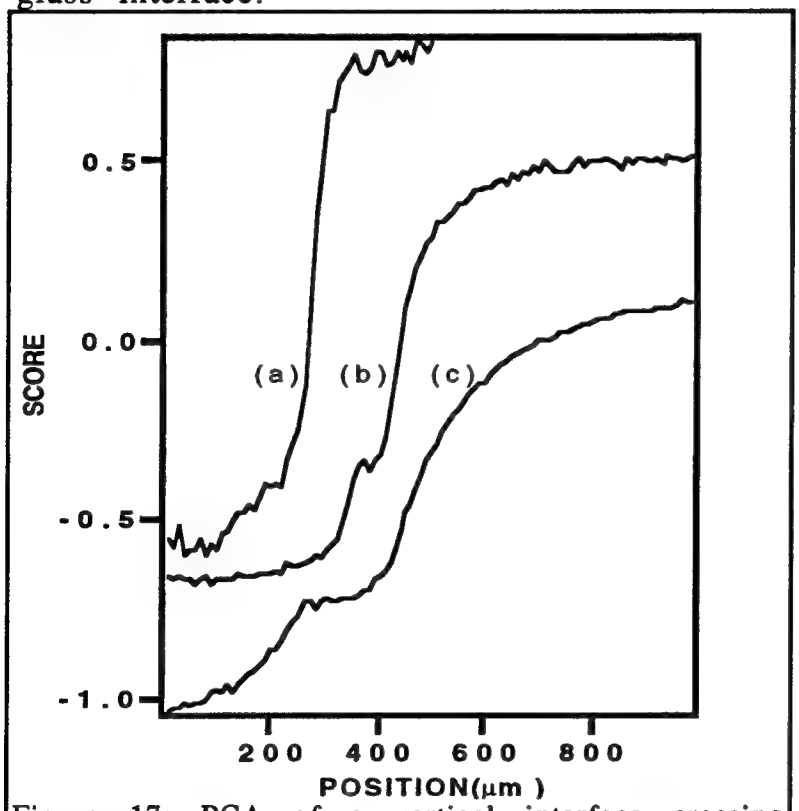

Figure 17: PCA of a vertical interface crossing detected with Raman scattering using the USC microRaman with a (a) 52X objective, (b) 20X objective, and (c) 10X objective

These results show that the effective vertical resolution was somewhat greater than the predicted - approximately 40 μm vertical resolution as compared to the predicted 20 μm. No suitable explanation has yet been found for this reduced resolution.

Microwave Curing Studies

A major interest which evolved in the pursuit of this project arose from an interaction with researchers at the FAA in Atlantic City, New Jersey. One of the advanced polymer synthesis methods under current development is the application of microwave sources to provide the heat necessary to drive reactions to completion. A major difficulty with microwave curing of polymers is inhomogeneity of exposure to the microwave radiation. For microwave curing applications to achieve widespread use in larger composite parts, a real-time monitoring system is

necessary. Due largely to the rapid measurements of which a fiber-optic Raman system is capable, we were able to successfully follow the curing of a polymer sample (the DER332/T-403 epoxy) under high-intensity microwave heating. Figure 18 below shows the experimental setup for the studies, publication of which is in progress in the optics journal Applied Spectroscopy.

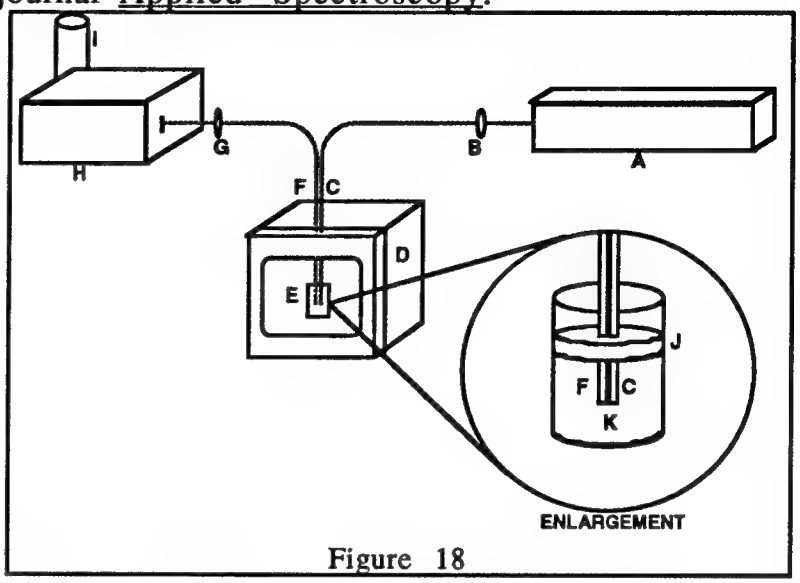

Figure 18

The sample interrogation procedure was fairly standard, except that the extreme heating rate and the microwave sources required special procedures in probe design and sample preparation. Metal casings are standard in most currently-available fiber probes. To produce a probe without a metal casing, the probe was prepared (two fibers embedded in a metal sheath) via the standard method and the metal casing was etched away electrochemically in a sulfuric acid bath. The polymer used to seal the fibers together was removed from the distal ends of the fibers by flame treatment, as this polymer (another epoxy) served to catalyze the decomposition of the DER332/T-403 polymer, with the predictable result that polymer charring at the probe tip at an early stage in the polymerization process obstructed the probe's view of the remainder of the process. A third sample pretreatment was extensive de-gassing of the liquid monomers prior to polymerization, and sealing the unreacted liquid beneath a cap to prevent expansion during reaction. These steps were necessary to prevent extensive bubbling of the cure mix. Prior to taking this step, the cured epoxy would often be produced as a "froth" rather than a clear polymer.

Figure 19 shows unprocessed spectra acquired during the curing of a polymer under microwave excitation.

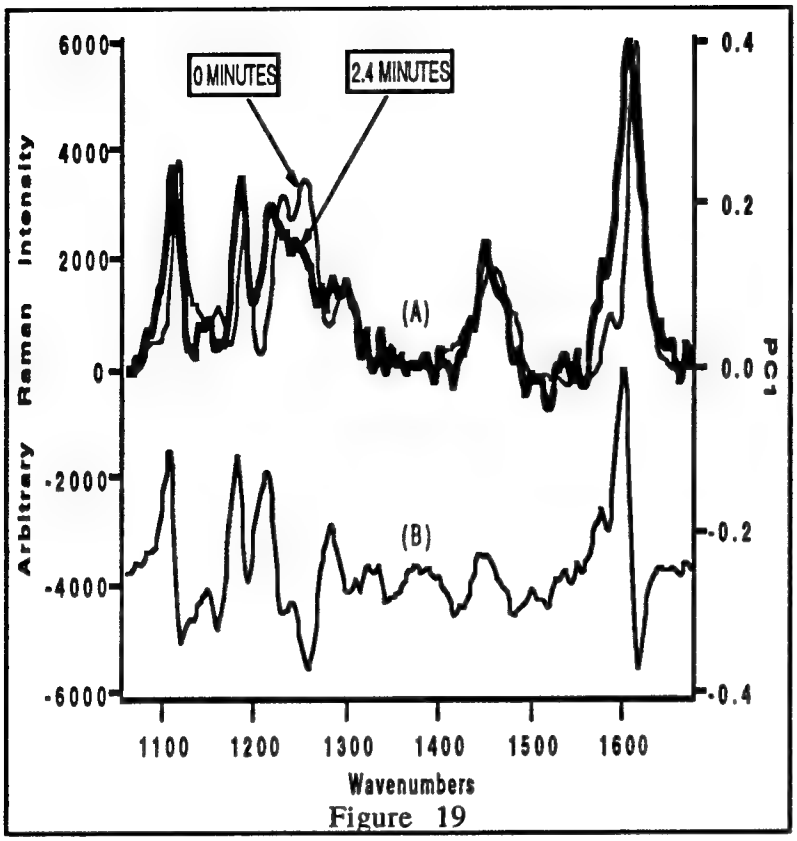

Figure 19

As this figure shows, the reaction was complete in about 2 minutes - the 2.4 minute spectrum was the last acquired before the hot polymer burst into flames. The curve B in Figure 19 is the first principal component of the optical spectra. This curve contains all the spectral peak shifts and magnitude changes that are observed during the curing of this polymer, and explained over 90% of the variability of the spectra. The residual variability of the spectra was noise.

When the projection of each spectrum onto the first principal component is plotted (giving an optical curing curve) the results allow us to observe the rate and extent of curing of the polymer. This is shown in Figure 20. Since this curing was performed with microwave excitation, no thermocouples could be placed into the polymer, and the temperature was not monitored optically

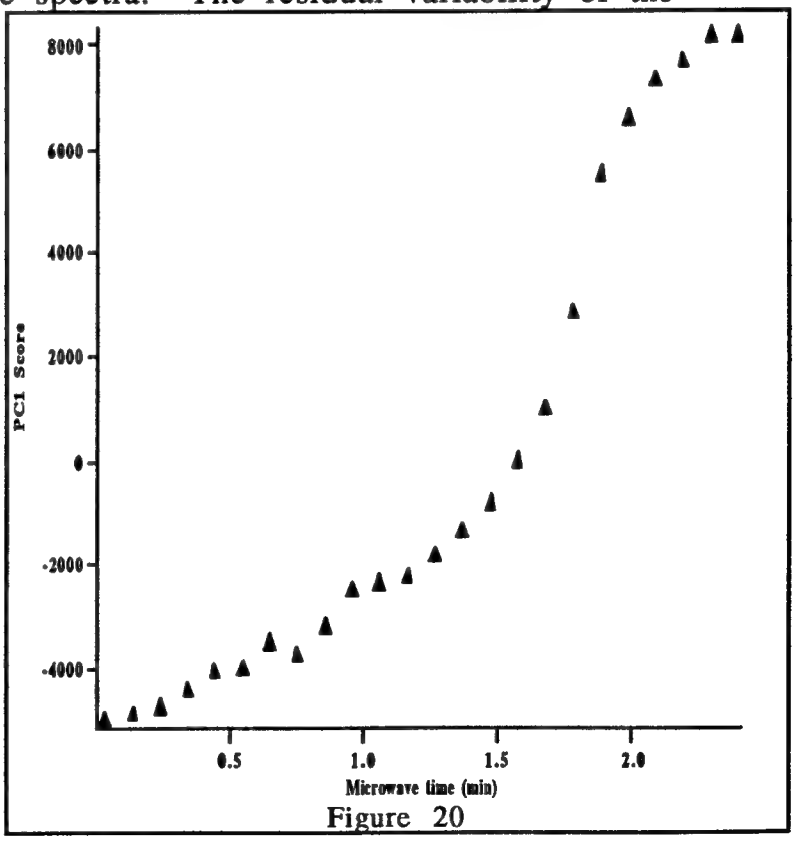

Figure 20

(although this can be done with more advanced equipment than that used for this study). Even under these extreme conditions, the Raman spectra (acquired every 5 seconds) clearly showed a plateau of reaction - a period in which the polymer had completely reacted but had not yet begun to decompose. Sensors based on this technology could be employed that would direct automated curing systems to de-energize the microwave source at the appropriate time for optimal curing.

Mode-Hopping Removal

A major difficulty with portable Raman systems using NIR excitation (necessary for fluorescence rejection) is the need for a compact, portable, stable, long-lived laser source. At present, the selection of lasers operating in the appropriate spectral region is limited to lasers which are very expensive to maintain (e.g., Nd:YAG lasers doubled to pump a dye laser or Argon-ion lasers pumping a dye laser or Krypton ion lasers) or diode lasers. Diode lasers would make ideal sources except for the phenomenon of mode-hopping.

Mode-hopping is the term used to describe the (apparently) random change of laser wavelength in a diode laser due to slight shifts in the gain band or cavity length of the laser with fluctuations in temperature. These discrete shifts of laser wavelength make Raman spectra obtained with diode lasers difficult to handle analytically over extended periods.

We have developed a new computational algorithm which aligns optical spectra of unknowns prior to processing based upon principal component analysis and comparison with calibration samples. The process results in accuracy which can be varied arbitrarily. As an example, Figure 21 shows a set of 5 Raman spectra acquired for a sample of Delrin (a Dupont polymer) acquired with a diode laser over a period of several minutes. These 5 spectra were selected from over 1600 spectra acquired in a single set of measurements in order to illustrate the mode-hopping alignment algorithm.

The four spectra shown in Figure 21 are unaligned - meaning effectively "raw" data. Although the sample is unchanged, the spectra are subtly distinct due to shifting of the laser wavelength with time and temperature drift. While minimal over the space of a few minutes, this shift can be quite substantial over the course of an entire day or week - often several nanometers or tens of wavenumbers. While the shifts shown in Figure 21 are slightly smaller than the width of the Raman peaks, shifts larger than the

width of Raman peaks are not uncommon, rendering unaligned data using a diode laser almost valueless in information content.

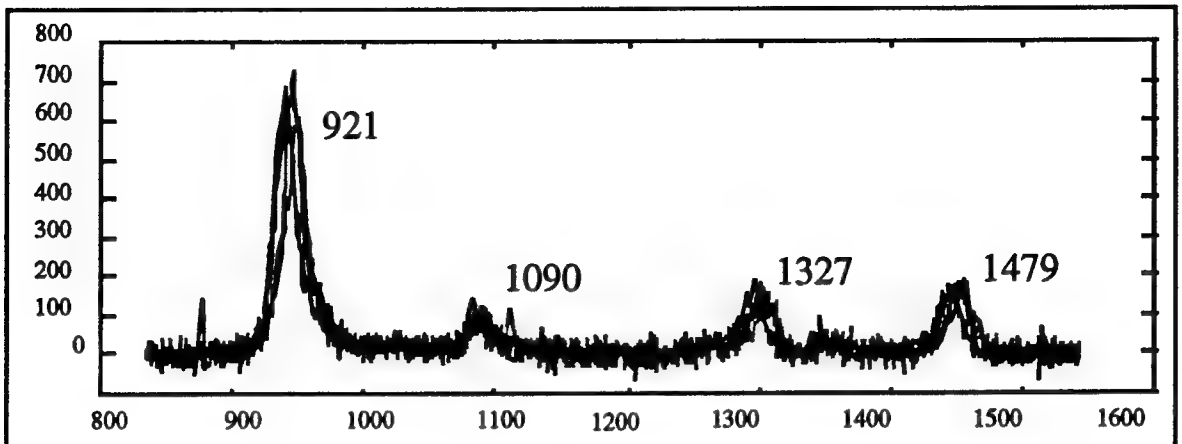

Figure 21 - Unaligned Raman of Delrin polymer using a Diode Laser excitation source at approx. 785 nm. Peaks do overlap perfectly due to laser mode hopping with time. The x-axis is given in wavenumber shifts from the nominal wavelength of the diode laser, rather than actual.

Application of the computational algorithm allows real-time alignment of spectra as they are acquired so that chemical information contained in the spectra is not obscurred. Figure 22 shows the same four spectra following alignment of the complete 1600-sample set of spectra.

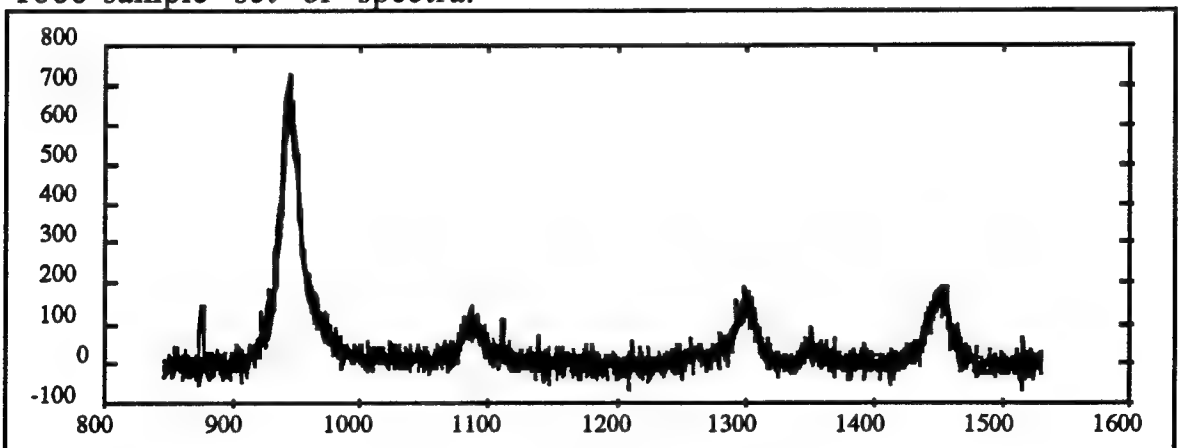

Figure 22. Same data as Figure 21, but following application of Algorithm for Spectral Alignment. The Raman shifts in this figure are on a "true" wavenumber scale, since laser drift is corrected for.

This alignment method is the subject of a patent disclosure and will be published following a patent review.

Chemometric Imaging

Just as PCA can be applied to individual spectra, the images acquired with the micro-Raman/micro-Fluorescence system can be analyzed to produce chemical mapping. Standard microspectroscopy systems produce "bright-field" images - total photon density maps or integrated spectral window maps. These types of images, while useful, do not always convey detailed information on subtle chemical or physical variations in a sample because they depend on the intensity of a light in a specified wavelength range instead of recognizing the patterns of spectral intensities in the image. One focus of our work has been the application of PCA to imaging for the purpose of determining cure heterogeneity in composites.

The micro-spectroscopy system described in a section above can be used to acquire complete optical spectra for a given point in a sample. By allowing a computer to translate the sample via motorized actuators, spectra can be acquired for arrays of points inside the sample and interpreted in image format.

Figure 23 shows two images of a gold contact (total width of 200 micrometers) sputtered onto a Delrin sample, a DuPont polymer. Figure 23a is a "univariate" image - a bright field image using the intensity of a single Delrin Raman peak to define the area occuppied by Delrin and the area occupied by gold. This is a very simple example, yet the univariate image is complicated by noise and is ill-defined. Figure 23b shows the same spectral data interpreted following mode-hop removal and principal component analysis. In Figure 23b, the magnitude of the first principal component, the most important pattern recognized in the data, is used as the source of the image information. This improves the signal-to-noise in the image and allows us to view more detailed information in the image.

Figure 24 shows a bright-field image of a composite - the red areas of the image are a fibrous support surrounded by a DuPont nylon of a proprietary nature. The yellow-blue region of Figure 24 is a particle of a nylon-related byproduct of the polymerization which has become embedded in the material. This image is taken in a fluorescence mode, with the magnitude of the fluorescence at 530 nm plotted vs. position to produce the view. The area viewed is approximately 450 X 250 micrometers.

Figure 25 shows the results of PCA on the images. Figure 25a is an image based on the first principle component, which highlights the areas occupied by the polymer impurity. Note that this image shows the spatial extent of the defects to be substantially greater than the original bright-field image. Figure 25b is an image based on the second principal component, which highlights the regions

surrounding the defects and which may contain information about diffusional mixing between the defects and the surrounding nylon. In these images, the weave of the fiber support is also more apparent than in the original bright field image.

Figure 26 is a PC1 image of a glass fiber embedded in an epoxy. The red ring surrounding the fiber is a second polymer - a polyimide that was coated onto the fiber prior to polymerization in epoxy. Figure 27 is a second view of the same subject, placed into 3-D perspective. It is apparent that the PCA treatment of images from microspectroscopy can be used to increase the information content of images and even to increase data acquisition rates, since the PCA treatment provides a substantial increase in signal-to-noise in analysis.

Figure 28 shows another PC1 image of a fiber embedded in epoxy without a coating of a second polymer. The blue regions of this image include the fiber face, which in these images should appear as a circle with a diameter of 220 μm. The apparent size of the fiber is in approximate agreement with the known size of the fiber, although the shape is not regular. This is partially due to optical irregularities in the material being studied. In this case, the sample was cut and polished with a fine Al_2O_3 lapping film. The "rays" extending away from the fiber are actually cracks and crevasses in the polymer exposed during polishing. These cracks are not apparent in the "bright-field" image of the surface, but the confocal nature of the MicroRaman system reveals them as it performs an "optical section" on the sample. Even following spectral normalization these rays are prominent in the spectroscopy of the surface due to residue from the polishing which contaminates the crevasses. Such contamination is exceedingly difficult to remove, although ultrasonication may be effective in producing a pristine surface for study.

Better signal-to-noise and closer spacing of the measurement points should substantially improve our ability to resolve any irregularities surrounding fibers in epoxy or other matrices.

Nanometer-Scale Analysis Of Graphite Interfaces

A major thrust of this project has been to develop methods for studying the interfaces of polymers with surfaces. The reason for this is to improve the binding of polymers to substrates for adhesive, composite and other purposes which require mechanical strength between these two dissimilar materials.

Graphitic fibers are a common component of composite materials, with epoxies being the most common binding agent. Generally, fibers are coated with uncured liquid monomers and

(a)

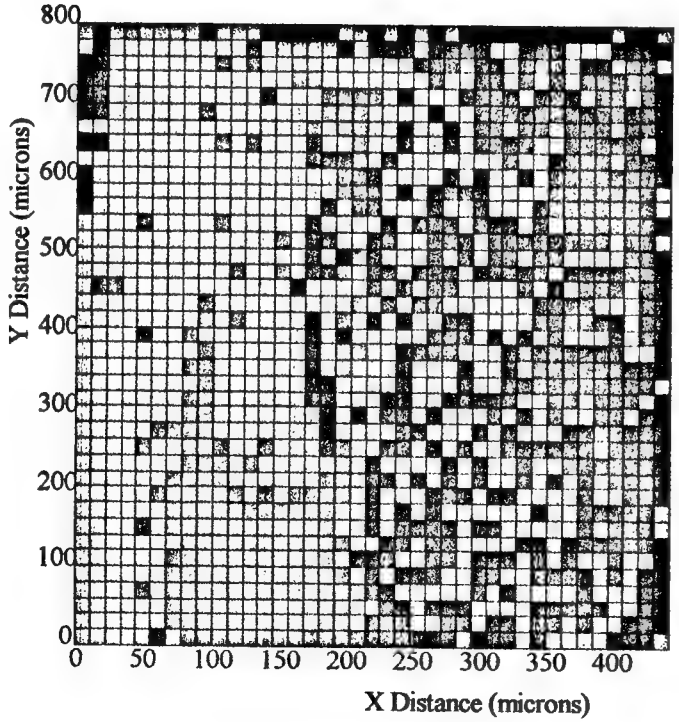
800
700
600
500
400
300
200
100
0
Y Distance (microns)
0
50
100
150
200
250
300
350
400
X Distance (microns)

(b)

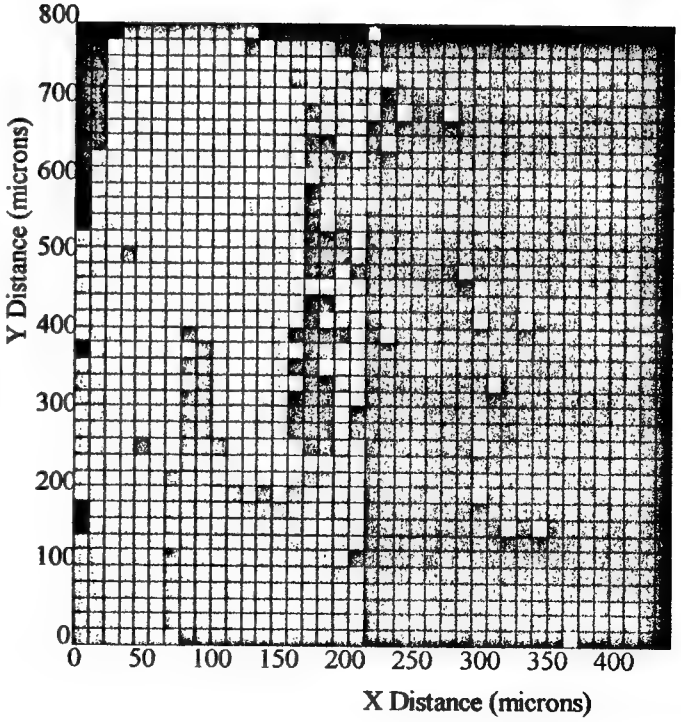
800
700
600
500
400
300
200
100
0
Y Distance (microns)
0
50
100
150
200
250
300
350
400
X Distance (microns)

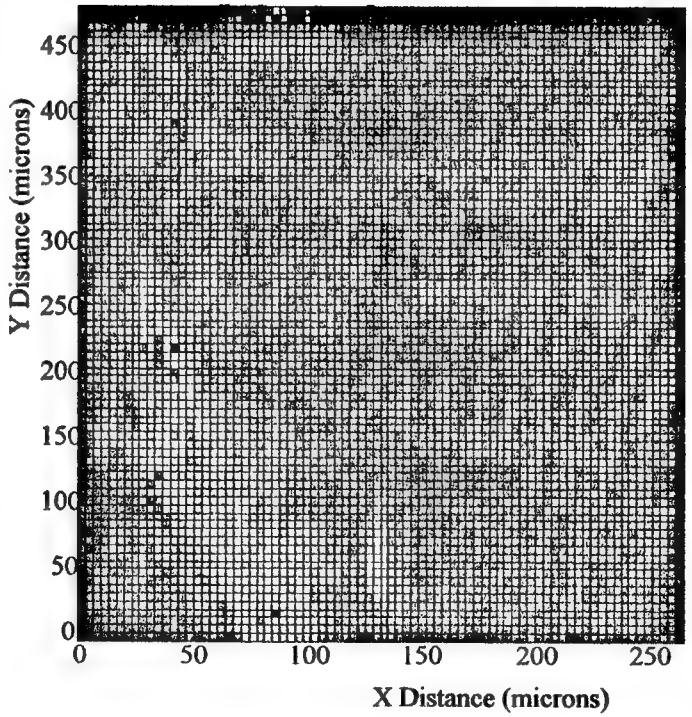
Y Distance (microns)
450
400
350
300
250
200
150
100
50
0
0
50
100
150
200
250
X Distance (microns)

(a)

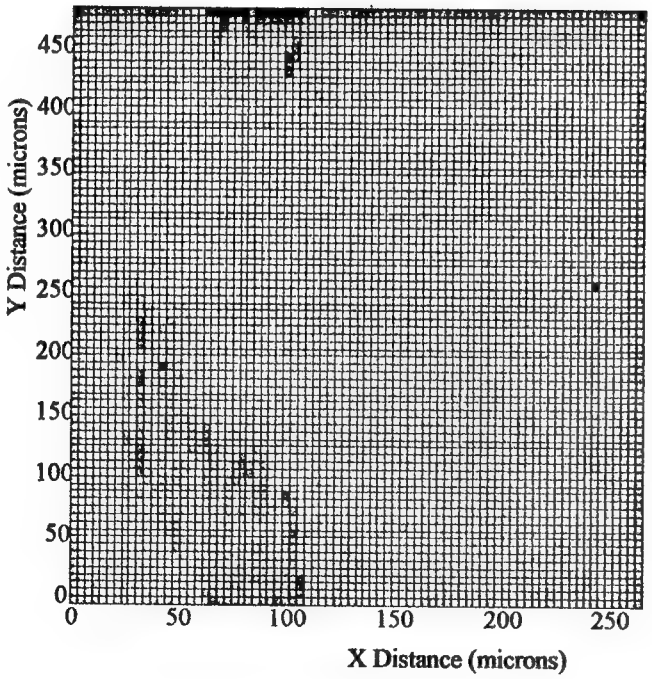
Y Distance (microns)
0
50
100
150
200
250
300
350
400
450
0
50
100
150
200
250
X Distance (microns)

(b)

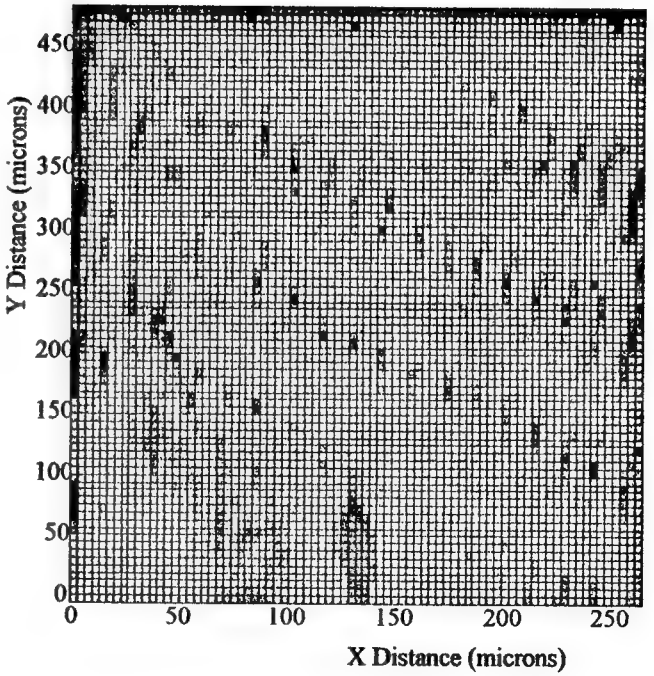
Y Distance (microns)
0
50
100
150
200
250
300
350
400
450
0
50
100
150
200
250
X Distance (microns)

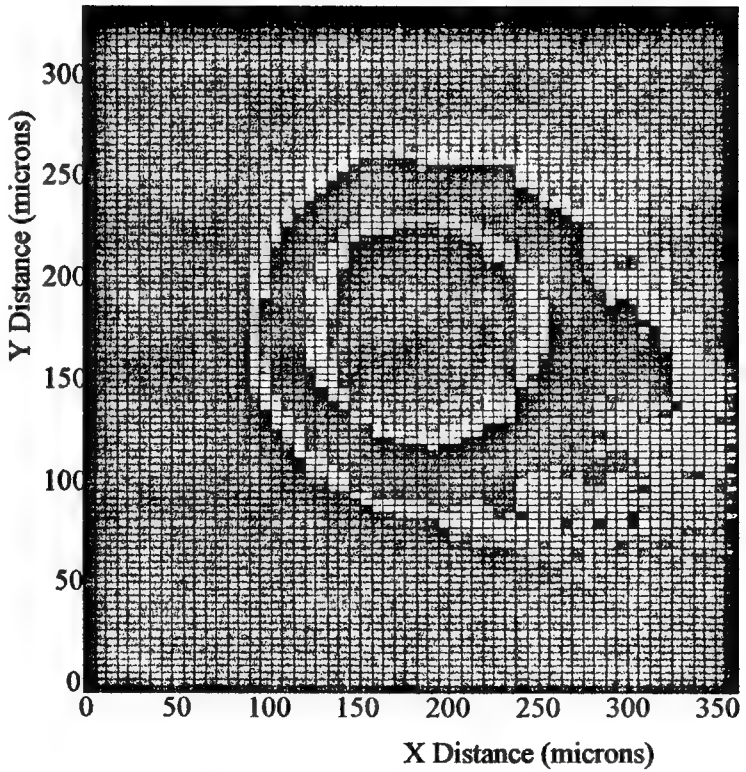
Y Distance (microns)
300
250
200
150
100
50
0
0
50
100
150
200
250
300
350
X Distance (microns)

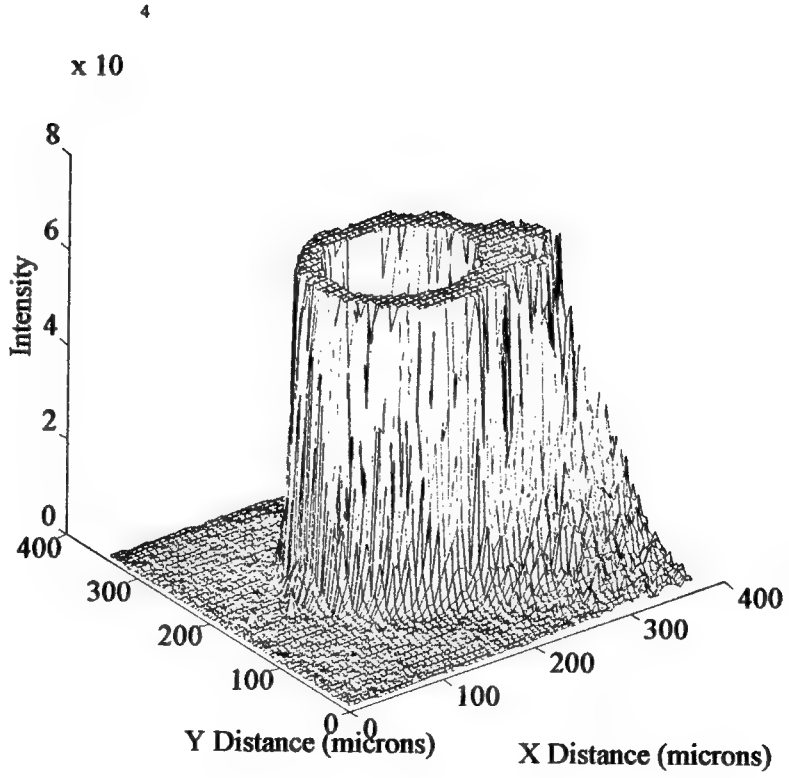
4
x 10
8
6
4
2
0
Intensity
400
300
200
100
0
0
100
200
300
400
Y Distance (microns)
X Distance (microns)

PC1 - Unit Area

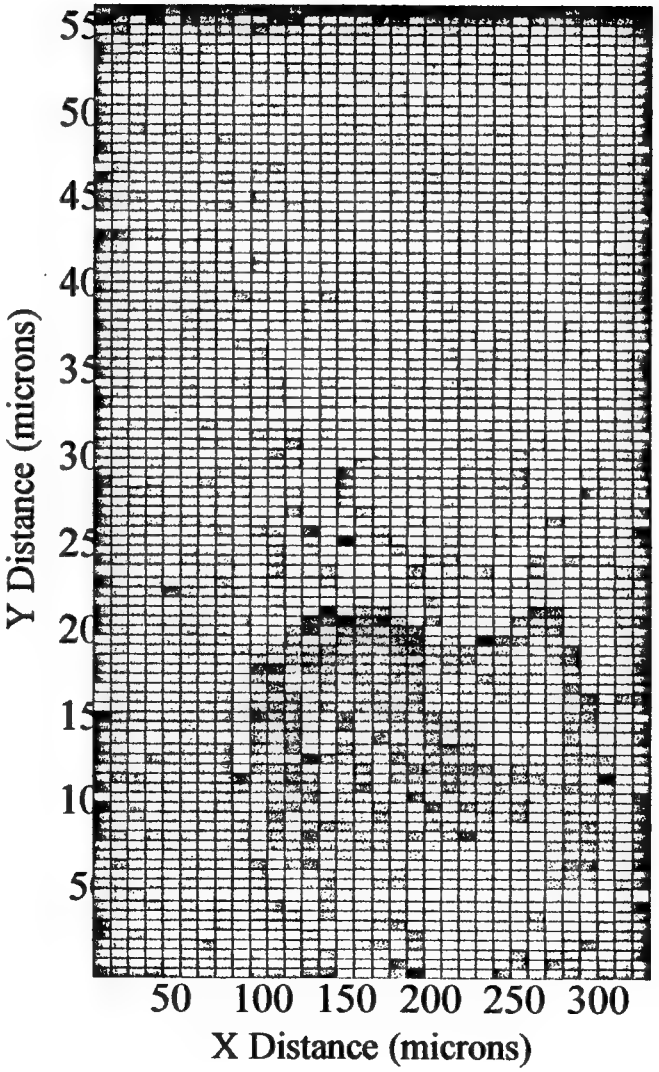

heated until the polymers set and cure. This provides an interface of unknown character between the polymer and fiber.

Recent work in this laboratory has focused on the analysis and chemical derivitization of graphitic domains. For these studies, highly-ordered pyrolytic graphite (HOPG) was selected because of its limited number of defect sites - this provided a controlled substrate for study.

A project recently funded by the NSF resulted in instrumentation capable of imaging the surface of HOPG at near-atomic resolution while chemical reagents are added. The importance of this instrumentation to the present project is that it allows us to visualize whether covalent bonding is occurring between the graphite and anything in the reagent solution. We have observed that the basal plane of graphite is (as expected) highly unreactive toward any mild chemical agents. However, we have observed reactivity on the molecular scale at the edge plane of HOPG.

Graphite is the most stable form of carbon at room temperature and atmospheric pressure. It consists of layers of a two-dimensional atomic lattice comprised of "benzene-like" rings with six carbon atoms each.

Figure 29 shows the structure of one layer of graphite, with the basal plane and edge plane of the layer indicated.

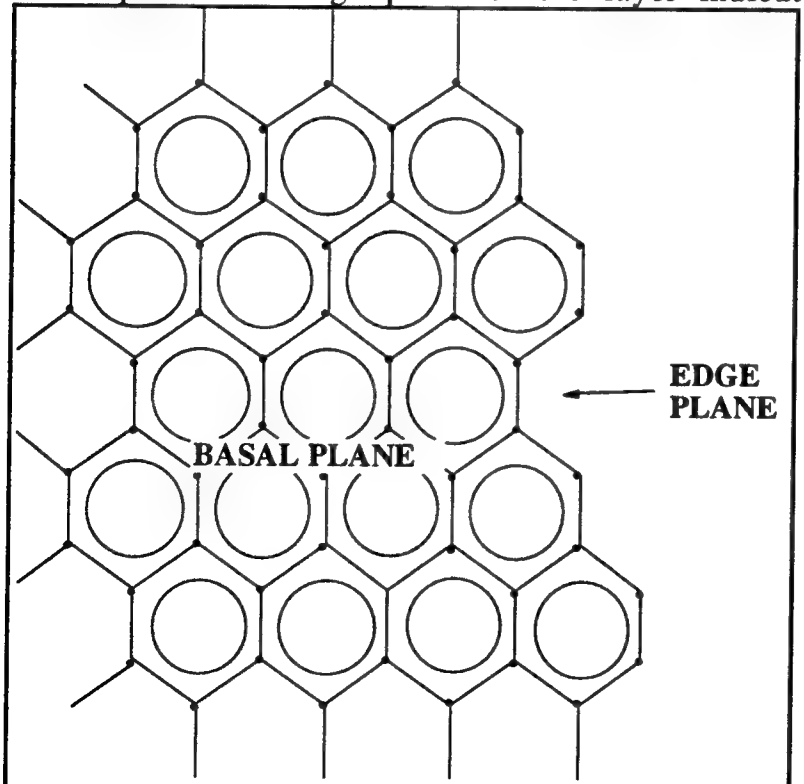

Figure 29

Chemical reactivity of graphite is highly anisotropic. The basal plane of graphite is relatively unreactive. The edge plane, however, is more reactive; simple organic chemical functionalities can be added and manipulated at this edge in much the same manner as is done with large aromatic molecules in solution.

Figure 30 shows the chemical pretreatment necessary to functionalize the

graphitic edge plane with amine-groups.

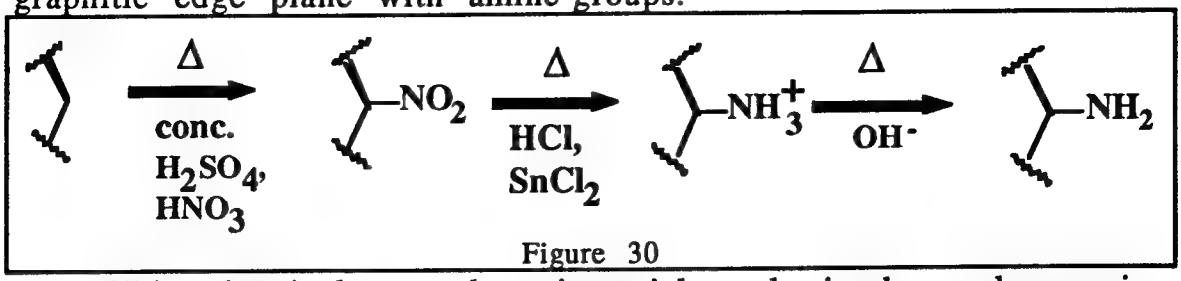

Figure 30

This chemical procedure is quick and simple, and scanning tunneling microscope studies done in this laboratory indicate that little damage is done to highly ordered pyrolytic graphite during this treatment so long as conditions are not extreme (e.g., too much heating results in delamination of the graphite planes and oxidation).

Once functionalized, the amine groups can serve as anchor points for polymer attachment. Many simple polymer precursors such as those shown in Figure 31 depend upon bonds between other chemical functions (in this case the anhydride chemical group) and amine groups to form the backbone of the polymer. .

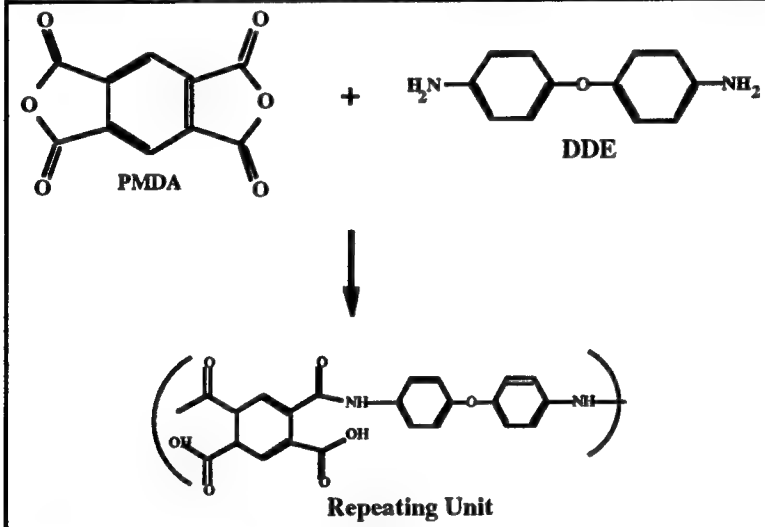

Figure 31
A simple dianhydride (pyromelletic dianhydride) and diamine (diaminodiphenylether) form polymers that can be attached to graphitic edge planes.

The polymer shown in Figure 31 forms quickly and readily, and was chosen as a model polymer for studies of covalent attachment to graphite.

One purpose for this work was to demonstrate chemical derivatives of graphite that could strengthen the interface between graphite fibers and epoxies. Epoxies use one component (such as DER332, Figure 1 above) containing epoxide groups that combines with an amine to form a copolymer. If the surface of graphite is modified to contain covalently-attached polymer units terminating in aliphatic or aromatic amines, then the interface between the polymer and fiber can be strengthened.

Figure 32 shows the proposed method for attachment of the test polymer to the derivitized graphite edge plane.

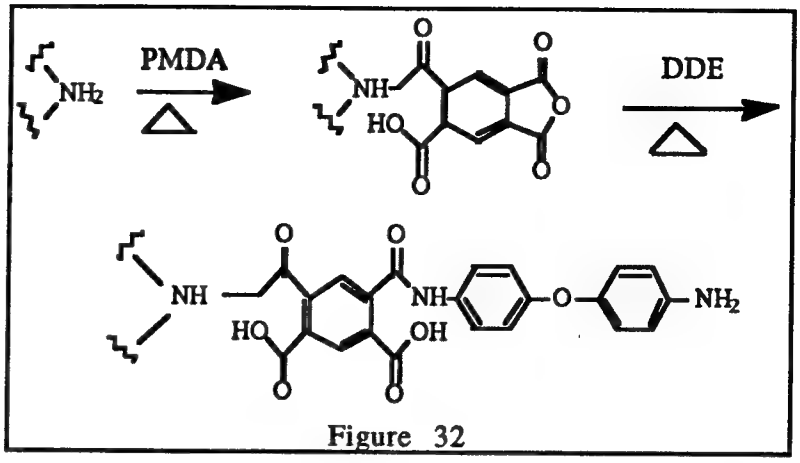

Figure 32

This attachment is far too fine a detail to observe under an optical microscope or even a scanning electron microscope. However, we have observed the effects of attachment in two ways. First, we were able to visualize the attachment of the polymer using a scanning tunneling microscope (developed with support of the National Science Foundation) that records images of surfaces *in situ* during chemical treatments. Figure 33 shows an example of a surface before and after treatment with DDE and PMDA monomers in ten steps (enough for ten complete dianhyride-diamine units).

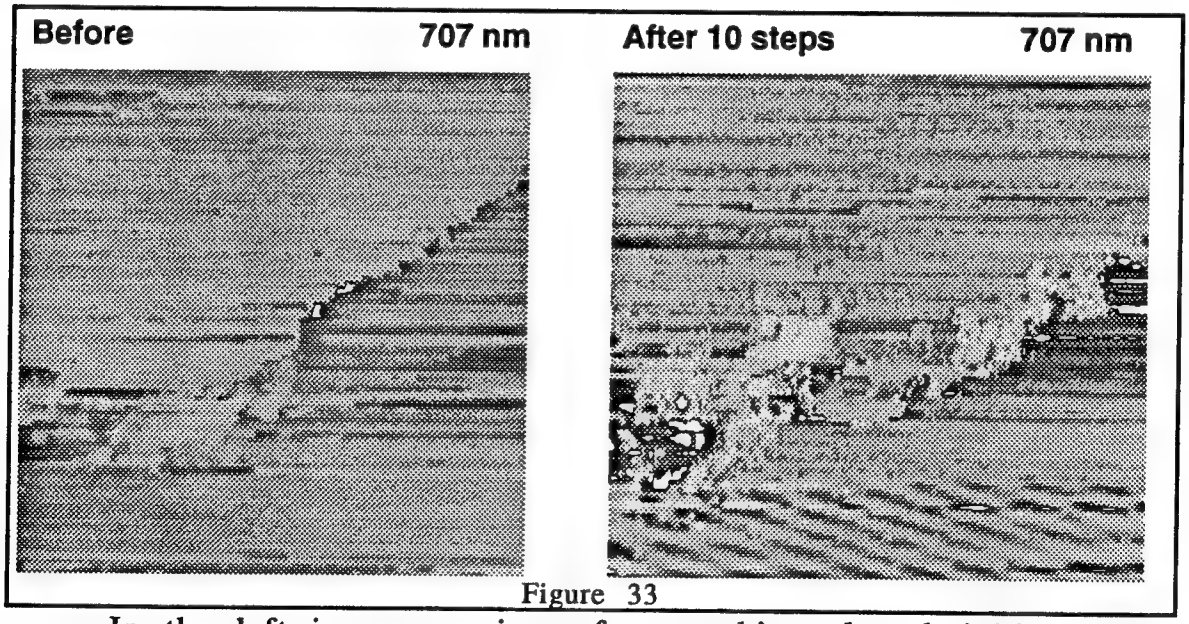

Figure 33

In the left image, a view of a graphite edge derivitized with amine groups beneath a flowing stream of N,N-Dimethylformamide (DMF) is presented. The right image shows the same edge (imaged continuously during treatment) following exposure to the monomer precursors, PMDA and DDE, in ten sequential steps in the flowing DMF. The residue building up on the edge is covalently attached,

since the scanning tip does not displace it nor does the flowing DMF wash it away.

A second method of observation of this derivitization is via fluorescence microscopy using the micro-spectroscopy system developed in this project. If the surface is prepared with ten steps of the polymer as in the Figure above, and the final treatment step leaves an amine group from the DDE monomer as the functionality presented to solution, an amine-sensitive fluorescent tag molecule can be added to the flowing stream in the scanning tunneling microscope. In the case of Figure 34 below, the tag molecule fluorescamine was added. This molecule becomes fluorescent when it binds to amine groups and is highly specific for this type of binding. Figure 34 shows two views of a graphite surface. In this case, the surface is that of highly-ordered pyrolytic graphite of the highest quality - very few edge-plane defects on the surface. The top view is approximately a 100 μm X 75 μm area of graphite illuminated with 488-nm laser light from an Argon ion laser. The bright details on the surface are scattering from dust and other particles which have settled on the surface since treatment. The lower image is of the same view, but with a 488-nm-rejection filter placed into the microscope. This rejects 99.9999% of the 488-nm light, but permits 85-90% of the longer-wavelength fluorescence of the fluorescamine bound on the surface to pass to the detector. As a result, the highlights on this image are due to the derivatized edge planes, and the width of the fluorescent lines is diffraction limited (only about 1 μm thick) because the edge defects are actually much smaller than the microscope is capable of resolving.

In conclusion, we have demonstrated the successful attachment of polymers to graphite via covalent bonding, potentially useful for strengthening the interface between graphite and polymers in composites.

(A) - Scattered 488-nm-light image

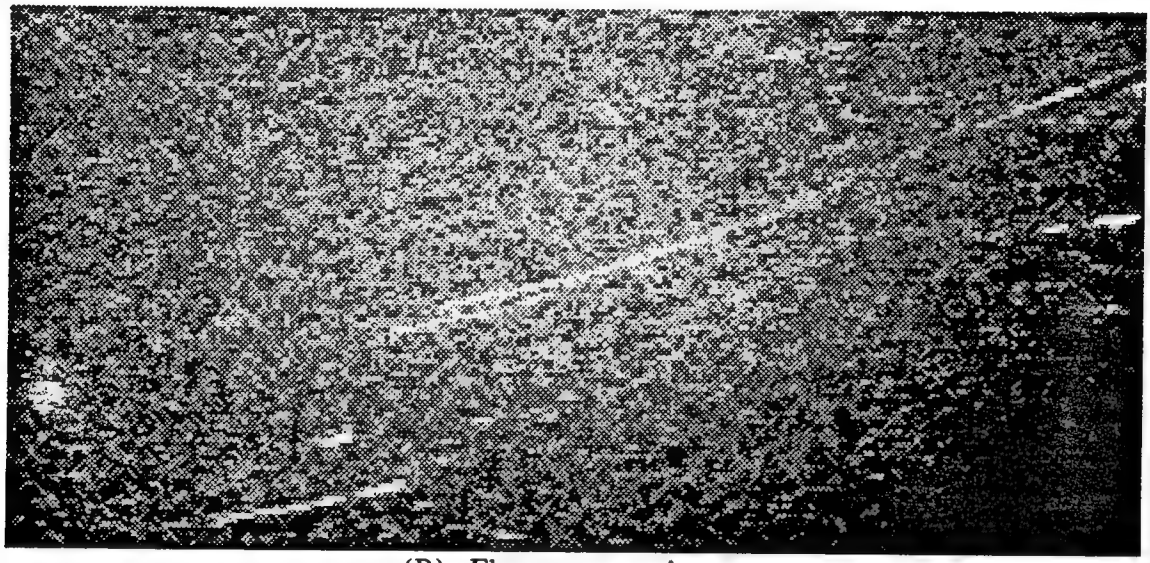

(B) Fluorescence image

Figure 34
100 μm x 75 μm image of graphite surface derivatized with polymers and exposed to fluorescamine.

Epoxy-Metal Interfacial Chemistry via SERS

Recently this laboratory has developed a method for producing metal colloidal suspensions in commercial polymers capable of producing surface-enhanced Raman scattering. These suspensions have a variety of uses, one of which is to study the chemistry of molecular adhesion at the metal-polymer interface.

Surface-enhanced Raman scattering (SERS) was discovered in the mid-1970's, and has been the subject of intense study[6]. While

normal Raman scattering is a relatively weak phenomenon, adsorption of a molecule at a metal surface can lead to enhancements of the Raman scattering of the molecule by factors approaching 10^5-10^6. This gives a spectroscopic entry to the study of monolayer surface-adsorbed species -- particularly of the chemical bonding present at a metal surface. The drawback of SERS is that only a few metals are known to produce it (Ag, Au, Cu and a few others weakly), and the surfaces must be prepared properly: they should be fresh and rough. Colloidal metal particles produced *in situ* provide such metal surfaces.

The preparation method developed by this laboratory involves preparing a concentrated solution of Ag^+ in Jeffamine T-403, mixing this solution in proportion with DER332, adding solid $NaBH_4$ to reduce the mixture, and curing the resulting brown solution. Ag metal particles precipitate from solution during the curing of the polymer. The exact proportions of T-403 and DER332 along with the rate of heating appear to determine the size distributions of the Ag particles, with aggregate sizes $<0.5\ \mu m$. The resulting polymer is brown and cloudy in color, but exhibits less fluorescence than a clear, unreduced sample of the same polymer because of the fluorescence-quenching effects of the metal in suspension.

Figure 35 shows the Raman spectrum of the DER332/T-403 polymer with the precipitated Ag colloid. The spectrum of this material changed upon intense illumination with a laser -- new features already present in this material (but not normally present in the clear polymer) increased in magnitude. Figure 35 shows the spectrum prior to intense illumination, along with the spectrum of the differences caused by laser annealing. The difference spectrum nearly recovers a spectrum of a new species produced by the laser heating. Further SERS work in this laboratory has shown that the same new spectrum is obtained by post-curing of the polymer in a normal curing oven. The new peaks are, however, present in the spectrum even before additional heating is provided -- they merely increase in magnitude with heating. A slight shifting of the vibrational frequencies is also observed with additional heating.

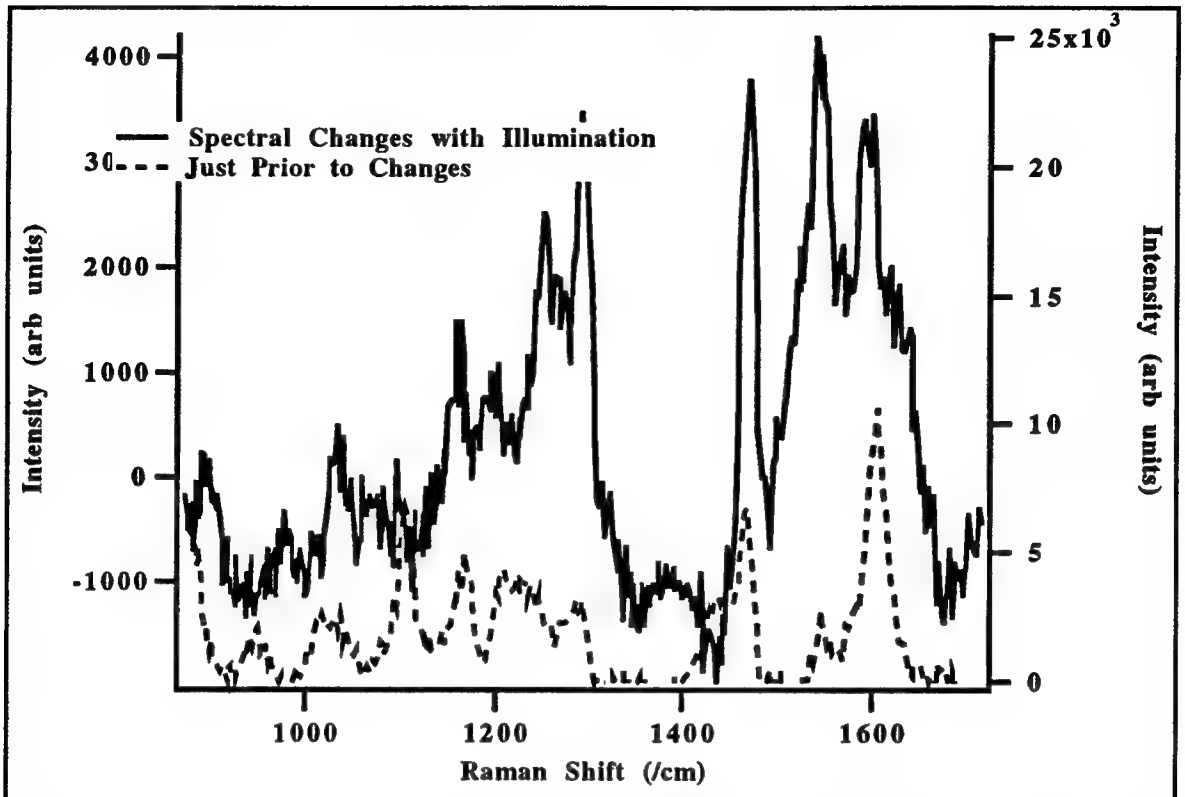

Figure 35: (dashed line) spectrum of the DER332/T-403 polymer prior to laser annealing. New peaks appear in the spectrum even prior to annealing. (solid line) difference spectrum showing approximate spectrum of "new" species observed upon annealing -- actually increased intensity of the new peaks seen before annealing.

The origin of the new features observed in the spectrum upon introduction of the Ag colloid apparently lies in surface-adsorbed DER332 which has not reacted to form part of the polymer. Figure 36 shows the same difference spectrum in Figure 35 plotted on a scale with the SERS of monomer DER332 obtained from a standard water-based colloid. These are essentially identical, given that the difference spectrum is complicated by subtle differences in fluorescence of the polymer and other heating effects.

The nature of the bonding between the DER332 and the metal surface can be deduced from the SERS spectrum. The orientation of the DER332 units on a metal surface is apparently the same whether the DER332 is in a dilute aqueous solution (we were able to observe <200 ppb DER332 in water using SERS) or at a high concentration in a polymer. The surface-enhanced effect is normally greatest for vibrational modes of the molecules which are vibrating perpendicular to the metal surface. In the case of DER332 at the metal surface, some sort of attachment to the metal is indicated by the large shifts of vibrational energies; the enhancement of out-of-

plane vibrational modes rather than the in-plane vibrations of the phenyl rings seems to indicate the molecule adsorbs to the surface via a π-bonding interaction of the aromatic electron clouds of the phenyl rings. Hence, the molecule appears to "lie flat" on the metal surface, held in place by an electrophilic attraction of the metal surface for the electrons in the π system of the DER332.

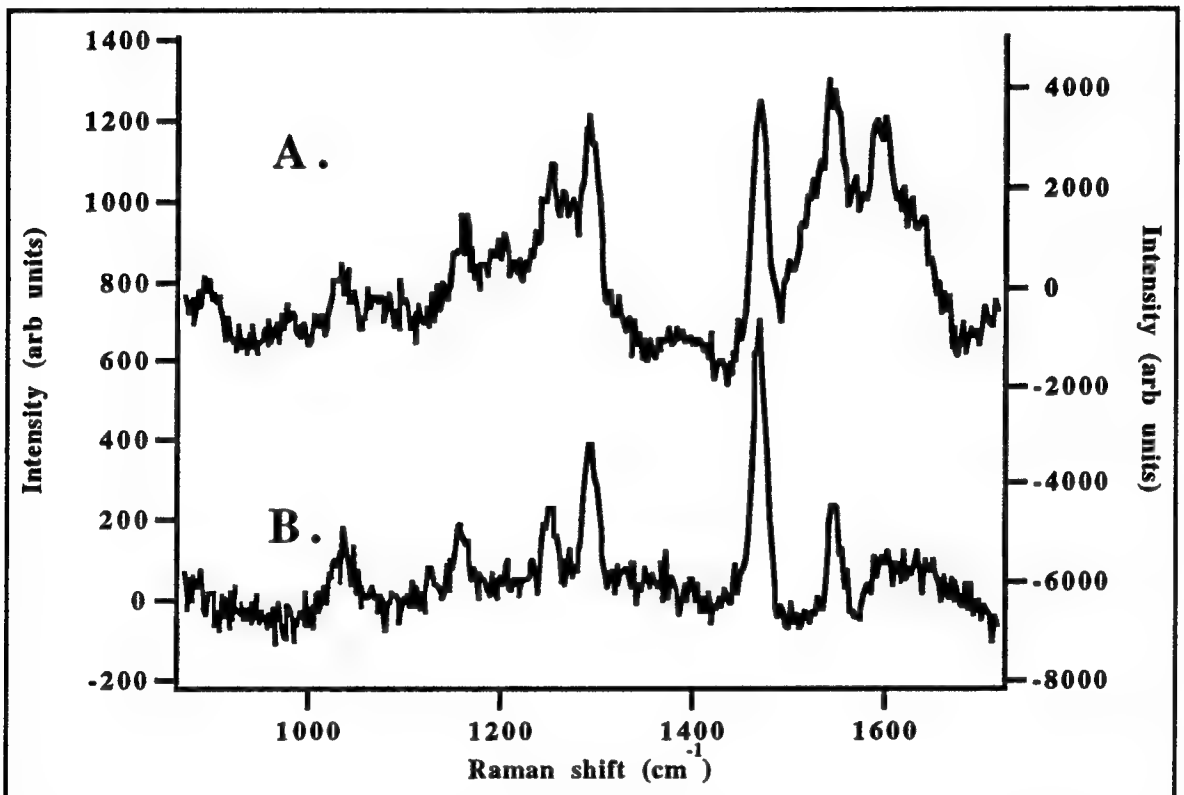

Figure 36: (A) difference spectrum shown in Figure 35. (B) SERS spectrum of 200 ppb DER332 monomer in aqueous solution using an aqueous Ag colloidal suspension.

4.C. LIST OF ALL PUBLICATIONS AND TECHNICAL REPORTS

A number of publications and presentations have resulted from this work. Publications and manuscripts in press or submitted are included as Appendices to this report.

The presentations which acknowledged ARO grant #DAAL-03-92-G-0316 are:

Fiber-Optic Raman Spectroscopy for Cure Monitoring of Advanced Polymer Composites
Myrick, M.L., Angel, S.M., Lyon, R.E., and Vess, T.M.
Proceedings of the SPE 50th Annual Technical Conference and Exhibits (Detroit, May 4-8, 1992) pp. 2052-2055.

Raman in the Real World
Myrick, M.L., Kolis, J., Parsons, E., Chike, K., Lovelace, M., Scrivens, W., Holliday, R., and Williams, M. presented at Gordon Conference on Analytical Chemistry, Hew Hampton, NH, August 11, 1993.

Raman and Near-IR Studies of the Curing of an Epoxy
M.L. Myrick, K.E. Chike, R. Lyon, S.M. Angel, and T. Vess, presented at Pittsburgh Conference, Atlanta, Ga., March 1993

Factor Analysis of Fiber-Optic Raman Spectroscopy Data From Thermoset Polymers During the Curing Process
M.K. Higgins, J.F. Aust, S.L. Morgan and M.L. Myrick, presented at Pittsburgh Conference, Atlanta, Ga., March 1993.

Remote Cure Monitoring of Polymeric Resins by Laser Raman Spectroscopy
K.C. Hong, T.M. Vess, R.E. Lyon, K.E. Chike, J.F.Aust, and M.L. Myrick
Proc. 38th Intern. SAMPE Symp. (Anaheim, CA, May 10-13, 1993), in press.

Reduction of Dimensionality Concepts for Spectroscopic and Chromatographic Data
S.L. Morgan, M. Higgins, J.F. Aust and M.L. Myrick
presented at Pittsburgh Conference, Chicago, Ill, March 1994.

A New Fiber-Optic-Interfaced Micro-Raman Spectrometer
C. Stellman, M.L. Myrick
presented at Pittsburgh Conference, Chicago, Ill, March 1994.

Variable-pathlength Cell for Thin-Film Raman Spectroscopy
K.E. Chike, M.L. Myrick
presented at Pittsburgh Conference, Chicago, Ill, March 1994.

Comparison of thin-film and evanescent Raman Spectra for an Epoxy Curing Reaction
K.E. Chike, M.L. Myrick
presented at Pittsburgh Conference, Chicago, Ill, March 1994.

New Concepts in Polymer Processing
Richard Lyon
presented at the 1994 Polymers Gordon Conference, New Hampshire. July 1994.

SERS Using an Ag Colloid in a Commercial Polymer: Interfacial Chemistry
J. Wu, M.L. Myrick
to be presented at the Pittsburgh Conference, New Orleans, LA, March 1995.

Papers and Manuscripts which Acknowledged Grant # DAAL-03-92-G-0316 are:

Raman and Near-Infrared Studies of an Epoxy Resin
Chike, K.E., Lyon, R.E., Angel, S.M., and Myrick, M.L.
Appl. Spectrosc. 47(1993), 1631.

Microwave Studies of the Curing of an Epoxy
Stellman, C., Aust, J., Myrick, M.L.
Appl. Spectrosc. (in press, 1995).

Comparison of Spectral Normalization Alternatives in Cure Reaction Monitoring via FT-Raman Spectroscopy
Aust, J.F., Booksh, K.S., and Myrick, M.L.
Anal. Chim. Acta , submitted(1995).

Design and Evaluation of a Fiber-Optic Micro-Raman Spectroscopy System for Multidimensional Chemometric Imaging
Stellman, C., Reddick, J., and Myrick, M.L.
Rev. Sci. Instrum., (submitted, 1995)

Nanofabrication of Organic Materials and Structures
J.D. Noll, C.M. Stellman, P.G. Van Patten, and M.L. Myrick
J. Vac. Sci. Tech. A (submitted, 1995)

Reduction of Spectral Imprecision Induced by Laser Mode-Hopping in Raman Spectroscopy
Booksh, K.S., Stellman, C.M., Cannon, W.J., and Myrick, M.L.
Appl. Spectrosc. (manuscript in preparation, 1995).

SERS Using an Ag Colloid in a Commercial Polymer: Interfacial Chemistry
J.L. Wu, and M.L. Myrick
(manuscript in preparation, 1995)

4.D. LIST OF ALL PARTICIPATING SCIENTIFIC PERSONNEL

The personnel involved in this research over its term are:

Dr. M.L. Myrick, PI
Dr. S.L. Morgan, Co-PI
Dr. Eric Markel, collaborator, USC-Chemical Engineering
Chris Calling, Oriel Instruments, Inc. (equipment loans)
Dr. John Cooper, post-doctoral associate
Dr. Karl Booksh, NSF Post-Doctoral Fellow
Katherine Chike, research assistant
Chris Stellman, research assistant
James Noll, research assistant
Jeffrey Aust, research assistant
Melinda Hale, research assistant
Wendy Bell, research assistant

Melinda Hale received a Ph.D. in Analytical Chemistry (S.L. Morgan, advisor) in 1994. She is currently pursuing a second degree in Statistics at USC.

Dr. Cooper is now an Assistant Professor of Chemistry at Old Dominion University, to which he moved in the Summer of 1993.

Dr. Booksh arrived at USC in August 1994, and is currently planning to stay with this research group until his NSF Post-Doctoral Fellowship expires in 1996.

Mr. Stellman and Ms. Bell are currently each in their third year of graduate studies and we anticipate their timely completion of work and graduation in 1996.

Mr. Noll and Mr. Aust are each in their fourth year of graduate studies, and we anticipate their completion of work and graduation in 1995.

5. REPORT OF INVENTIONS (BY TITLE ONLY)

1) Fiber-Optic Interfaced Micro-Spectroscopy System for Chemical Speciation and Imaging Using Multivariate Statistical Algorithms (disclosed for Patent, 1994)

2) Alignment Method for Mode-Hopped Raman Spectra (Disclosed for Patent, 1994)

6. BIBLIOGRAPHY

1) Maddams, W.F. and I.A.M. Royaud, "The Characterization of Polycyclic Aromatic Hydrocarbons by Raman spectroscopy," Spectrochim.Acta, **46A**, 309(1990).

2) Gerrard, D.L. and W.F. Maddams, "Polymer Characterization by Raman Spectroscopy," Appl.Spectrosc.Rev., **22(2&3)**, 251(1986).

3) Mertzel, E. and J.L. Koenig, "Application of FTIR and NMR to Epoxy Resins," Adv.Polym.Sci. **75**, 74(1986).

4) Lee, H. and L. Vincent "The Use of Infrared Quality Control in the Manufacture of Epoxy Resin Adhesives," Adhesives Age, Sept. 1961.

5) I. T. Jollife, "Principal Component Analysis", Springer-Verlag, New York, 1986.

6) M. Fleishman, P. Hendra, and A. McQuillan Chem.Phys.Lett. **26**,163(1974).

LIST OF APPENDICES

APPENDIX I - Raman and Near-IR Studies

Raman and Near-Infrared Studies of an Epoxy Resin

K. E. CHIKE, M. L. MYRICK,* R. E. LYON,† and S. M. ANGEL‡
University of South Carolina, Department of Chemistry and Biochemistry, Columbia, South Carolina 29208

A quantitative comparison of Raman and Fourier transform near-infrared (FT-NIR) spectroscopic techniques for the analysis of epoxy curing is performed. It is shown that the Raman technique yields a linear calibration curve much like FT-NIR. Band assignments in the Raman spectrum of diglycidyl ether of bisphenol-A (DGEBA) were performed by studying Raman spectra of smaller model compounds.

Index Headings: Analytical methods; NIR spectroscopy; Raman spectroscopy.

INTRODUCTION

Raman spectroscopy of polymeric compounds is becoming increasingly popular and successful since the advent of lasers and techniques to minimize background fluorescence.[1-3] Raman spectroscopy has been used in a wide range of applications, including the analysis of elastomers,[4] biomolecules,[5,6] synthetic polymers,[7-9] fuel mixtures,[10] advanced composites,[11] and molecular complexes.[12] This paper will focus mainly on monitoring the cure of an epoxy resin.

Epoxy resins are used widely in composite materials as adhesives, surface coatings, and fiber (carbon, polyamide, or glass) matrices. These usually involve complex mixtures of more than one epoxy resin with various hardeners, where solvents and catalysts are sometimes required for reaction.

The chemical and mechanical properties of a cured epoxy are sensitive to variations in the starting material. Mechanical properties of finished composites such as hardness show a sensitive dependence on the conditions of curing. Therefore, strict quality control is needed in the processing of an epoxy matrix. Analytical spectroscopy can meet this need by providing pertinent structural and kinetic data. The most common spectroscopic techniques employed to date exploit Fourier transform infrared (FT-IR)[13-16] and near-infrared (NIR) absorption.[17,18]

Characterization of polymers and epoxy resins can be achieved by NIR spectroscopy. This absorption method can analyze uncured bulk samples and raw materials without the need for extensive sample preparation, and samples can be monitored in a rapid and nondestructive manner. However, the NIR spectral region only provides the absorptivities of combination and overtone bands of higher-frequency fundamental vibrations. Since polymers possess an abundance of active vibrational combination and overtone bands, band overlap complicates spectra, though quantitative NIR for the cure of an epoxy resin has been reported.[18]

Although Raman spectroscopy of polymers and epoxy resins is a recognized analytical technique,[7-9,19,20] applications in cure monitoring have been slow to follow. Recent literature reports have investigated Raman spectroscopy as a quantitative tool.[10,21-24] However, obtaining consistent measurements is difficult because the intensity and frequency reproducibility of the Raman bands are dependent on instrumental parameters such as laser power, excitation frequency, detector response, and sample volume and alignment. These instrumental factors make it difficult to obtain reproducible spectra. One effective method for correcting most of these instrumental factors is to employ internal standards.

The object of this report is to demonstrate a linear correlation between the epoxide concentration and its Raman response utilizing Fourier transform Raman (FTR) spectroscopy, which is similar to that obtained by quantitative FT-NIR.

EXPERIMENTAL

Diglycidyl ether of bisphenol-A (DGEBA or DER 332, Dow Chemical) at 99% purity was degassed to remove excess moisture and trapped gases. Then a stoichiometric amount of diethylamine (DEA, Aldrich, 99%) was combined with DGEBA (epoxy equivalent weight = 173 g; amine hydrogen equivalent weight = 73.14 g) in a 250-mL round-bottom flask to form an end-capped molecule which mimicked a cured epoxy (i.e., DGEBA with an amine hardener). The flask was purged with nitrogen, sealed, and heated to 50°C. The viscosity of the product was low due to the absence of cross-linking reactions. The final product was mixed in 10% (w/w) increments with neat DGEBA to form a calibration curve of known epoxide concentration.

A Perkin-Elmer 1600 Series Fourier transform infrared spectrometer with a thermoelectrically cooled detector was used to acquire the NIR spectra. The DGEBA/DEA final product, termed 0% DGEBA/DEA, was heated to reduce its viscosity and mixed with the appropriate amounts of neat DGEBA, and then the samples were placed between two 1.00-mm-thickness glass microscope slides with a 1.00-mm aluminum spacer. Six sets of samples for each concentration were prepared and inserted into the spectrometer, and approximately five minutes were allowed to elapse before spectra were taken (16 scans at 4 cm^{-1} resolution) to allow the sample compartment to be purged with N_2 and to stabilize.

Quantitative FT-NIR and FTR were performed on the DGEBA/DEA stock solutions, ranging from 0% DGEBA/DEA to 100% or neat DGEBA in 10% (w/w) increments. These stock solutions of the DGEBA/DEA

Received 19 February 1993; revision received 23 April 1993.
* Author to whom correspondence should be sent.
† Present address: Federal Aviation Administration Technical Center, Atlantic City International Airport, NJ 08405.
‡ Present address: Lawrence Livermore National Laboratory, P.O. Box 808, L-524, Livermore, CA 94550.

0003-7028/93/4710-1631$2.00/0

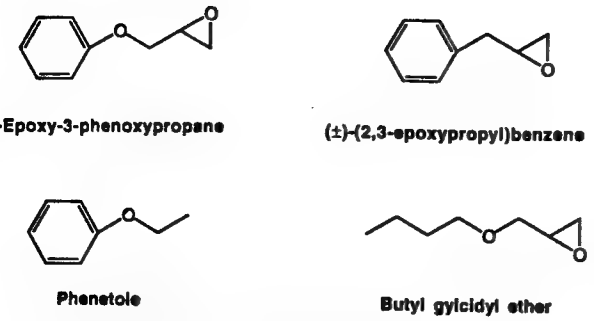

FIG. 1. Molecular structures of model compounds.

mixtures were prepared and analyzed first by the FT-IR in the NIR region. Due to fluctuations of the baseline, a corrected absorbance was calculated for the epoxide band according to the method of Dannenberg.[17]

The FT-Raman studies were performed with a Perkin-Elmer FT-Raman 1700X series spectrometer with an InGaAs detector. Six samples for each concentration were prepared by weighing each component into 3-g glass vials. Then the mixtures were heated to reduce the viscosity. The samples were analyzed with the use of a Nd:YAG laser operating at 1.00 W of power with 32 scans at 4 cm^{-1} resolution. As with the FT-NIR studies, corrected intensities were calculated with the use of the baseline method for the peaks of interest. This method is similar to that used by Dannenberg,[17] whereby the intensities and wavenumbers at either side of the epoxide frequency in the FTR spectra were recorded and a straight line was plotted. Then the intensity at the baseline of the epoxide band was extrapolated according to its frequency. This correction factor was then subtracted from the observed intensity of the epoxide band to yield the corrected intensity. An internal reference was also utilized to account for instrumental parameters and for variations in sample volume and alignment by calculating Raman peak ratios.

Mid-infrared (MIR) spectra of DGEBA, DEA, and the DGEBA/DEA samples were collected with a Fourier transform MIR spectrometer with a DTGS detector by Mattson Polaris (Model Number IR-10410). The samples were placed between two NaCl plates, and a total of 16 scans at 4 cm^{-1} resolution for each sample were taken.

Butyl glycidyl ether (98%), phenetole (99%), (±)-(2,3-epoxypropyl)benzene (98%), and (±)-1,2-epoxy-3-phenoxypropane (99%) (Fig. 1) were obtained from Aldrich Chemical Company, and were used as model compounds for FT-NIR and Raman studies without any further purification.

TABLE I. Tentative band assignments in the NIR region.

NIR (cm^{-1})	Assignment
4167	Combination bands of the terminal methylene group[a,b]
4348	Combination bands of the aliphatic methyl group[a]
4525	Combination band of the second overtone of the C-O fundamental stretch (~900 cm^{-1}) with the fundamental C-H stretch (~2725 cm^{-1})[c]
4680, 4622	Combination band of the aromatic conjugated C=C stretch (~1625 cm^{-1}) with the aromatic C-H fundamental stretch (~3050 cm^{-1})[b,c]
5970	Phenyl C-H stretching overtone band[b,d]
6052	First overtone of the terminal (methylene) C-H fundamental stretching vibration[a]

[a] Reference 25.
[b] Reference 18.
[c] This paper.
[d] Reference 17.

TABLE II. NIR band comparison of neat DGEBA with the model compounds. EPP: (±)-1,2-epoxy-3-phenoxypropane; EPB: (±)-(2,3-epoxypropyl)benzene, PHE: phenetole; BGE: butyl gylcidyl ether.[a]

	NIR bands (cm^{-1})						
Compound	4167	4348	4525	4680	4622	5970	6052
DGEBA	P	P	P	P	P	P	P
EPP	P	P	P	P	P	P	P
EPB	P	P	P	P	P	P	P
PHE	A	P	A	P	P	P	A
BGE	P	P	P	A	A	A	P

[a] P = Band present in spectrum; A = band absent in spectrum.

RESULTS AND DISCUSSION

Detailed NIR characterization of DGEBA and other compounds possessing terminal epoxides have been reported previously.[17,25] By analyzing model compounds with an FT-NIR spectrometer, we made some additional band assignments. The NIR spectra of butyl glycidyl ether, phenetole, (±)-(2,3-epoxypropyl)benzene, and (±)-1,2-epoxy-3-phenoxypropane were employed to identify some of the peaks present in the NIR spectrum of DGEBA. Tentative band assignments and the corresponding NIR frequencies are listed in Table I. A summary for the FT-NIR spectral comparison of DGEBA with the model compounds is listed in Table II.

The chemical structures of DGEBA and the final product are depicted in Fig. 2. FT-NIR spectra were obtained on the starting materials and the final product. Figure 3 illustrates the decreasing intensity of the 4525-cm^{-1} band as a function of the lessening concentration of the epoxide. A calibration curve for the analysis of the NIR response with respect to the epoxide concentrations in the DGEBA/DEA mixtures gave a linear plot when the frequency at 4525 cm^{-1} was examined. Figure 4 illustrates the linearity achieved when the DGEBA/DEA solutions were examined by the FT-NIR spectrometer. The error bars depict a 95% confidence interval (CI) in the NIR calibration curve. The CIs for the FT-NIR and FTR

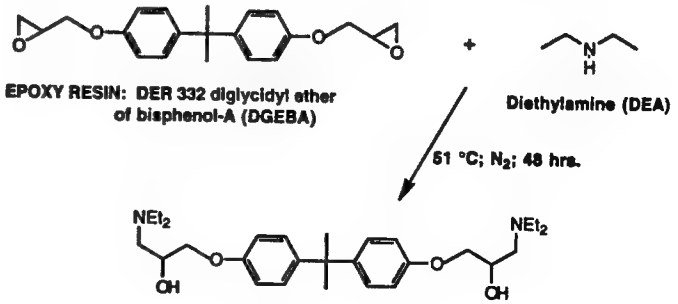

FIG. 2. Chemical structures of DGEBA and final product.

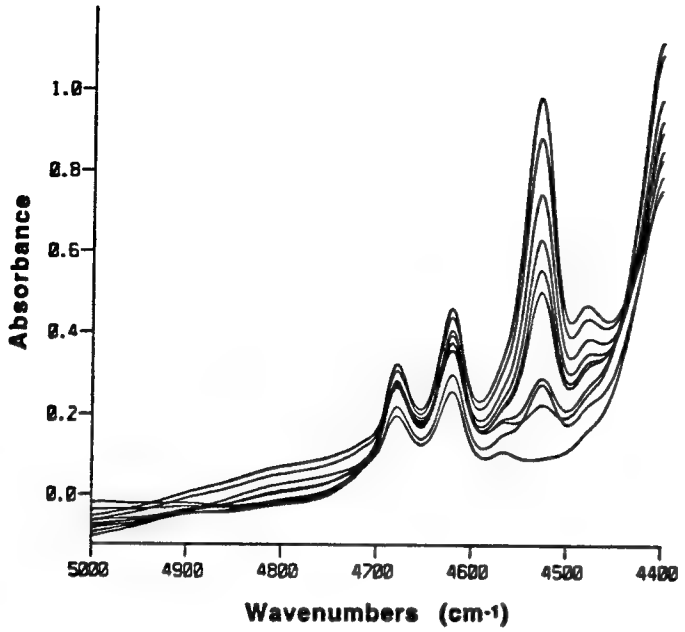

FIG. 3. FT-NIR spectra of the DGEBA/DEA concentration series. Epoxide concentration ranges from pure DGEBA (top) to pure DGEBA/DEA adduct (bottom). The 40% (w/w) DGEBA/DEA is omitted due to limitations in computer software.

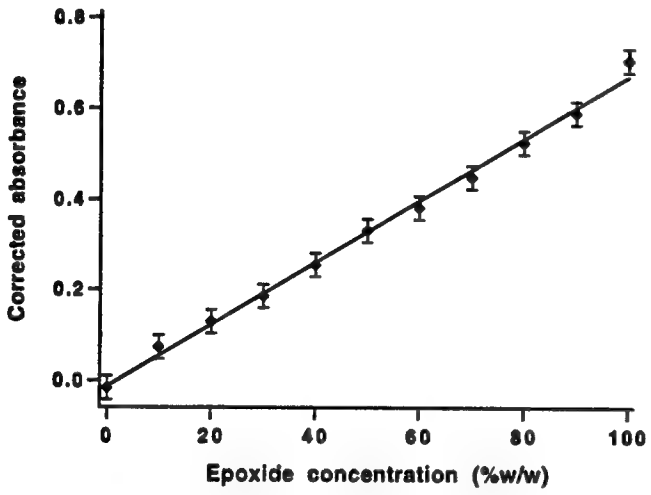

FIG. 4. FT-NIR calibration curve of DGEBA/DEA.

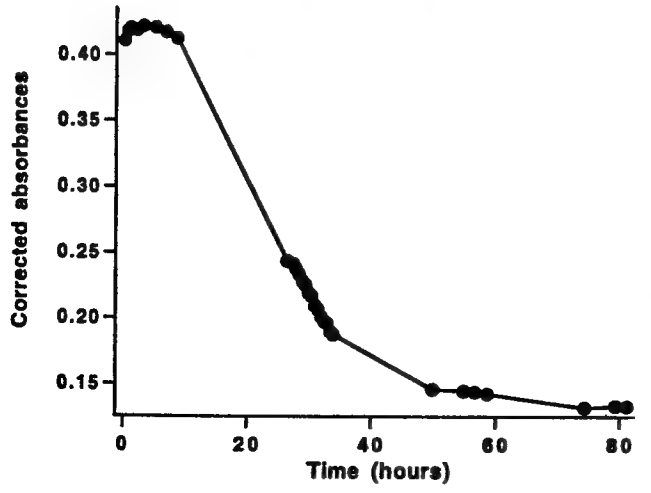

FIG. 5. Stability plot of 70% (w/w) DGEBA/DEA solution.

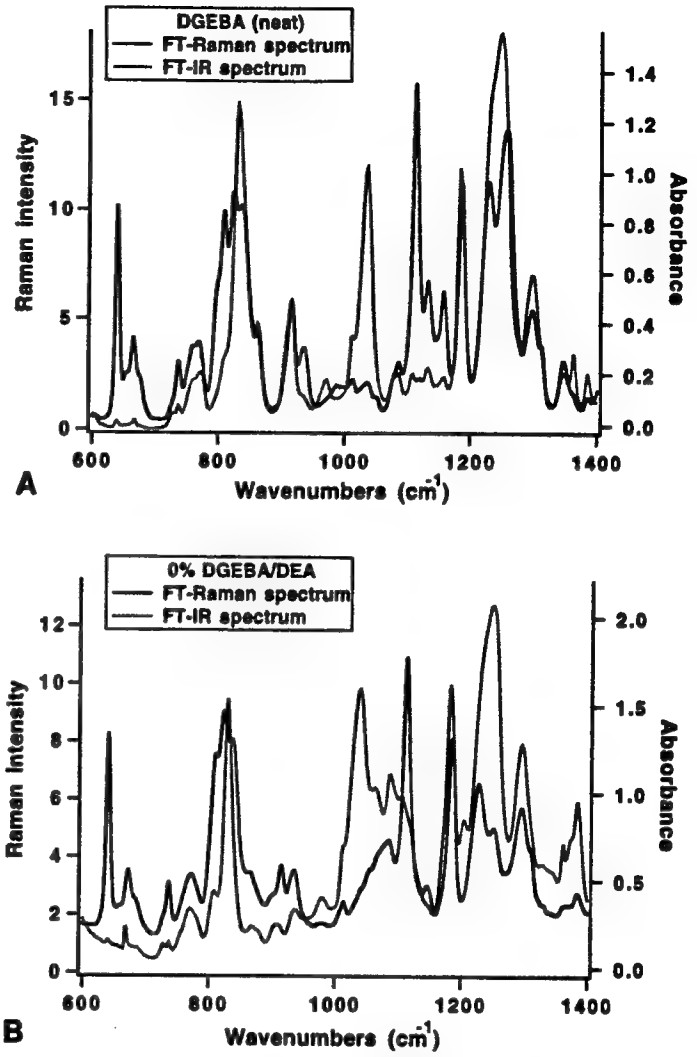

FIG. 6. (A) Mid-IR vs. Raman spectra (noncorrected background) of neat DGEBA. (B) Mid-IR vs. Raman (background corrected) spectra of 0% DER 332/DEA.

studies represent the deviation of the six samples of each concentration. In addition, no volume corrections for the sample mixtures were made.

A 70% (w/w) sample of DGEBA/DEA was prepared and its corrected absorbance was recorded for approximately 80 hours. After approximately 6 h the absorbance of the epoxide band began to decrease rapidly (Fig. 5), suggesting that a homopolymerization reaction catalyzed by the formation of a tertiary amine is occurring between the 0% DGEBA/DEA solution and the added neat DGEBA. In an effort to avoid chemical degradation of the epoxide functionality during examination, the DGEBA/DEA samples are prepared and studied within approximately five hours.

The interpretation of both Raman and infrared spectra requires knowledge of the structural origins of the vibrational bands which are present. Although quality spectra of an epoxy resin, both mid-IR and Raman, may be acquired (Fig. 6), complete band assignments are difficult to perform due to the complexity of these spectra. With the aid of previous Raman characterization of DGEBA,[19,20,26] use of both Raman and MIR spectra from the model compounds, normal mode calculations, and

TABLE III. Infrared and Raman band assignments for DGEBA. Note: s = strong; m = medium; w = weak; vw = very weak; sh = shoulder; str = stretch; and def = deformation.

IR	Raman	Assignments
1298 m	1272 w	C-O str. (ether groups)[a]
1248 s	—	C-O str. (ether groups) and C-C str.[a,b]
—	1232 s	C-O str. and phenolic C_4-O_2 str.[b]
—	1211 s	Epoxy group?
1184 s	1186 s	CH_3/gem-dimethyl def. and C_6-$C_{7/8}$ str.[a,b]
—	1113 s	Aromatic C-H str. and in-plane def.[a-d]
1065 vw	—	Phenolic C_4-O_2 str.[a]
1036 s	—	Substituted aromatic[a,d,e]
1010 sh	—	Substituted aromatic[a,d,e]
916 m	924 sh	Epoxy group[a,b,e]
862 sh	908 m	Epoxy group[a,b,e]
806 s	819 s	Substituted aromatic[a,d,e]
772 m	762 m	C_3-C_2 skeletal[b]
—	736 sh	C_3-C_2 skeletal[b]
—	667 m	Aromatic C-H out-of-plane def.[c,d,e]
—	641 s	Aromatic C-H out-of-plane def.[c,d,e]

[a] Reference 26.
[b] This paper.
[c] Reference 19.
[d] Reference 20.
[e] Reference 16.

comparison with the MIR[13-16,26] spectra of DGEBA, some additional assignments have been made for DGEBA and are listed in Table III. Note this is not a complete assignment of bands because the spectral range only covers the 600–1350 cm^{-1} region in the Raman spectra.

The peak assigned to epoxide-stretching is at approximately 1240 cm^{-1} in the Raman spectrum of DGEBA. As illustrated by the Raman spectra in Fig. 7, this peak is part of unresolved bands. The Raman peak at 1220 cm^{-1} is thought to be due to the fundamental Φ-O-C phenolic stretch. This assignment was deduced by examining the Raman spectrum of phenetole, which contains a peak at approximately the same frequency. Moreover, phenetole possesses a small peak at approximately 1240 cm^{-1}, and this may indicate that another overlapping peak is present in the DGEBA spectrum. These

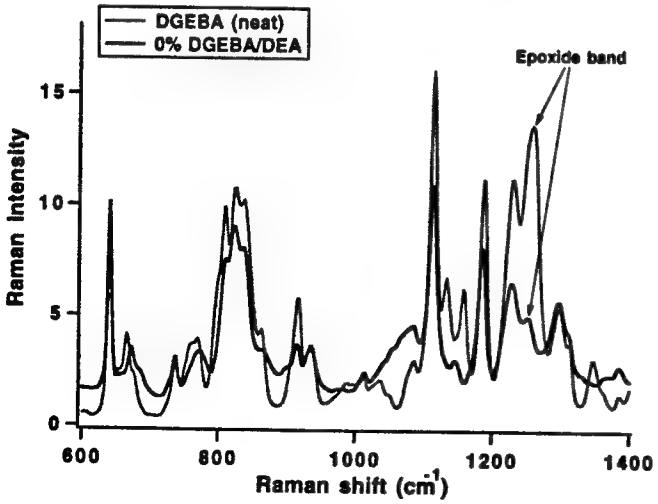

FIG. 7. Raman spectra of DGEBA (neat) and DGEBA/DEA reaction product.

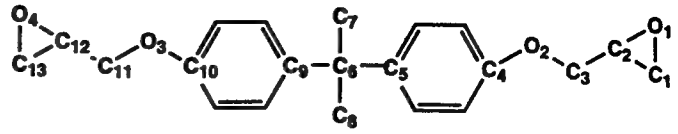

FIG. 8. Atomic labeling of DGEBA.

phenolic stretches may be the reason why the 1240-cm^{-1} band does not apparently disappear completely in the Raman spectrum of 0% DGEBA/DEA. However, since the phenolic vibrations do not change during the cure, they should not mask the relative intensity changes in the C_1-O_1-C_2 (see Fig. 8 for atomic labels) epoxy peak of interest.

To normalize spectra in the FTR studies, we chose a reference band. For this purpose, the in-plane deformation of the gem-dimethyl group of DGEBA at 1186 cm^{-1} was selected. This assignment was made by comparing Raman spectra of the model compounds with that of the neat DGEBA. In addition, it was deduced that the aromatic ring mode is located at approximately 1113 cm^{-1}. The intensity of neither one of these vibrations changes during the reaction of DGEBA with DEA and thus could be used interchangeably as the reference band. Nevertheless, the peak at 1186 cm^{-1} was chosen in this study, and a calibration plot resulted which appears to be very similar to that of the FT-NIR calibration plot obtained (Fig. 9).

It is apparent from Fig. 9 that the reproducibility for the six sets of samples of each concentration is better in the FTR curve than the FT-NIR. Variations in sample cell pathlength and positioning in the FT-NIR spectrometer are the most likely causes for the fluctuation in the observed absorbances.

CONCLUSION

The comparison of FTR with FT-NIR is excellent and consistent, which confirms that quantitative Raman is possible on an epoxy resin. Additional studies are needed

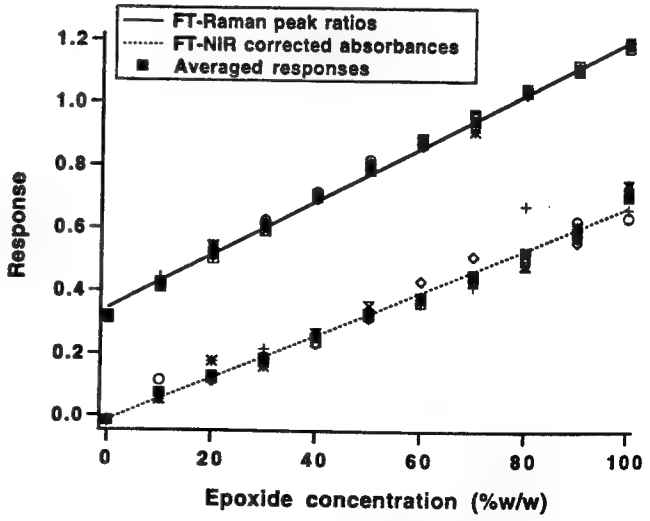

FIG. 9. Comparison of FT-NIR and FTR correlation curves. The responses from the six samples of each concentration are plotted against their respective epoxide concentration. An average response and linear curve fit were also calculated and plotted.

to extend Raman band assignments and to examine the quantitative capabilities on the actual cure of an epoxy matrix. Nevertheless, previous literature[21-24] has demonstrated that the reproducibility of these curves is sufficient for quantitative analysis of curing. Studies are now in progress to improve the aforementioned difficulties and to test the quantitative capabilities of Raman spectroscopy on actual epoxy matrices (e.g., DGEBA with Jeffamine T-403, a polyoxypropylene triamine hardener).

ACKNOWLEDGMENTS

M.L.M. and K.E.C. gratefully acknowledge the Army Research Office (Grant Number DAAL03-92-G-0316) for support of this work. They especially thank Dr. Edward S. Chen (ARO) for his interest and encouragement. R.E.L., S.M.A., and K.E.C. thank the Department of Energy and Lawrence Livermore National Laboratory (LLNL) (Contract Number W-7405-ENG-48) for supporting part of this research. For technical advice and supervision, the authors thank Dr. Thomas Vess (LLNL) and Dr. Eric Markel (USC). For additional normal mode calculations of model compounds, DGEBA, and DGEBA/DEA, we thank Dr. Fred Wolters of Clorox Corporation, Pleasanton, California.

1. M. L. Myrick and S. M. Angel, Appl. Spectrosc. **44**, 565 (1990).
2. D. L. Gerrard and J. Birnie, Anal. Chem. **64**, 502R (1992).
3. P. J. Hendra, G. Ellis, and D. J. Cutler, J. Raman Spectrosc. **19**, 413 (1988).
4. K. D. O. Jackson, M. J. R. Loadman, C. H. Jones, and G. Ellis, Spectrochim. Acta **46A**, 217 (1990).
5. J. J. Baraga, M. S. Feld, and R. P. Rava, Appl. Spectrosc. **46**, 187 (1992).
6. E. N. Lewis, V. F. Kalasinsky, and I. W. Levin, Anal. Chem. **60**, 2658 (1988).
7. S. Chadha, E. Ghiamati, R. Manoharan, and W. H. Nelson, Appl. Spectrosc. **46**, 1176 (1992).
8. J. K. Agbenyega, G. Ellis, P. J. Hendra, W. F. Maddams, C. Passingham, H. A. Willis, and J. Chalmers, Spectrochim. Acta **46A**, 197 (1990).
9. J. L. Koenig, Appl. Spectrosc. Rev. **4(2)**, 233 (1971).
10. M. B. Seasholtz, D. D. Archibald, A. Lorber, and B. R. Kowalski, Appl. Spectrosc. **43**, 1067 (1989).
11. S. F. Parker, S. M. Mason, and K. P. J. Williams, Spectrochim. Acta **46A**, 315 (1990).
12. S. M. Angel and M. L. Myrick, Anal. Chem. **61**, 1648 (1989).
13. W. R. Moser, J. R. Berard, P. J. Melling, and R. J. Burger, Appl. Spectrosc. **46**, 1105 (1992).
14. D. A. C. Compton, S. L. Hill, N. A. Wright, M. A. Druy, J. Piche, W. A. Stevenson, and D. W. Vidrine, Appl. Spectrosc. **42**, 972 (1988).
15. K. C. Cole, A. Pilon, D. Noel, J. J. Hechler, A. Chouliotis, and K. C. Overbury, Appl. Spectrosc. **42**, 761 (1988).
16. H. Lee and L. Vincent, Adhesives Age, Sept. (1961).
17. H. Dannenberg, SPE Transactions **3**, 78 (1963).
18. Charles E. Miller, Appl. Spectrosc. Rev. **26A**, 277 (1991).
19. W. F. Maddams and I. A. M. Royaud, Spectrochim. Acta **46A**, 309 (1990).
20. D. L. Gerrad and W. F. Maddams, Appl. Spectrosc. Rev. **22(2&3)**, 251 (1986).
21. T. Jawhari, P. J. Hendra, H. A. Willis, and M. Judkins, Spectrochim. Acta **46A**, 161 (1990).
22. K. P. J. Williams and S. M. Mason, Spectrochim. Acta **46A**, 187 (1990).
23. T. J. Vickers, C. K. Mann, J. Zhu, and C. K. Chong, Appl. Spectrosc. Rev. **26(4)**, 341 (1991).
24. C. D. Newman, G. G. Bret, and R. L. McCreery, Appl. Spectrosc. **46**, 262 (1992).
25. R. F. Goddu and D. A. Delker, Anal. Chem. **30**, 2013 (1958).
26. E. Mertzel and J. L. Koenig, Advances Polym. Sci. **75**, 74 (1986).

APPENDIX II - Comparison of Spectral Normalization

Effects of Spectral Normalization Alternatives on Qualitative Analysis with Raman Spectroscopy

Jeffrey F. Aust, Karl S. Booksh, and M. L. Myrick*

Department of Chemistry and Biochemistry

The University of South Carolina

Columbia, SC 29208

Abstract

The effect of different spectral normalization alternatives is discussed and applied to monitoring of a polymer curing process by FT-Raman. It is shown that for qualitative applications is in not critical that the spectra be normalized to immutable reference bands.

Introduction

Normalization of Raman spectra to the intensity of a reference peak or peaks is employed to remove unwanted variance resulting from changes in sampling size or efficiency between measurements. Therefore, the precision and accuracy of quantitative analysis employing Raman spectroscopy often depends upon the choice of Raman bands used for spectral normalization. In analytical applications of Raman spectrometry, much mental effort is expended to determine the proper Raman band or bands used for spectral normalization. The normalization bands are usually chosen for their intrinsic lack of variation between samples of different composition. For example, when monitoring the curing of a polymer by Raman spectroscopy, bands that are relatively cure insensitive are traditionally chosen for normalization. This selection is easy when the reaction mechanism and products are known, but may be quite difficult with out such *a priori* knowledge. Furthermore, in some applications, no such invariant internal reference band exists.

In many applications the quality of analysis is not contingent on the choice of normalization bands. The importance of normalization peak selection begs the question: What are the goals of analysis? If the aim of analysis is to construct a quantitative model for prediction with future unknown samples, then, yes, the selection of the normalization peak is very crucial in affecting the outcome of analysis. However, for non-quantitative applications, such as process monitoring and sample classification, the choice of normalization bands is often not critical. Examples of such applications include the monitoring of a polymer curing and the determination of ownership of aqueous petroleum discharge based on relative organic concentrations.

Orthogonal projection methods, in particular principal component analysis, are popular for analyzing multivariate data.[1] Here the data is reduced from a high dimensional space, equal to the number of measurements, to a lower dimensional sub-space. This sub-space is of the minimal dimensionally that contains all spectral variation resultant from changes in chemical content among the samples. The location of each sample in this sub-space is indicative of the sample's chemical content. This method of data analysis has advantages of simultaneous multiple analyte analysis, signal averaging, enhanced outlier detection, and ease of data visualization.

However, the presence of unwanted variance in the Raman data stemming from changes in laser intensity or sampling efficiency degrade the quality of analysis. Fortunately, the effects of these variations

can be minimized by spectral normalization. In this letter it is discussed by way of a brief mathematical discussion and illustrative example the influence normalization band selection has on analysis of Raman data. It is shown that with multivariate analysis the choice of normalization bands does not influence the rank (dimensionality) of the model used to describe the spectral information present in the data set. That is, information is neither lost or gained by judicious or injudicious choice of normalization bands. Only the distribution of the data within the multidimensional space defined by the model changes with choice of normalization bands. This distribution, while critical in quantitative analysis, is of lesser consequence in qualitative applications.

Discussion

The choice of normalization band does not alter the rank of the model, only the distribution of the samples in the multidimensional space defined by the model is transformed. This is evident when considering the effect of normalization on a generalized four band spectrum of a mixture with two components varying in concentration,

$$\mathbf{r}_i = \gamma_i \left[\alpha_1 a_i \quad \alpha_2 b_i \quad \alpha_3 a_i + \alpha_4 b_i \quad 1\right]^T \qquad (1)$$

where a_i and b_i are the concentrations of two components in the i^{th} sample, the αs are relative Raman scattering efficiencies and γ_i is the relative sampling efficiency for the i^{th} sample. Here the intensity of the first band is proportional only to the concentration of compound A, while the second is similarly related to compound B's concentration. The third band is a linear combination of a and b, and the fourth band is independent of both A and B.

Table 1, row 1 presents the generalized spectrum in equation 1 normalized to the ideal reference band (band 4), the band related to only compound A (band 1), and the band related to both compound A and B (band 3). For each normalization method, the spectrum of any sample lies in a two dimensional sub-space parallel to the plane defined by the vectors in row 2. If the vectors in row two are translated to originate at the location of any sample in the four dimensional space defined by the normalized data (e.g. w = $\alpha_1 a$, x=

$\alpha_2 b$, y= $\alpha_3 a + \alpha_4 b$, z=1), all the samples, and the principal components derived from principal component analysis, would then lie in the plane defined by the these two vectors. Hence normalization does not change the rank of the model used to describe the spectral variation.

Rows 3 and 4 of table 1 show the change in location of a sample in the four dimensional spectral space with respect to changes in component concentrations. With normalization to an inherently stable reference band, the samples are uniformly distributed about the spectral space. Since $\delta r/\delta a$ and $\delta r/\delta b$ are independent of a and b, samples that differ by x units of concentration will be separated by y units of spectral distance regardless of the absolute component concentrations. The other normalization options perform a nonlinear transformation on the distribution of samples. When the spectra are normalized to the band proportional to compound A, changes in the normalized spectra resultant from changes in the concentration of A are greater for small a and large b than for large a and small b. Normalizing to a band that is a product of both A and B produces changes in **r**, associated with changes in a or b, that are dependent on both a and b.

The transformation of the sample distribution by normalization can best be observed in actual principal component plots. To highlight this, 80 samples based in a 8x10 blocked experimental design were constructed based on equation 1 where $\alpha_1 = 1$, $\alpha_2 = 10$, $\alpha_3 = 1.5$, α_4=3, a varied uniformly from 1 to 10, b from 1 to 8, and γ_i was randomly selected from a uniform distribution ranging from 0.9 to 1.1. Also presented are the spectra normalized to unit area. This option was not presented in table 1 due to the cumbersome size of the algebraic notation associated with its derivatives and principal component spaces. For a linear transformation of the samples, the form of the experimental design should be reproduced in the lower dimensional space defined by the principal components. This is indeed seen in figure 1a where the spectra are normalized relative to an inherently constant spectral band. When the spectra are normalized to a band that changes with respect to component concentration (Figures 1b and 1c) or when the spectra are normalized to unit area (Figure 1d) the distribution of the experimental design is distorted in the spectral space.

Johansson *et al.* note the change of sample distribution in the principal component plots brought by normalization, but, offering only a warning, include no practical insights of use to analytical chemists who

are forced to normalize their spectra.[2] It is important to note that any apparent localized gains or losses in sensitivity in the principal component plots are offset by equivalent scale reducing or enlarging transformations applied to the spectral noise during normalization. Therefore, provided that the chemist is aware of the potential distortion of the between sample distances in the principal component plots induced by the transformations, no interpretability or utility of the plots are lost by "incorrect" spectral band normalization choice.

Results

The change in the distribution of the samples along the principal components is evident in the following re-analysis of data from a polymer curing process monitored by FT-Raman spectroscopy. Here twenty-four Ciba-Geigy Matrimid® 5292 samples are analyzed to monitor the percent cure. The question arises of which Raman bands are cure independent and hence "ideal" for normalization. In the original work the 1638 cm^{-1} band was chosen based on a Michael-type addition reaction mechnism between methylene dianiline bismaleimide (component A) and O,O'-diallyl bisphenol A (component B)(Figure 2a).[3] An alternative mechanism suggests that this band changes with cure percentage. The polyimide reaction is actually more complex and is believed to involve Ene, Diels-Alder, and isomerization reactions (Figure 2b).[4] The revised mechanism suggests that different bands, e.g. 1515 cm^{-1} or 1610 cm^{-1}, are "ideal" for normalization because the functional group responsible for these vibrations are conserved in the mechanism.

For illustrative purposes, four normalization alternatives have been chosen for presentation. Normalization to 1515 cm^{-1} was suggested by the currently accepted mechanism. Peaks at 1773 cm^{-1} and 1161 cm^{-1} were chosen as "non-ideal" normalization choices. The 1773 cm^{-1} band dramatically decreases in intensity with cure percent while the 1161 cm^{-1} band increases with curing. The fourth alternative presented is normalization of each Raman spectrum to unit area.

The effects of these four normalization methods are shown in figure 3. As expected normalization to the 1773 cm^{-1} band increases the sensitivity in the principal component plot at high cure percentages since, as the band intensity decreases, the total intensity of the normalized spectra increase. Similarly, normalization to the 1161 cm^{-1} Raman band results in increased sensitivity at low cure percentages. Note

that the samples normalized to 1773 cm^{-1} show relatively little change in position along the first principal component between 0% and 60% reacted compared to the samples when normalized to the 1161 cm^{-1} band. Concurrently, the samples normalized to 1773 cm^{-1} demonstrate a larger change in position along the first principal component between 60% and 70% cured than does the samples normalized to 1161 cm^{-1}. Normalization to the immutable 1515 cm^{-1} band or normalization to unit area spawn no localized inhomogenaities of sensitivities in the principal component plots. Note that the samples normalized to 1515 cm^{-1} and unit area lie between the samples subjected to the other normalization alternatives at both high and low cure percentages. With normalization to unit area, the localized sensitivity changes stemming from changes decreases in Raman bands are partially offset by increases in other Raman bands. Therefore, the net result is a more uniform sensitivity in the principal component plots than is seen with normalization to the "mercurial" 1773 cm^{-1} or 1161 cm^{-1} bands.

Conclusions

Although the choice of normalization bands is not critical for effective qualitative analysis via Raman spectroscopy, these conclusions should not be generalized to all quantitative applications. Here both the distribution of samples in the principal component space and distribution of instrumental errors after normalization heavily influence the precision and accuracy of results from the quantitative model. Unfortunate selection of normalization band for quantitative analysis could: a) necessitate a complex nonlinear model for analysis instead of a simple linear one, or b) result in heteroscadastic instrumental errors that violate the assumption of identically distributed errors for all samples that is implied for most common statistical methods.

Acknowledgments

Support for this work was provided by the Office of Naval Research (ONR) grant number N00014-92-J-183. J. F. A. and M. L. M. gratefully acknowledge Dr. Kenneth J. Wynne of ONR for his interest and support. K. S. B. received support from a National Science Foundation Postdoctoral Fellowship (CHE-9403179).

Bibliography

1. S. D. Brown, T. B. Blank, S. T. Sum, and L. G. Weyer, *Anal. Chem.* **66**, 315R (1994).

2. E. Johansson, S. Wold, and K. Sjodin, *Anal. Chem.* **56** 1685 (1984).

3. J. F. Aust, M. K. Higgins, P. Groner, S. L. Morgan, and M. L. Myrick, *Anal. Chim. Acta* **293** 119 (1994).

4. J. J. King, M. A.Chaudari, and S. A. Zahir, Proceedings of the 29th National SAMPE Conferrence (1984).

Table 1: Comparison of three normalization alternatives

Normalized by:	Reference Band	Component A Band	Overlapping A-B Band
Generalized Response	$\begin{bmatrix} \alpha_1 a \\ \alpha_2 b \\ \alpha_3 a + \alpha_4 b \\ 1 \end{bmatrix}$	$\begin{bmatrix} \alpha_1 a/\alpha_1 a \\ \alpha_2 b/\alpha_1 a \\ (\alpha_3 a + \alpha_4 b)/\alpha_1 a \\ 1/\alpha_1 a \end{bmatrix}$	$\begin{bmatrix} \alpha_1 a/(\alpha_3 a + \alpha_4 b) \\ \alpha_2 b/(\alpha_3 a + \alpha_4 b) \\ (\alpha_3 a + \alpha_4 b)/(\alpha_3 a + \alpha_4 b) \\ 1/(\alpha_3 a + \alpha_4 b) \end{bmatrix}$
PC Space[b]	$\begin{bmatrix} -2\alpha_1 & \alpha_3 \\ \alpha_2 & -2\alpha_2 \\ -2\alpha_3 + \alpha_4 & \alpha_3 - 2\alpha_4 \\ 0 & 0 \end{bmatrix}$	$\begin{bmatrix} 0 & 0 \\ -1 & \alpha_2 \\ -6\alpha_3 + 6\alpha_4 & 3\alpha_4 \\ 1 & 0 \end{bmatrix}$	$\begin{bmatrix} \alpha_1\alpha_3\alpha_4 & \alpha_1\alpha_4^2 \\ -\alpha_2\alpha_3^2 & -\alpha_2\alpha_3\alpha_4 \\ 0 & 0 \\ \alpha_3^2 + \alpha_4 - \alpha_3\alpha_4 & \alpha_4^2 + \alpha_3 - \alpha_3\alpha_4 \end{bmatrix}$
$\delta R/\delta a$ [c]	$\begin{bmatrix} \alpha_1 \\ 0 \\ \alpha_3 \\ 0 \end{bmatrix}$	$\begin{bmatrix} 0 \\ -\alpha_2 b/\alpha_1 a^2 \\ -\alpha_4 b/\alpha_1 a^2 \\ -1/\alpha_1 a^2 \end{bmatrix}$	$\begin{bmatrix} \alpha_1/(\alpha_3 a + \alpha_4 b) - (\alpha_1\alpha_3 a)/(\alpha_3 a + \alpha_4 b)^2 \\ -(\alpha_2\alpha_3 a)/(\alpha_3 a + \alpha_4 b)^2 \\ 0 \\ \alpha_3/(\alpha_3 a + \alpha_4 b)^2 \end{bmatrix}$
$\delta R/\delta b$ [d]	$\begin{bmatrix} 0 \\ \alpha_2 \\ \alpha_4 \\ 0 \end{bmatrix}$	$\begin{bmatrix} 0 \\ \alpha_2/\alpha_1 a \\ \alpha_4/\alpha_1 a \\ 0 \end{bmatrix}$	$\begin{bmatrix} -(\alpha_1\alpha_4 b)/(\alpha_3 a + \alpha_4 b)^2 \\ \alpha_2/(\alpha_3 a + \alpha_4 b) - (\alpha_2\alpha_4 b)/(\alpha_3 a + \alpha_4 b)^2 \\ 0 \\ \alpha_4/(\alpha_3 a + \alpha_4 b)^2 \end{bmatrix}$

a. Generalized response of the normalized spectra where a and b represent the varying concentration of two species A and B respectively.

b. Two non-orthogonal vectors that define the space containing the first two principal components of the mean centered data.

c. Change in instrument response with respect to a change in concentration of component A.

d. Change in instrument response with respect to a change in concentration of component B.

Figure Captions

Fig. 1: Effect of normalization method on sample distribution in the principal component space: (A) normalized by reference peak, (B) normalized by peak unique to one species, (C) normalized by peak in common with both species, (C) normalized to unit spectral area.

Fig. 2: Postulated reaction mechanisms: (A) Michael-type addition, (B) Ene, Diels-Alder, and isomerization.

Fig. 3: Score on first principal component with respect to cure percentage and normalization alternatives: (o) normalization by 1161 cm^{-1} band, (+) normalization by 1515 cm^{-1} band, (*) normalization to unit area, (x) normalization by 1773 cm^{-1} band.

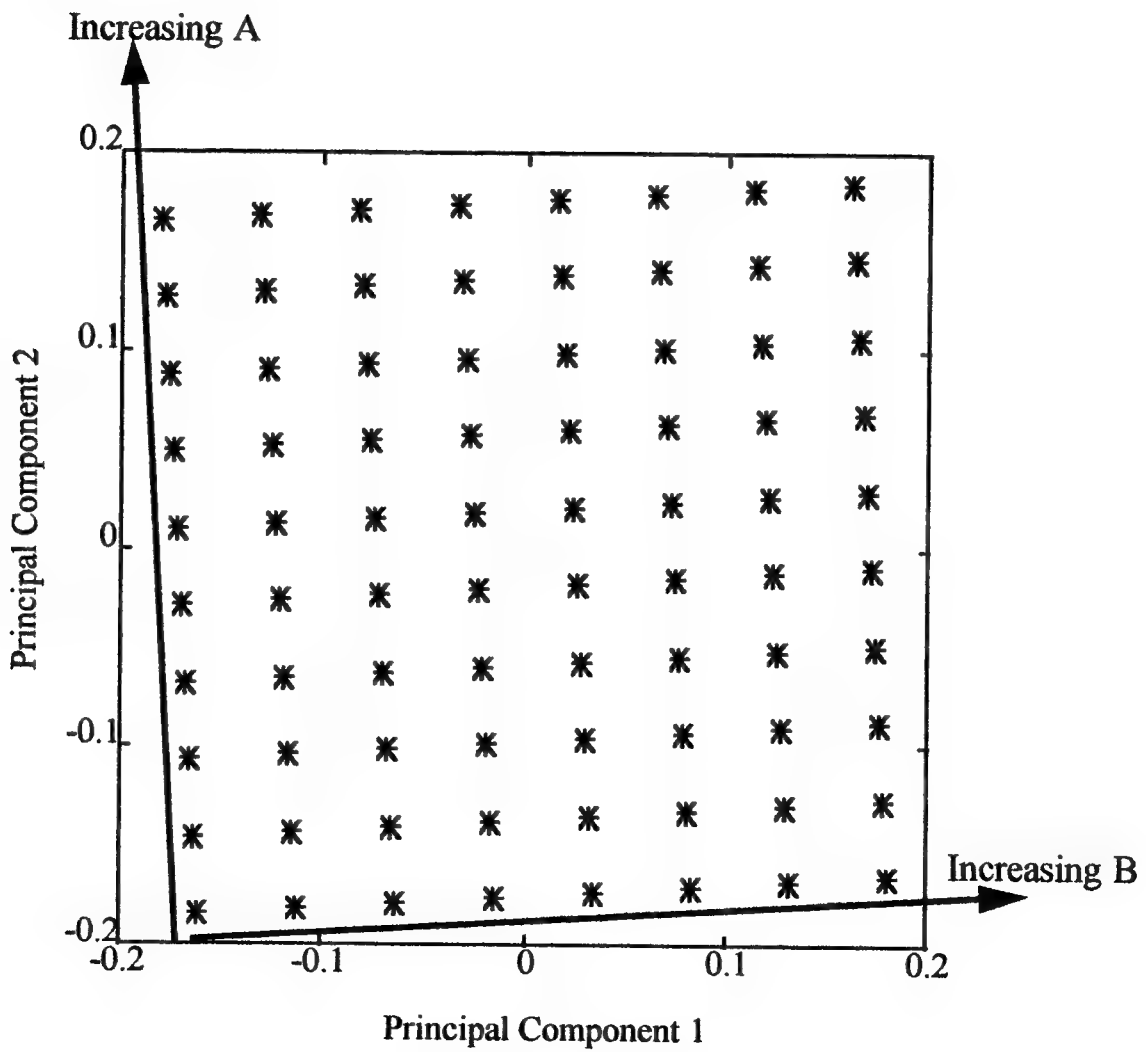
Increasing A
0.2
0.1
0
-0.1
-0.2
Principal Component 2
Increasing B
-0.2
-0.1
0
0.1
0.2
Principal Component 1

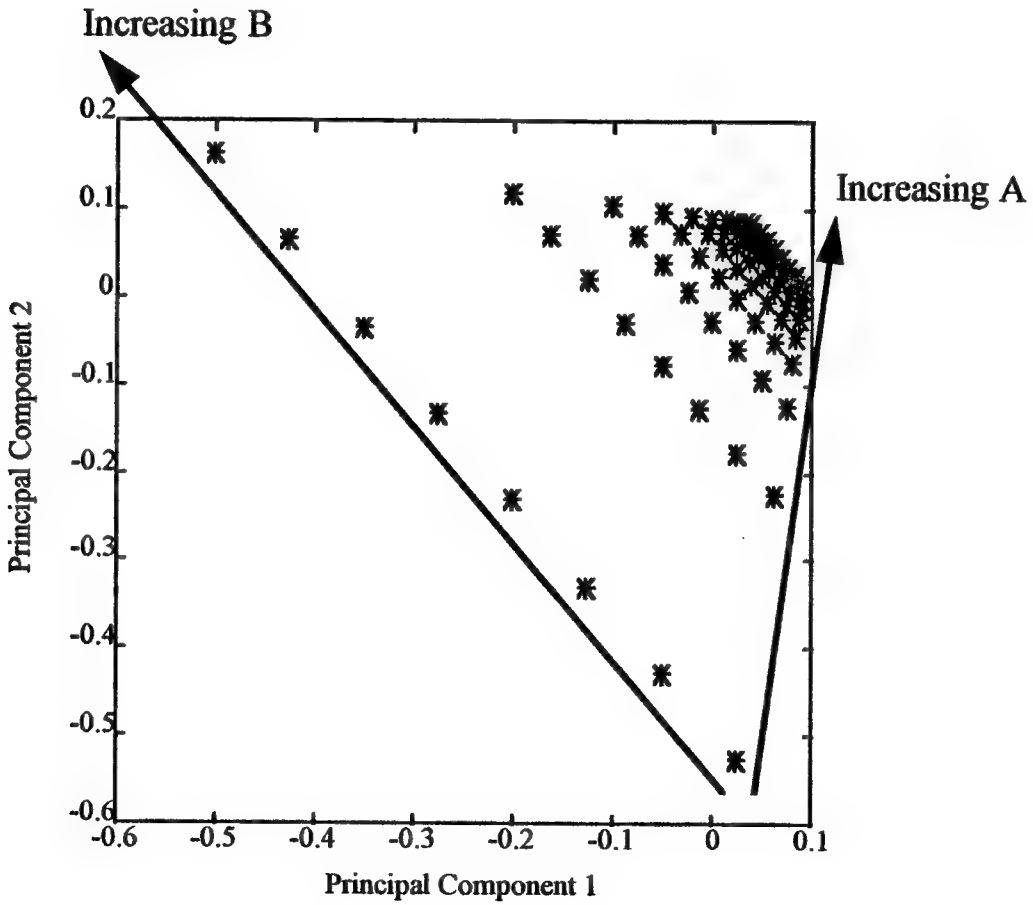
Increasing B
Increasing A
Principal Component 2
Principal Component 1
0.2
0.1
0
-0.1
-0.2
-0.3
-0.4
-0.5
-0.6
-0.6
-0.5
-0.4
-0.3
-0.2
-0.1
0
0.1

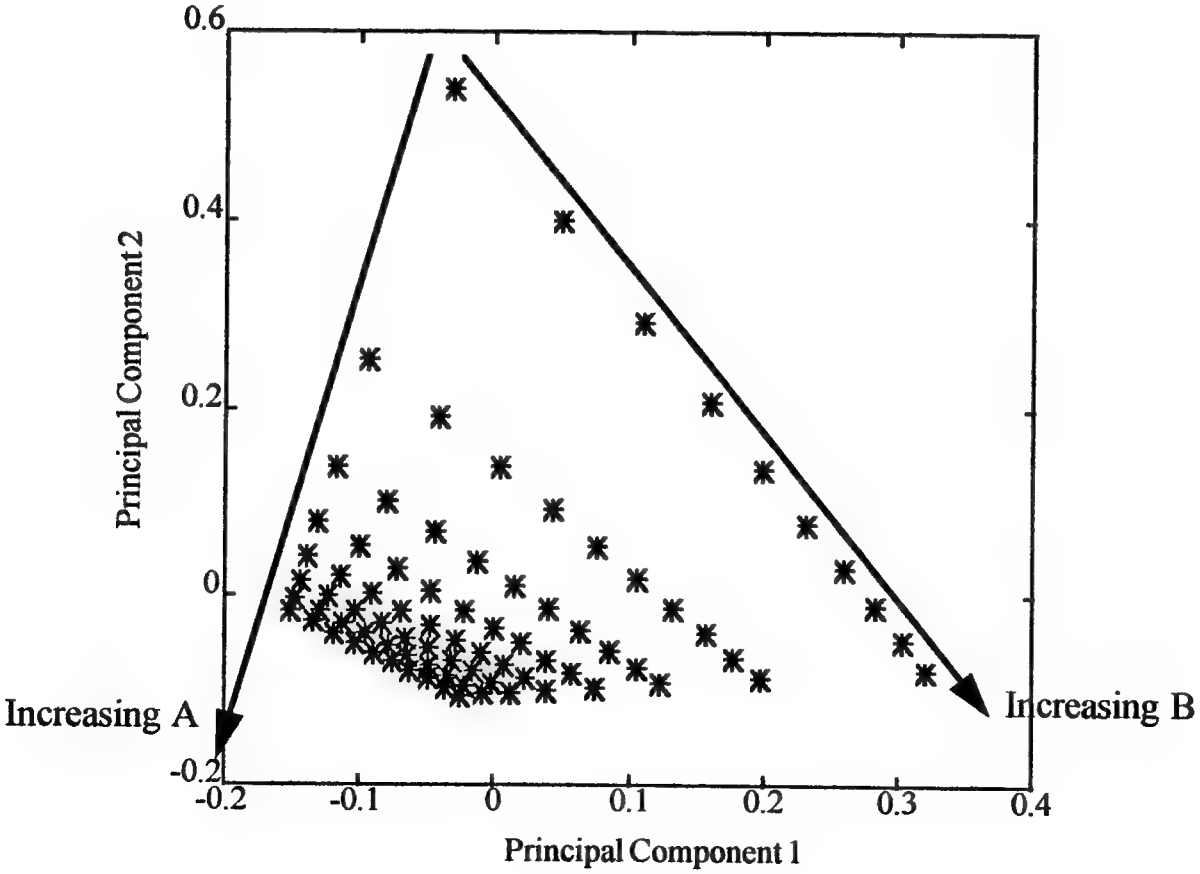
0.6
0.4
0.2
0
-0.2
Principal Component 2
Increasing A
Increasing B
-0.2
-0.1
0
0.1
0.2
0.3
0.4
Principal Component 1

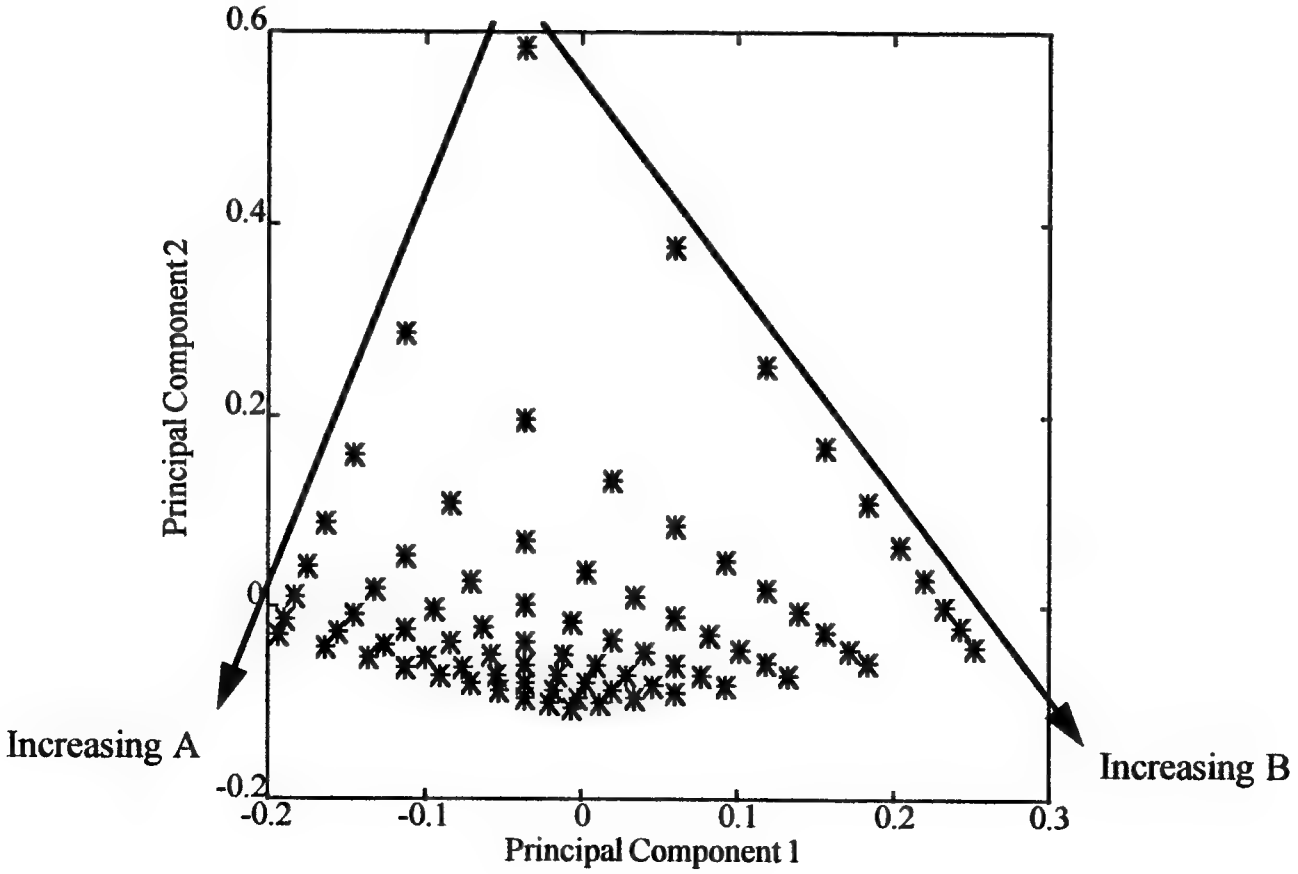
0.6
0.4
0.2
0
-0.2
Principal Component 2
-0.2
-0.1
0
0.1
0.2
0.3
Principal Component 1
Increasing A
Increasing B

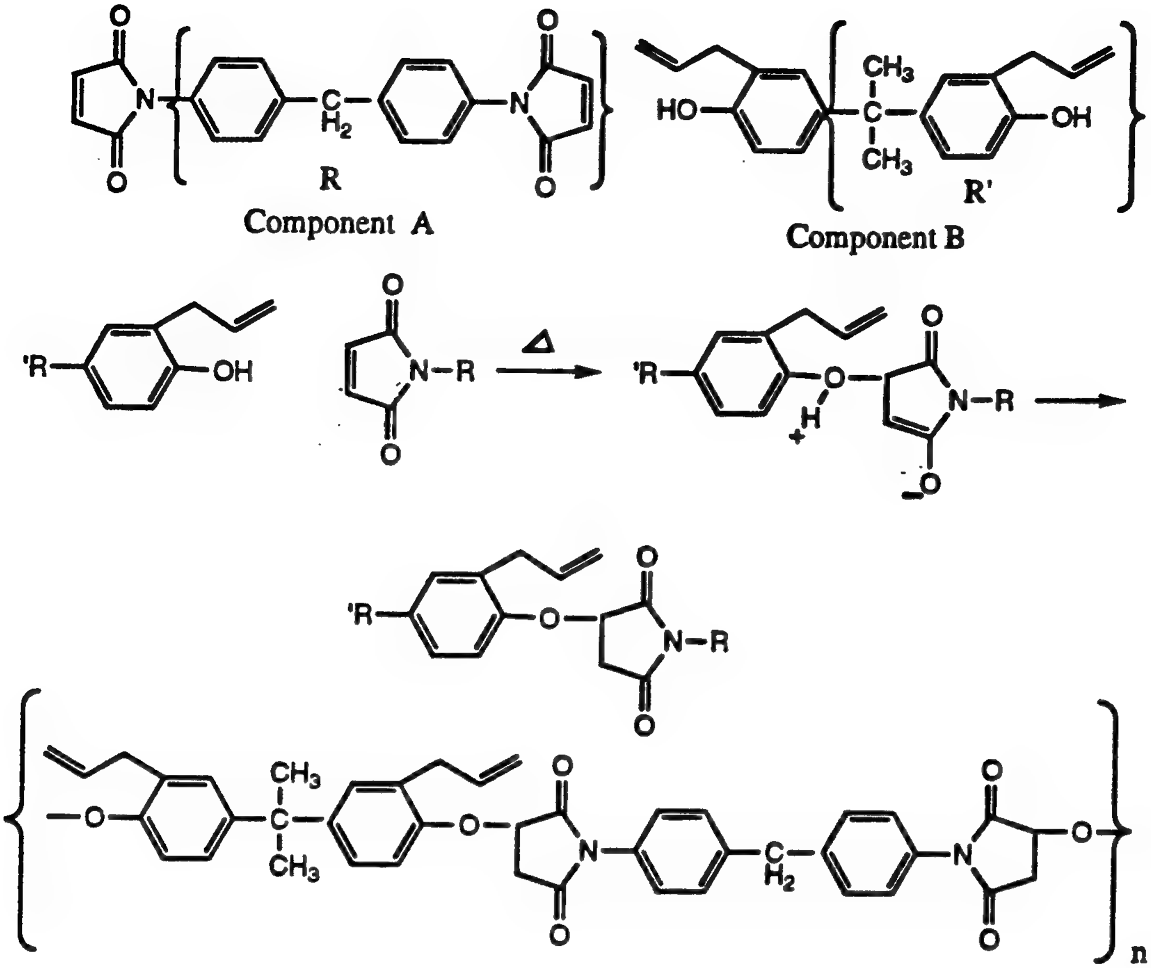
R
Component A
R'
Component B
'R
OH
N-R
HO
CH3
CH3
n

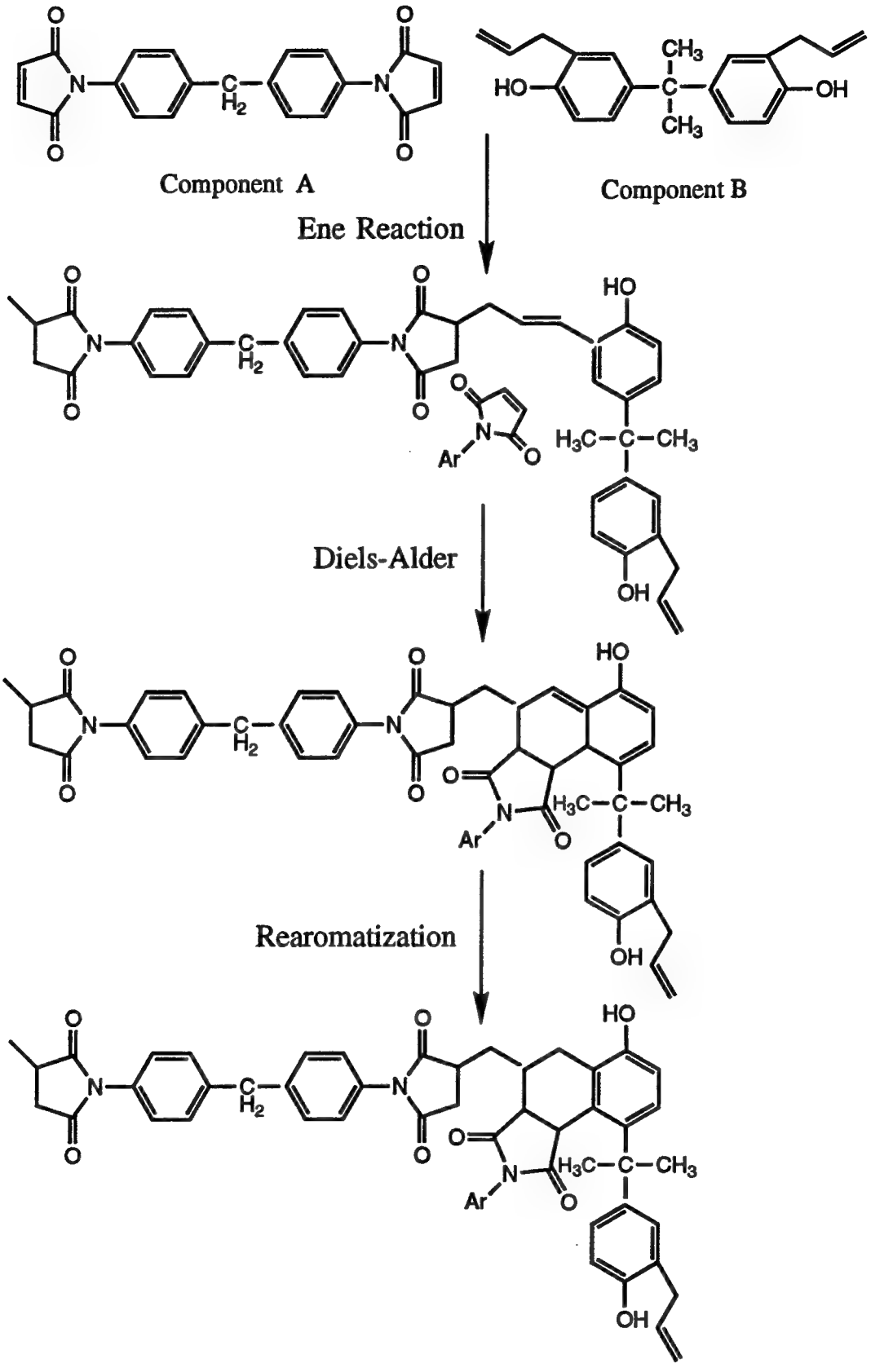
Component A
Component B
Ene Reaction
Diels-Alder
Rearomatization

Fig 2b

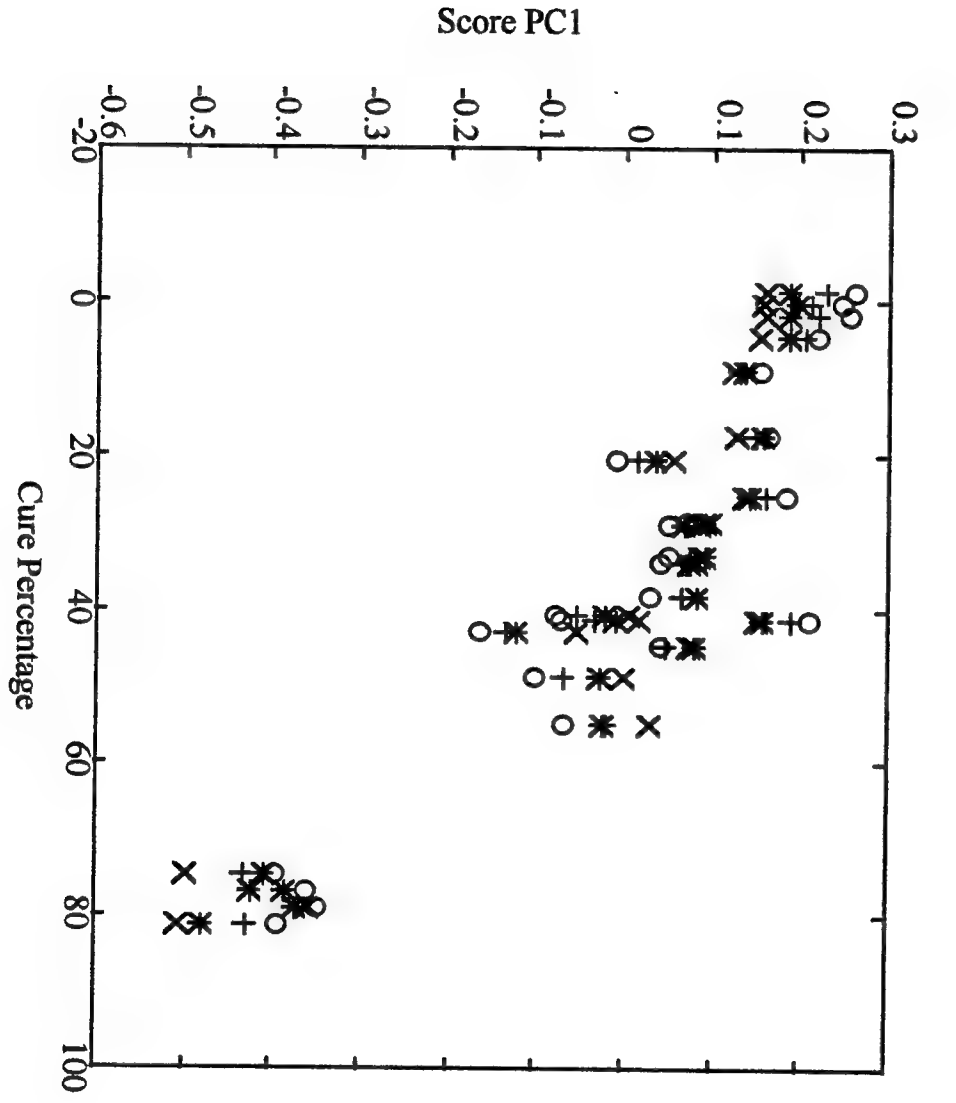
Score PC1
-0.6
-0.5
-0.4
-0.3
-0.2
-0.1
0
0.1
0.2
0.3
Cure Percentage
-20
0
20
40
60
80
100

APPENDIX III - Description and Performance of a Highly Versatile, Low Cost Fiber-Optic Confocal Raman Microscope

Description and Performance of a Highly Versatile, Low Cost Fiber-Optic Confocal Raman Microscope

C.M. Stellman, J.D. Noll, J.E. Reddic and M.L. Myrick*

Department of Chemistry and Biochemistry

University of South Carolina, Columbia, SC 29208

Abstract

A versatile fiber-optic confocal Raman microscope capable of using multiple excitation sources and detection schemes has been developed. Fiber-optics also provide remote capabilities for the microscope. The instrument is designed for facile interfacing with chemometric data analysis methods to improve data acquisition speed and data interpretation. The horizontal and vertical spatial resolution of the microscope is characterized experimentally using principal component data analysis methods.

I. Introduction

The Raman microscope has emerged as a powerful spectroscopic tool with applications to many different fields.[1-10] Since its introduction in the 1970's a large number of optical arrangements and instrumental designs have been used to achieve Raman spectra of micro-sized samples, each having its own advantages and disadvantages.[11,12] There have also been a large number of techniques employed to determine the spatial resolution of such instruments.[13-17] We report here the development of an automated highly versatile fiber-optic confocal Raman microscope which can be constructed for a base cost of $20K (compared to commercially available micro-Raman systems costing >$100K). Also presented is a novel statistical approach for determining the instruments' spatial resolution. The design and construction of our microscope as well as our analysis of resolution cater to planned future investigations of polymer adhesive bondlines. However, the fiber-optic interface provides tremendous excitation and detection versatility. Likewise, the statistical data analysis approach we apply may be modified for use with virtually all forms of confocal microspectroscopy (e.g., fluorescence, reflectance, Raman) to improve speed and accuracy.

II. Instrumental Design

The microscope (Figure 1) is designed with a front-surface dichroic beamsplitter dividing the prime focus of the objective into two arms. The front surface dichroic beamsplitter provides ≥99% reflection at 780 nm (the nominal excitation wavelength for the

studies presented here) and a transmittance of >90% from 815 nm to 950 nm. This allows the instrument to access Raman spectral shifts between 550 and 2295 cm^{-1}. The beamsplitter is anti-reflection coated on its rear surface to diminish stray reflections and is held in a 360° rotatable mount. One arm holds the excitation source placed at prime focus. The second arm holds a movable mirror that selects between a high resolution video image (see below) of the sample surface or a sampling fiber placed at the second prime focus. The sample is placed below the objective and may be moved in a manual or automated scanning fashion.

The microscope will accommodate any standard thread objective. This study employed a 10X and 20X refractive objective and a 52X reflective objective. The refractive objectives are not corrected for near-infrared operation and may suffer from chromatic aberration in this wavelength range. A reflective objective has been used in an effort to diminish chromatic aberrations associated with silica lenses; this does not eliminate spherical aberrations. The reflective objective usually offers a more economical alternative than well-corrected achromatic or apochromatic refractive objectives while still obtaining a reasonably high N.A. to provide good spatial resolution. It does provide less throughput than a refractive objective, but we can still obtain good spectra of weak Raman scatterers in less than 30 seconds, acceptable for many applications. The reflective objective may also be used with a large number of excitation sources, unlike refracting objectives which are corrected for specific wavelengths. Ideal objectives (well-corrected refractive) were not used in this study in an effort to keep instrumental costs

down and to test spatial resolution under less than ideal (but realistic) experimental conditions.

One method we have used for coupling an excitation source to the microscope is via fiber-optics. In this case, a laser of desired wavelength is focused onto an excitation fiber and mounted to the microscope via an xyz positioner. In past work we have used a Coherent 599 standing-wave dye laser (815 nm) pumped with a Coherent Innova 300 Argon ion laser focused onto a 200 μm-core fiber.[18] A second method of excitation is via a diode laser of desired wavelength fitted with a collimating lens and xyz positioner mounted directly to the microscope. All spectra presented in this paper were excited with a Spectra Diode Labs (780 nm) diode. Both excitation methods provide for remote capabilities. The laser source and/or its power source may be controlled from a distant environment that is only limited by fiber attenuation or diode head cable length.

As mentioned above, a high resolution video camera is used to view the sample while providing a safe means of monitoring the laser position and degree of focus. Images from video-rate cameras may be stored for future analysis by means of a computer controlled image grabber. Inexpensive CCD arrays (Santa Barbara Instrument Group ST-6) have also been used for full viewing data acquisition.[19]

Laser attenuation is achieved by use of a 785 nm holographic edge filter in a 360° rotatable mount. The filter provides >80% transmission above 785 nm and like the beamsplitter is easily replaced with any one inch filter of desired optical properties.

Detection schemes for Raman scattering are also highly versatile. Collection of the signal is achieved via a fiber-optic

mounted in an xyz positioner. Via this fiber, the Raman scattering is transferred to the detector of choice. All spectral data in this publication were dispersed by means of a Spex 270M imaging spectrograph and detected by a liquid N_2 cooled Spex Spectrum One CCD. Use of fiber-optics also provide for remote capabilities in collection which complement that of excitation, thus allowing for micro-Raman studies to be limited only by the environmental constraints of the microscope.

The use of fiber optics provide a confocal optical arrangement to enhance vertical resolution. Traditionally confocal microscopy has been performed by placing a pinhole in the back image plane of a microscope.[5,12,17] In our microscope, the 200 μm-core fiber serves as a pinhole. This vertical resolution enhancement is ideal for the study of transparent samples.

The sample is xy positioned by means of a motorized (Newport PMC300) 2-D actuator system and brought to focus by means of a manual z positioner. Programming written for this system offers the user sample positioning via keystroke inputs as well as several scanning options for imaging, and has the ability to collect spectra at desired scanning increments (≥2 μm) for subsequent statistical analysis and image formation. The system operates automatically after the necessary spectral parameters and scanning modes have been set. All samples were manually positioned in this study because increments of movement less than those obtainable by the actuators (2 μm) were desired.

III. Resolution

A. Data Processing

Horizontal and vertical resolution for our microscope have been determined by monitoring Raman spectra while scanning through a known interface. Variability in a spectral data set, such as that caused by scanning across an interface, is best analyzed by a statistical method such as Principle Component Analysis (PCA). Spectral data of n points per spectrum can be viewed as points in an n-dimensional space. PCA is effectively a coordinate transformation which attempts to express the variability of a data set in the fewest possible dimensions. Accounting for the variability requires a number of principle components (PCs) equal to the smaller of the number of variables or the number of samples.[20-21] The first PC (PC1) is the single curve that best explains the variability of the data. The second (PC2) and higher PCs are orthogonal to this axis (PC1) and are ranked in decreasing order of correlation with the data variability. PCA decomposition of the data matrix can be obtained by eigenvalue-eigenvector analysis. The resulting eigenvalues are measures of the variance explained by each PC. The amount of explained variability decreases for each additional PC; beyond the number of PCs necessary to explain real variability, the remaining PCs consist mostly of "noise". PCA of the collected spectral scans was performed with the chemometrics software package "Pirouette" (Infometrix Inc., Seattle WA).

All data was baseline subtracted using a polynomial baseline fit to remove fluorescence. Also, collected data was statistically pre-

treated to account for spectral variance resulting from the diode laser phenomena known as mode hopping. Mode hopping is a discrete shift in excitation wavelength and/or power resulting from a fluctuation in the gain band of the diode. Mode hopping is visually discernible in Raman spectra by the abrupt shifting of peaks by several wavenumbers. All data were monitored for mode hop wavelength fluctuations and corrected by shifting spectra the appropriate number of pixels. Mode hop intensity fluctuations were diminished by means of vector length normalization. Each intensity value in a spectrum was divided by the length of the sample vector f_i where m* contains only the included variables. In this case the spectra were integrated over their total area.

$$f_i = \sqrt{\sum_{j=1}^{m^*} x^2_{ij}} \qquad (1)$$

$$x_{ij(norm)} = \frac{x_{ij}}{f_i} \qquad (2)$$

Finally all data was mean centered by computing the mean over each variable (pixel number) and then subtracting the mean from each data point to produce the mean centered matrix:

$$x_j = \frac{1}{n}\sum_{i=1}^{n} x_{ij} \qquad (3)$$

$$x_{ij(mc)} = x_{ij} - x_j \qquad (4)$$

All pre-treatment of data may be easily and routinely performed with the assistance of self-authored and commercial software.

B. Horizontal Resolution

Horizontal resolution of our microscope has been determined by analyzing spectral changes with PCA while scanning over an epoxy/Delrin interface. The sample was prepared by boring a 1 cm diameter hole in a 3 cm slice of 5 cm diameter Delrin rod. The hole was filled with the epoxy (tripolyoxypropylenetriamine encapped diglycidylether of bisphenol-A (DGEBA) epoxide), allowed to cure, and polished smooth with multiple grades of polishing paper, finishing with a .3 μm grit. The sample was manually scanned at 1μm intervals and spectra were collected at each point. The spectrograph was outfitted with a 300 groove/mm grating and a slit width of 200 μm was used. The spectra were integrated for 30, 30 and 60 seconds with sample surface powers of 45 mW, 35 mW, and 5 mW for the 10X, 20X, and 52X objectives respectively.

After pre-treatment, a PCA of data for all three objectives was performed. Initial examination of PC1 versus sample position showed an increase in PC1 score with micrometer position corresponding to the microscope's horizontal resolution. However, it was difficult to define where this region began and ended because of a slow change in slope with respect to position. Close examination of the data revealed that PC1 accounted for approximately 70% of the data variability and that PC2 accounted for approximately 25% of the variability, for each of the objectives. Ideally, PC1 should contain upward of 90% of the variance if the spectral changes are due to one

change in chemical structure. Examination of the PC loadings versus wavelength (Figure 2) showed that PC1 and PC2 were similar to the Delrin and epoxide spectra, respectively (Figure 3). Ideally, PC1 should be a difference of the two spectra corresponding to the appearance or disappearance of the spectral peaks with changing position. Hence, to enhance identification of the interfacial region we perform a rotation transformation on our data. In essence the first two PCs may be forced into one non-orthogonal direction by choosing an appropriate linear combination of the two. By examination of our data in the form of 3-D scores plots it was found that by rotating PC1 45° into PC2 an ideal combination could be obtained. Rotation from the old PC1 and PC2 axes into the new sum and difference axes requires a rotation transformation of Cartesian coordinates:

$$S = PC1 + PC2 \qquad (5)$$

$$D = PC1 - PC2 \qquad (6)$$

PC1-PC2 provides a data representation which noticeably enhances the definition of the interface (Figure 4). The loadings of PC1-PC2 versus wavelength produce the necessary form (one component increasing while the other decreases) of the spectral data as a function of changing position. From these plots we determine that our microscope has a horizontal spatial resolution of 15 μm, 10 μm, and 5 μm for the 10X, 20X, and 52X objectives respectively.

At first glance the horizontal resolution of our microscope may seem to be larger than expected. Theoretically, the lateral resolution

of a microscope objective nearly corresponds to the diameter of the focused laser which we calculate at 3.8 μm, 2.4 μm, and 1.5 μm for the 10X, 20X, and 52X objectives respectively. The determined spatial resolutions are approximately 4.0X greater for the refractive objectives and 3.3X greater for the reflecting objective. Spatial resolution may change with samples based on the refraction, scattering, and absorption properties of the material being examined.[5] This is an important consideration in the determination of actual resolution, but due to the difficulty in quantifying these effects they are beyond the scope of this paper. Spatial resolution of a confocal Raman microscope is also highly dependent on the optical properties of the microscope objective.[5] Non-ideal behavior (see below) of the sample and microscope likely explain discrepancies between theoretical and experimental resolution values.

Spatial resolution degrades with increasing aberrations and depth of focus.[5,12] The refractive objectives have low magnifications and numerical apertures (N.A.) corresponding to a large depth of focus. Also, their silica-based composition makes them prone to chromatic aberrations. These two factors contribute to making the experimentally-determined spatial resolution larger than the theoretical. The reflective objective with a higher magnification and N.A. has a smaller depth of focus. This, combined with a lack of chromatic aberration, decreases the deviation between theoretical and experimental resolution. Spherical aberration is still present in reflective objectives and is likely a strong contributor to the remaining difference between experimental and theoretical resolution.

All three PC1-PC2 score plots seem to have a large degree of noise present. Spectral intensities not only change with material, as expected, but also change randomly with translation position. A scanning electron micrograph of the epoxide and Delrin surfaces (Figure 5) shows that both surfaces possess pits and grooves that may cause sample position to vary in the microscope's focus, resulting in a fluctuation in Raman intensity. This theory is consistent with the observation that the spectral intensities seem to fluctuate less in magnitude for the epoxy than the Delrin, which has a noticeably rougher surface.

"Naked-eye" determination of the interface-crossing region (and thus the resolution) from the spectra acquired in this study is nearly impossible with a reasonable degree of certainty. This is especially true in the case of the 52X objective that produces less intense spectra because of its lower throughput. PCA provides a strong tool for enhancing details of such interfaces. The horizontal spatial resolution for our microscope would likely reach theoretical values by the use of well-corrected high-N.A. refractive objectives coupled with the use of PCA.

B. Vertical Resolution

Vertical resolution of our microscope has been determined in a similar fashion, but the microscope's focal plane was scanned through a polystyrene/epoxy interface. The sample was prepared by filling a standard 1 cm polystyrene cuvet with epoxy and allowing it to cure. The cuvet was laid on its side, vertically scanned at intervals of 10 μm, and spectra were collected at each point. All spectrograph

settings, integration times, and excitation powers were equivalent to those used for determining horizontal resolution.

No linear transformation of the PCA data was required because PC1 had the appropriate characteristics already. Examination of the sample spectra (Figure 6) and the PC1 loadings plot (Figure 7) show that PC1 is a difference of the two polymer spectra with positive and negative peaks corresponding to the appearance and disappearance of spectral peaks with changing position. This is characteristic of a good PCA of a simple spectral change between two distinct materials and helps to support the validity of our analysis.

For all three objectives PC1 accounted for >95% of the variability. Unlike the horizontal resolution data, a PC loading plot (Figure 8) shows a gradual change in slope at the interfacial region. In order to enhance this characteristic region a first derivative of PC1 score as a function of position was taken (Figure 9). From this analysis the resolution was determined as the full width at half maximum (FWHM) of the PC1 score slope and was measured to be approximately 340 μm, 120 μm and 40 μm for the 10X, 20X, and 52X objectives respectively. (This differentiation technique was used on the horizontal resolution data to little effect and is not reproduced here.)

Theoretical calculations made using Beam Three Optical Ray Tracer (Stellar Software) place our microscopes vertical resolution at 8-10 μm for our 52X objective. The experimental resolution was calculated at approximately 4X this value. We feel that this deviation is largely due to the same causes that degraded the horizontal resolution, and is consistent with the 3.3X difference in

horizontal resolution between experiment and theory. Some variation may also be a result of an increasing attenuation of Raman scattering with increasing depth of penetration. No theoretical calculations were made for the refractive objectives.

IV. Conclusions

Fiber-Optic Confocal Raman microspectroscopy is a promising technique for spatially resolved quantitative analysis of polymeric materials. Analysis of virtually all Raman scatterers is made possible by versatility in excitation source and spectral detection and is further enhanced via remote capabilities. PCA provides an ideal statistical tool in analyzing spectral change as a function of position, thus making it conducive to monitoring spatial resolution as well as other material characteristics that may be monitored spectroscopically. Furthermore, PCA provides a method of enhancing indistinct spectral changes. This ultimately allows for the use of more economical and more versatile lenses in many studies, faster sampling times and greater analysis flexibility.

Acknowledgment

M.L.M and C.M.S gratefully acknowledge the Army Research Office (Grant Number DAAL03-9Z-G-0316) for support of this work. They especially thank Dr. Edward S. Chen for his interest and encouragement.

References

1. M. Bowden, G.D. Dickson, D.J. Gardiner, and D.J. Wood, Appl. Spectrosc. **44**, 1679-1684 (1990).

2. D.M. Hembree, J.C. Oswald and N.R. Smyrl, Appl. Spectrosc. **41**, 267-272 (1987).

3. H. Ishida, R. Kamoto, S. Uchida, A. Ishitani, Y. Ozaki, K. Iriyama, E. Tsukie, K. Shibata, F. Ishihara and H. Kameda, Appl. Spectrosc. **41**, 407-412 (1987).

4. F. Sureau, L. Chinsky, C. Amirand, J.P. Ballini, M. Duquesne, A. Laigle, P.Y. Turpin and P. Vigny, Appl. Spectrosc. **44**, 1047-1051 (1990).

5. R. Tabaksblat, R.J. Meier and B.J. Kip, Appl. Spectrosc. **46**, 60-68 (1992).

6. D.J. Gardiner, C.J. Littleton and M. Bowden, Appl. Spectrosc. **42**, 15-19 (1988).

7. P.J. Treado, A.G. Govil, M.D. Morris, K.D. Sternitzke and R.L. McCreery, Appl. Spectrosc. **44**, 1270-1275 (1990).

8. M. Bowden, D.J. Gardiner and G. Rice, J. Raman Spectrosc. **21**, 37-41 (1990).

9. M.L. McGlashen, U. Guhathakurta, K.L. Davis and M.D. Morris, Appl. Spectrosc. **45**, 543-545 (1991).

10. R.A. Dalterio, W.H. Nelson, D. Britt, J. Sperry and F.J. Purcell, Appl. Spectrosc. **40**, 271-272 (1986).

11. M. Delhaye and P. Dhamelincourt, J. Raman. Spectrosc. **3**, 33-43 (1975).

12. P.J. Treado and M.D. Morris, Appl. Spectrosc. Rev. **29(1)**, 1-38 (1994).

13. A.J. Sommer and J.E. Katon, Appl. Spectrosc. **45**, 527-534 (1991).

14. J. Barbillat, E. Da Silva and B. Roussel, J. Raman Spectrosc. **22**, 383-391 (1991).

15. R. G. Messerschmidt and D.B. Chase, Appl. Spectrosc. **43**, 11-15 (1989).

16. D.K. Veirs, J.W. Ager III, E.T. Loucks and G.M. Rosenblatt, Appl. Optics **29**, 4969-4980 (1990).

17. G.J. Puppels, W. Colier, J.H.F. Olminkhof, C. Otto, F.F.M. de Mul and J. Greve, J. Raman Spectrosc. **22**, 217-225 (1991).

18. C.M. Stellman, J.E. Reddic and M.L. Myrick, Pittsburgh Conference Poster Session (1994).

19. J.D. Noll, C.M. Stellman and M.L. Myrick, Submitted to Nature (1994).

20. E.R. Malinowski, *Factor Analysis in Chemistry, 2nd ed.*, (John Wiley, New York, 1991).

21. I.T. Jollife, *Principal Component Analysis*, (Springer-Verlag, New York, 1986).

List Of Figures

10X objective, (c) polystyrene for the 20X objective, (d) tripolyoxypropylenetriamine encapped diglycidylether of bisphenol-A (DGEBA) epoxide for the 20X objective, (e) polystyrene for the 52X objective and (f) tripolyoxypropylenetriamine encapped diglycidylether of bisphenol-A (DGEBA) epoxide for the 52X objective.

Figure 7: Loading versus wavenumber plots of PC1 for the (a) 10X objective, (b) 20X objective and (c) 52X objective.

Figure 8: Score versus position plot for the (a) 52X objective, (b) 20X objective and (c) 10X objective.

Figure 9: Score derivative versus position plot for the (a) 10X objective, (b) 20X objective and (c) 52X objective.

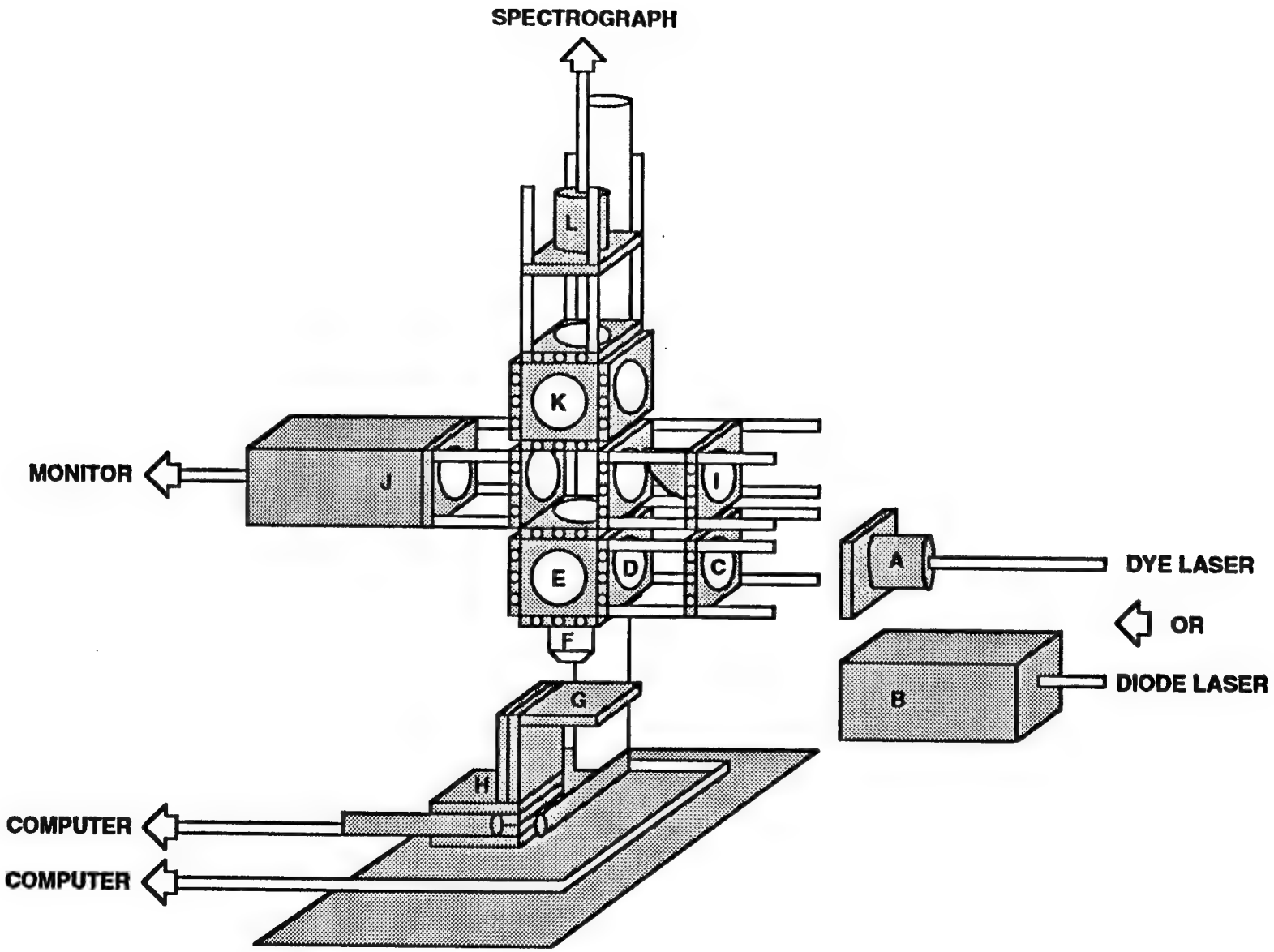
SPECTROGRAPH
L
K
MONITOR
J
I
A
DYE LASER
OR
E
D
C
B
DIODE LASER
F
G
H
COMPUTER
COMPUTER

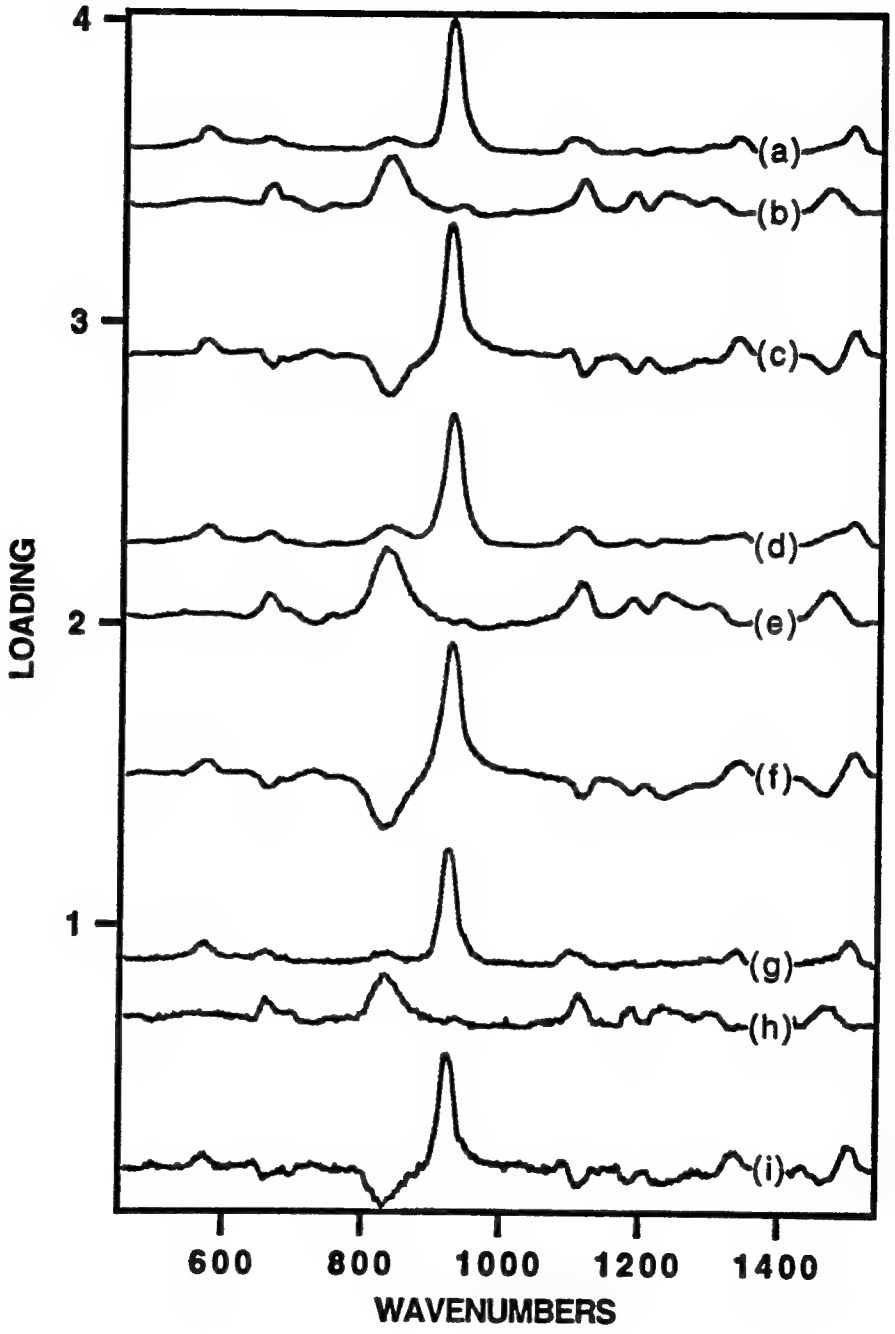
4
3
2
1
LOADING
(a)
(b)
(c)
(d)
(e)
(f)
(g)
(h)
(i)
600
800
1000
1200
1400
WAVENUMBERS

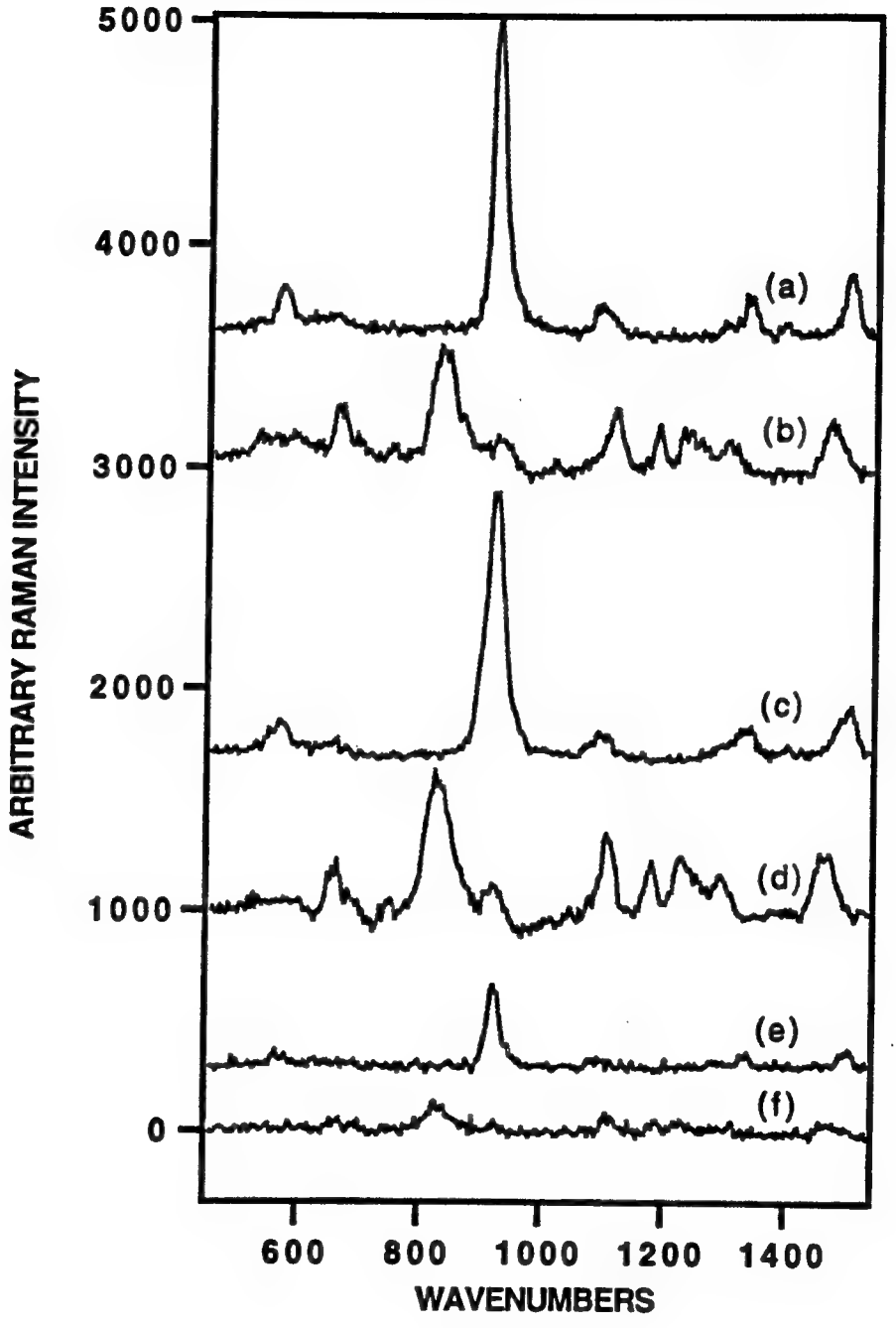
5000
4000
3000
2000
1000
0
ARBITRARY RAMAN INTENSITY
(a)
(b)
(c)
(d)
(e)
(f)
600
800
1000
1200
1400
WAVENUMBERS

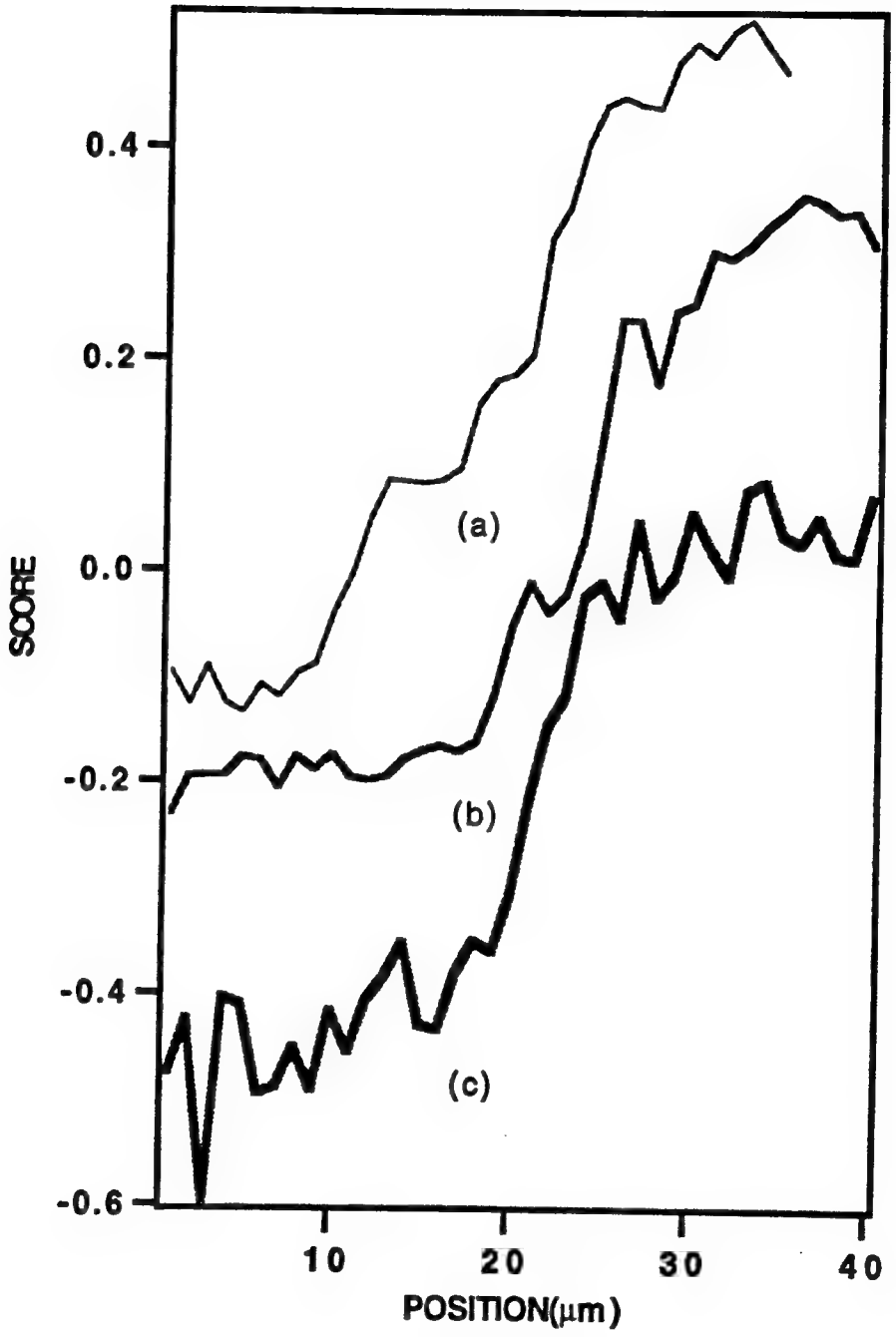
0.4
0.2
0.0
-0.2
-0.4
-0.6
SCORE
(a)
(b)
(c)
10
20
30
40
POSITION(μm)

EPOXY

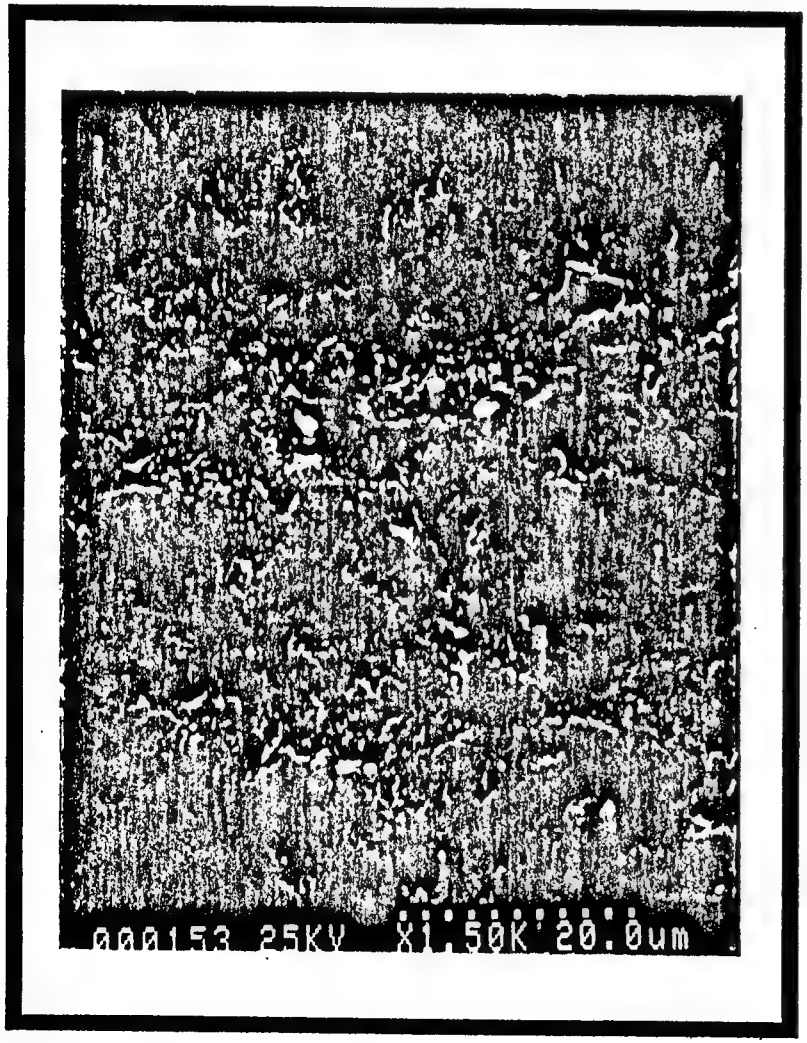

DELRIN

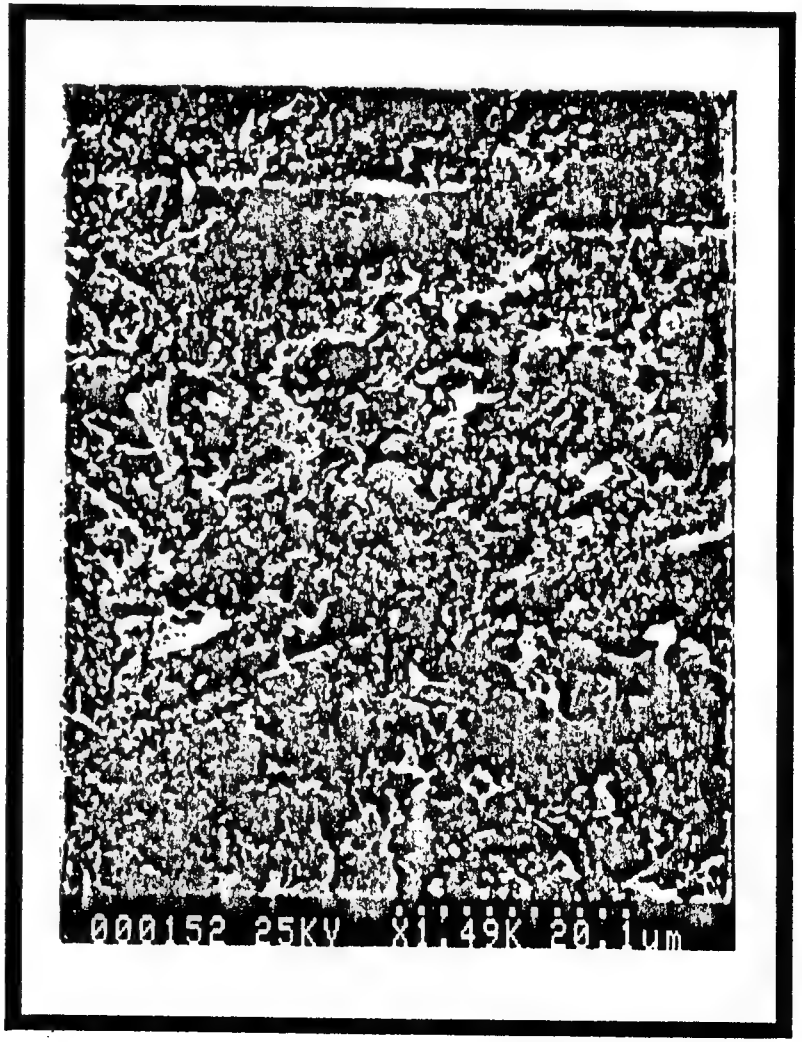

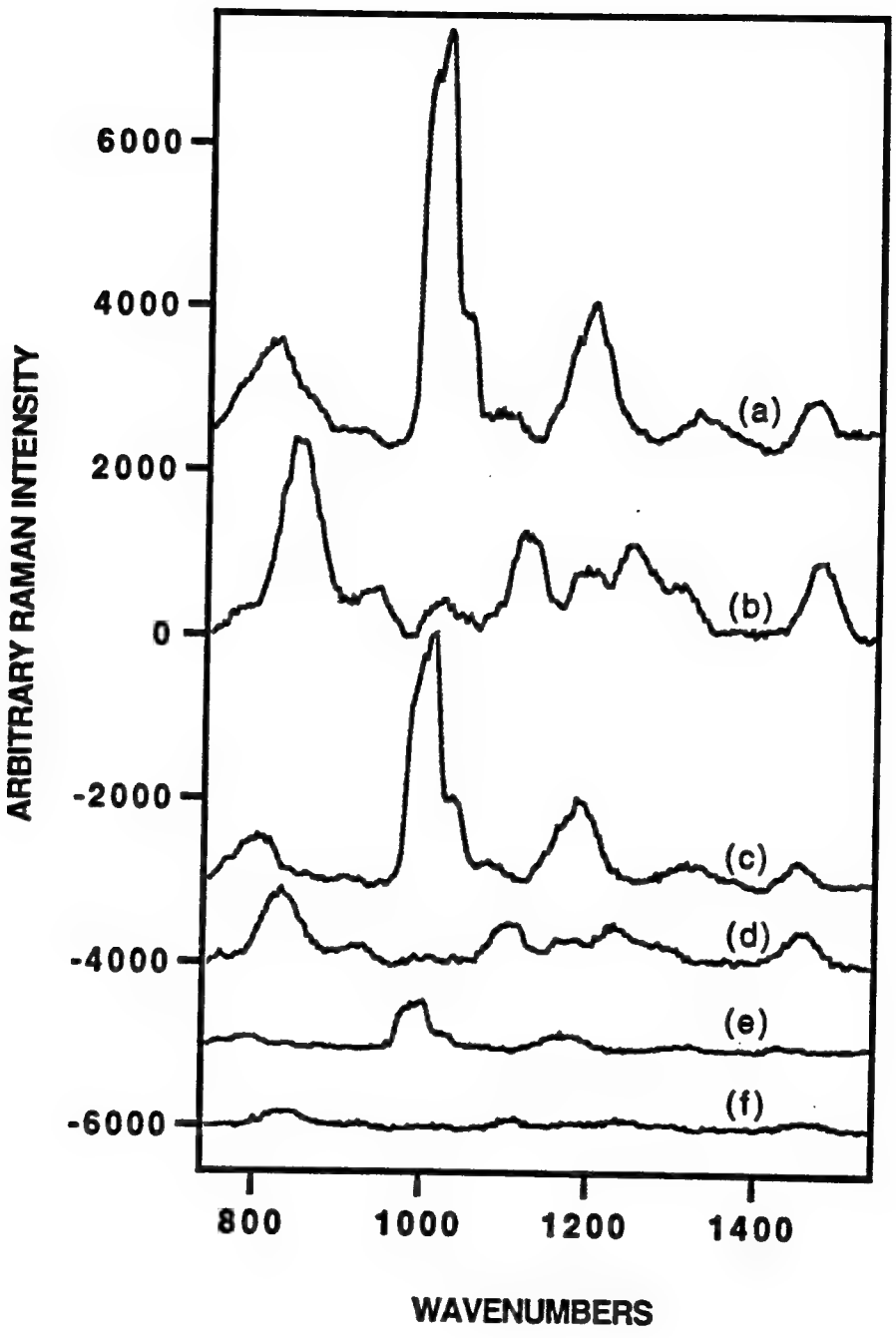
6000
4000
2000
0
-2000
-4000
-6000
ARBITRARY RAMAN INTENSITY
(a)
(b)
(c)
(d)
(e)
(f)
800
1000
1200
1400
WAVENUMBERS

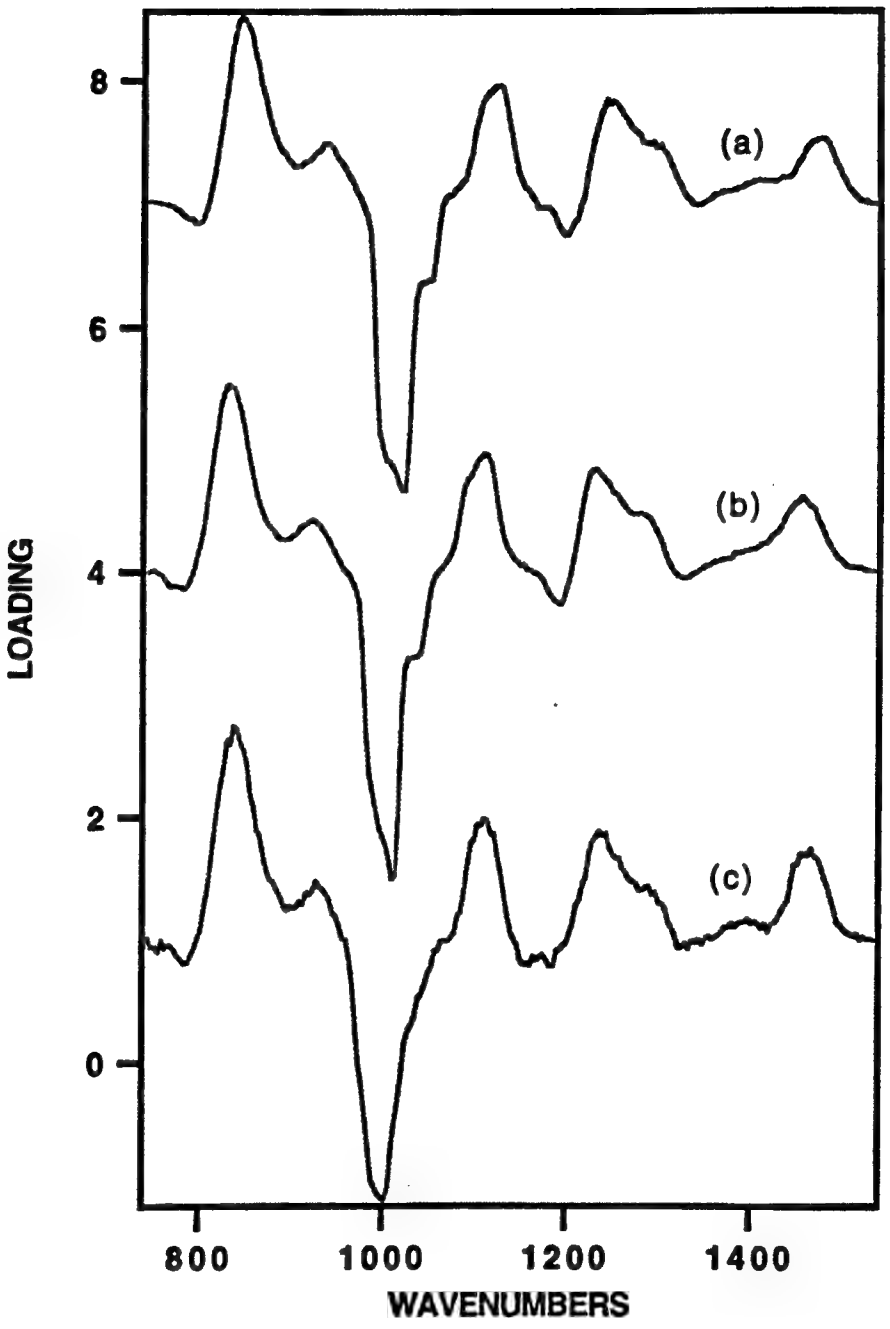
8
6
4
2
0
LOADING
(a)
(b)
(c)
800
1000
1200
1400
WAVENUMBERS

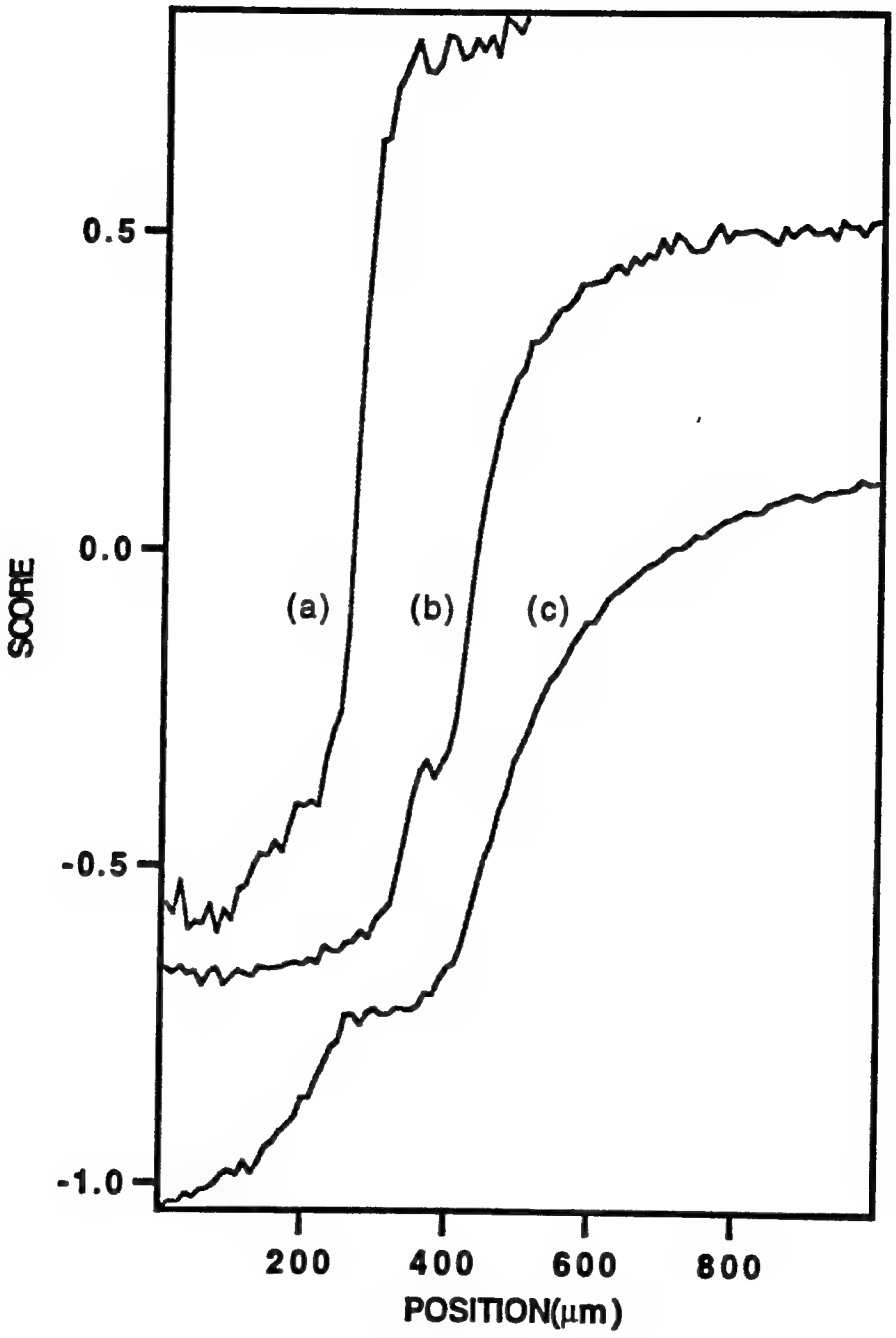
0.5
0.0
-0.5
-1.0
SCORE
(a)
(b)
(c)
200
400
600
800
POSITION(μm)

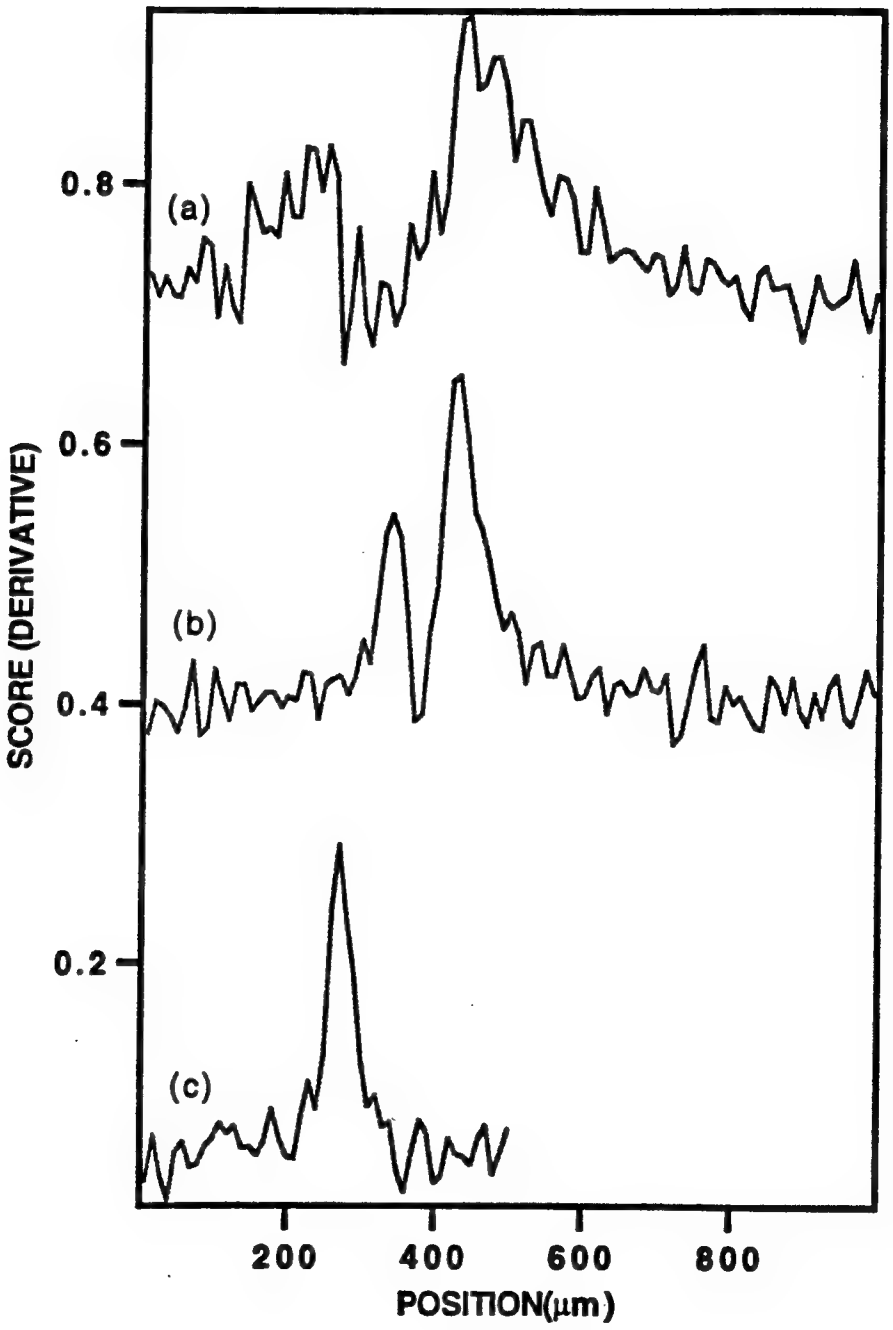
0.8
0.6
0.4
0.2
(a)
(b)
(c)
SCORE (DERIVATIVE)
200
400
600
800
POSITION(μm)

APPENDIX IV - In-Situ Spectroscopic Study of Microwave Polymerization

In-Situ Spectroscopic Study of Microwave Polymerization

Christopher M. Stellman, Jeffrey F. Aust, and Michael L. Myrick*

Department of Chemistry, University of South Carolina, Columbia, South Carolina 29208

ABSTRACT

Microwaves provide a commercially advantageous method of rapidly curing polymeric samples. Curing times of several hours with traditional ovens are easily reduced to several minutes by microwave curing. Many commonly-used sample monitoring probes (e.g., thermocouples) contain metallic elements that are incompatible with microwave processing. In this work we have used a dual-fiber optical probe to spectroscopically monitor the rapid microwave curing of an amine-cured epoxide as a function of time. Such probes can be free of metallic components and provide a relatively cheap and practical means of monitoring cure chemistry via Raman spectroscopy.

INDEX HEADINGS

Raman Spectroscopy, Fiber Optic Spectroscopy, Microwave Polymerization, Chemometrics.

INTRODUCTION

Microwaves provide a commercially advantageous method of rapidly curing polymeric samples. Curing times of several hours with traditional ovens are easily reduced to several minutes by microwave curing. Many commonly-used sample monitoring probes (e.g., thermocouples) contain metallic elements that are incompatible with microwave processing. Such accelerated polymer processing via rapid microwave heating would benefit from rapid *in-situ* monitoring techniques using optical spectroscopy.

Fiber-optic Raman spectroscopy has recently been applied to monitoring the cure of thermoset polymers[1-3], adhesives[4] and composites[5] *in-situ* via miniaturized sensors. Raman spectroscopy provides many advantages over other spectroscopic techniques for polymer cure monitoring, including broad applicability, high sensitivity and selectivity and freedom from large background fiber absorption.

In this work we have used a dual-fiber optical probe to spectroscopically monitor the rapid microwave curing of an amine-cured epoxide as a function of time. Such probes can be free of metallic components and provide a relatively cheap and practical means of monitoring cure chemistry via Raman spectroscopy. To the authors knowledge this is the first report of microwave polymer processing monitored by *in situ* fiber-optic Raman spectroscopy.

EXPERIMENTAL

Reagents. A tripolyoxypropylenetriamine-encapped diglycidylether of bisphenol-A(DGEBA) epoxide was prepared by reacting 100% w/w DGEBA (99%, Dow Chemical DER332, epoxide equivalent weight 173.0 g/eq) with 35% w/w polyoxypropylenetriamine (99%, Texaco Chemical Jeffamine T-403, amine hydrogen equivalent weight 50.9 g/eq). The mixture was degassed under vacuum for several minutes and stored under nitrogen in a sealed 500 ml flask until being transferred to the microwave sample container. The chemical structure and reaction of DGEBA and polyoxypropylenetriamine are shown in Figure 1.

Apparatus. The instrumental apparatus is shown in Figure 2. The fiber-optic Raman measurements were made using a two fiber probe inserted into a curing epoxide. The sample was cured in a low wattage microwave oven. Excitation was achieved by focusing 200 mW of the 488 nm line of a Coherent Innova 305 argon laser onto the polished face of the excitation fiber with a 20x microscope objective. A 488 nm bandpass filter (Chroma, Inc.) was employed to eliminate any stray laser emissions. The collected Raman scattering was collimated through a 488 nm holographic filter (Physical Optics, Inc.) to attenuate the excitation line and then focused onto the slit of a Spex 270M imaging spectrograph. The spectra were collected with a Spex Spectrum One liquid N_2 cooled CCD.

The probe was constructed from two 200 μm core one meter long silica fibers (Polymicro Inc.). The two fibers were sealed in a 21 gauge syringe with DER332-T403 epoxy and polished smooth. The

metal syringe barrel was then removed by electrochemical etching in a bath of 17% H_2SO_4.

The sample was placed in a disposable 1 dram vial and the probe was inserted into the center of the epoxide sample. The top of the vial was sealed with a 1 cm layer of 5-minute epoxy to minimize the formation of air bubbles in the curing sample as well as provide a practical means of supporting the probe during an experimental run.

Data Analysis. Variability in a spectral data set, such as that caused by sample curing, is best analyzed by a statistical method such as Principle Component Analysis (PCA). Spectral data of n points per spectrum can be viewed as points in an n-dimensional space. PCA is effectively a coordinate transformation which attempts to express the variability of a data set in the fewest possible dimensions. Accounting for the variability requires a number of principle components (PCs) equal to the smaller of the number of variables or the number of samples.[7,8] The first PC (PC1) is the single curve that best explains the variability of the data. The second (PC2) and higher PCs are orthogonal to this axis (PC1) and are ranked in decreasing order of correlation with the data variability. PCA decomposition of the data matrix can be obtained by eigenvalue-eigenvector analysis. The resulting eigenvalues are measures of the variance explained by each PC. The amount of explained variability decreases for each additional PC; beyond the number of PCs necessary to explain real variability, the remaining PCs consist mostly of "noise". PCA of the collected spectral scans was performed using the chemometrics software package "Pirouette"

(Infometrix Inc., Seattle WA). Spectra were baseline subtracted using a polynomial baseline fit and normalized using a cure-insensitive Raman band at 1612 cm^{-1}. This band is ideal because its chemical functionality does not change and it is environmentally stable in terms of neighboring changes in polarizability, thus leading to no significant change in integrated band intensity during the course of sample curing. Furthermore, it has been shown in related studies that in many cases the band choice for normalization has little effect on the overall performance of normalizing the data when used in conjunction with PCA.[9] PCA was performed with only mean-centering of spectra.

RESULTS AND DISCUSSION

Raman spectra of the microwave cured epoxide were continuously taken over a 2.4 minute curing time. The exposures were 4 seconds long with a time lapse of 1.9 seconds between spectral collections. It has previously been demonstrated that Raman bands at 1113 cm^{-1}, 1186 cm^{-1} and 1243 cm^{-1} provide a good means of following the sample curing chemistry[1,6]. Figure 3 shows the background corrected Raman intensities of this spectral region at two curing times. It can be seen that the 1243 cm^{-1} peak loses intensity relative to the 1113 cm^{-1} peak as the cure time increases.

Principal component analysis of the spectra showed that the first principal component (PC1) contained 86.4% of the spectral variance. A loading plot of PC1 (Fig. 3) shows that it contains the most important spectroscopic changes resulting from the curing processes. PC2 and other principal components appeared to contain

mostly random noise. The sigmoidal plot in Figure 4 shows the PC1 score versus cure time and correlates well with previous data taken of the same epoxide cured in a traditional oven. It can be seen that most of the curing occurs in the 1.5 to 2.0 minute range. Spectra collected after 2.4 minutes were eliminated from the analysis because the sample ignited at this point due to continued heating. However, Figure 4 shows that the sample curing reached completion after 2.0 minutes, well in advance of sample ignition.

The results reported here demonstrate the potential of fiber-optic Raman spectroscopy for monitoring the microwave curing of polymeric samples.

ACKNOWLEDGMENT

M.L.M., C.M.S. and J.F.A. gratefully acknowledge the Army Research Office (Grant Number DAAL03-92-G-0316) for support of this work. They especially thank Dr. Edward S. Chen (ARO) for his interest and encouragement.

REFERENCES

(1) M.L. Myrick, S.M. Angel and R.E. Lyon, SAMPE Journal, **28(4)**, 37-42, (1992).

(2) D.L. Gerrard and W.F. Williams, Appl. Spectrosc. Rev., **22**, 251 (1986).

(3) C.E. Miller, D.D. Archibald, M.L. Myrick and M.S. Angel, Appl. Spectrosc., **44**, 1297 (1990).

(4) R.E. Lyon, M.L. Myrick and S.M. Angel, Proc. 6th International Symposium on Structural Adhesives Bonding , Morristown NJ, **May 4-7** (1992).

(5) R.E. Lyon, M.L. Myrick, S.M. Angel and T.M. Vess, Proc. SPE Antec 92, Detroit MI, **May 3-7** (1992).

(6) K.C. Hong, T.M. Vess, R.E. Lyon, K.E. Chike, J.F. Aust and M.L. Myrick, 38th International SAMPE Symposium and Exposition, Anaheim CA, **May 10-13** (1993).

(7) E.R. Malinowski, *Factor Analysis in Chemistry*, 2nd ed., (John Wiley, New York, 1992).

(8) I.T. Jollife, *Principal Component Analysis*, (Springer-Verlag, New York, 1986).

(9) J.F. Aust, K.S. Booksh and M.L. Myrick, Anal. Chim. Acta., submitted (1994).

LIST OF FIGURES

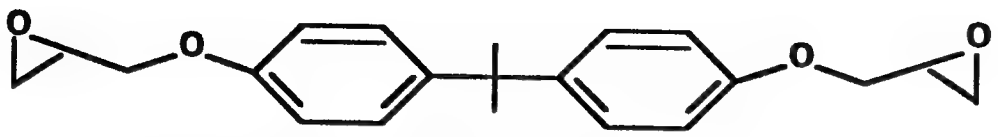

Diglycidyl ether of bisphenol-A
(DER332)

+

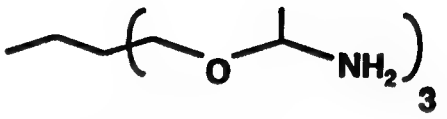

Polyoxypropylenetriamine
(Jeffamine T-403)

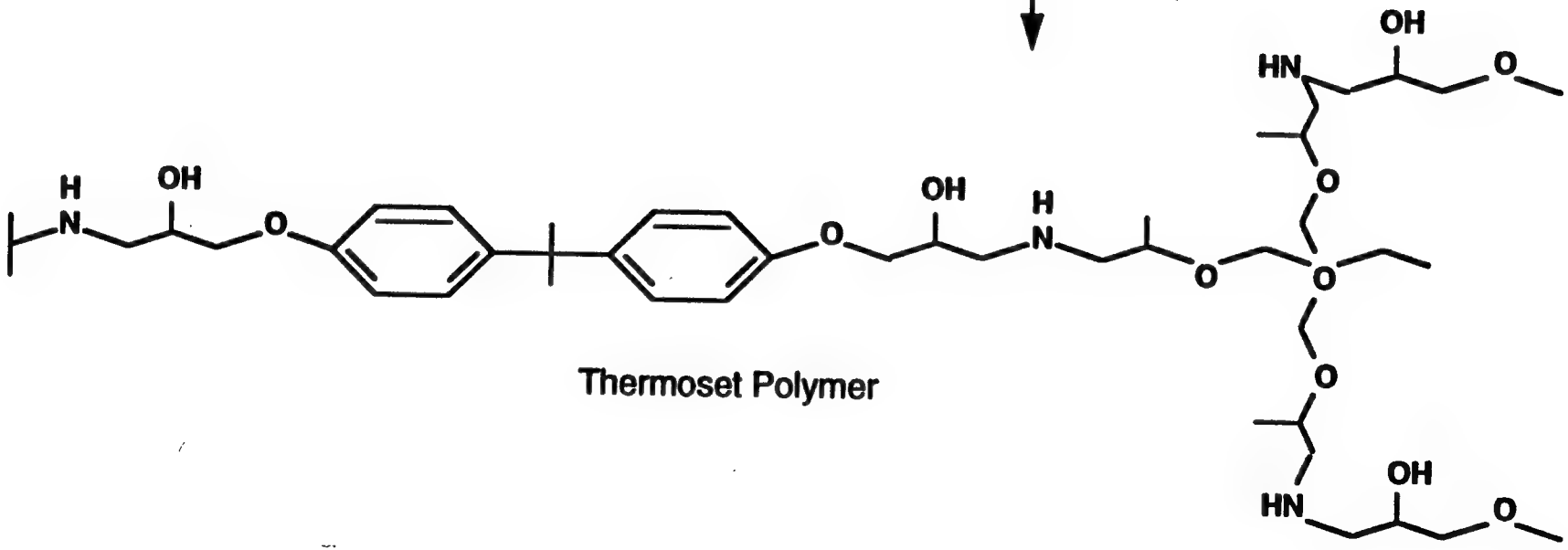

Thermoset Polymer

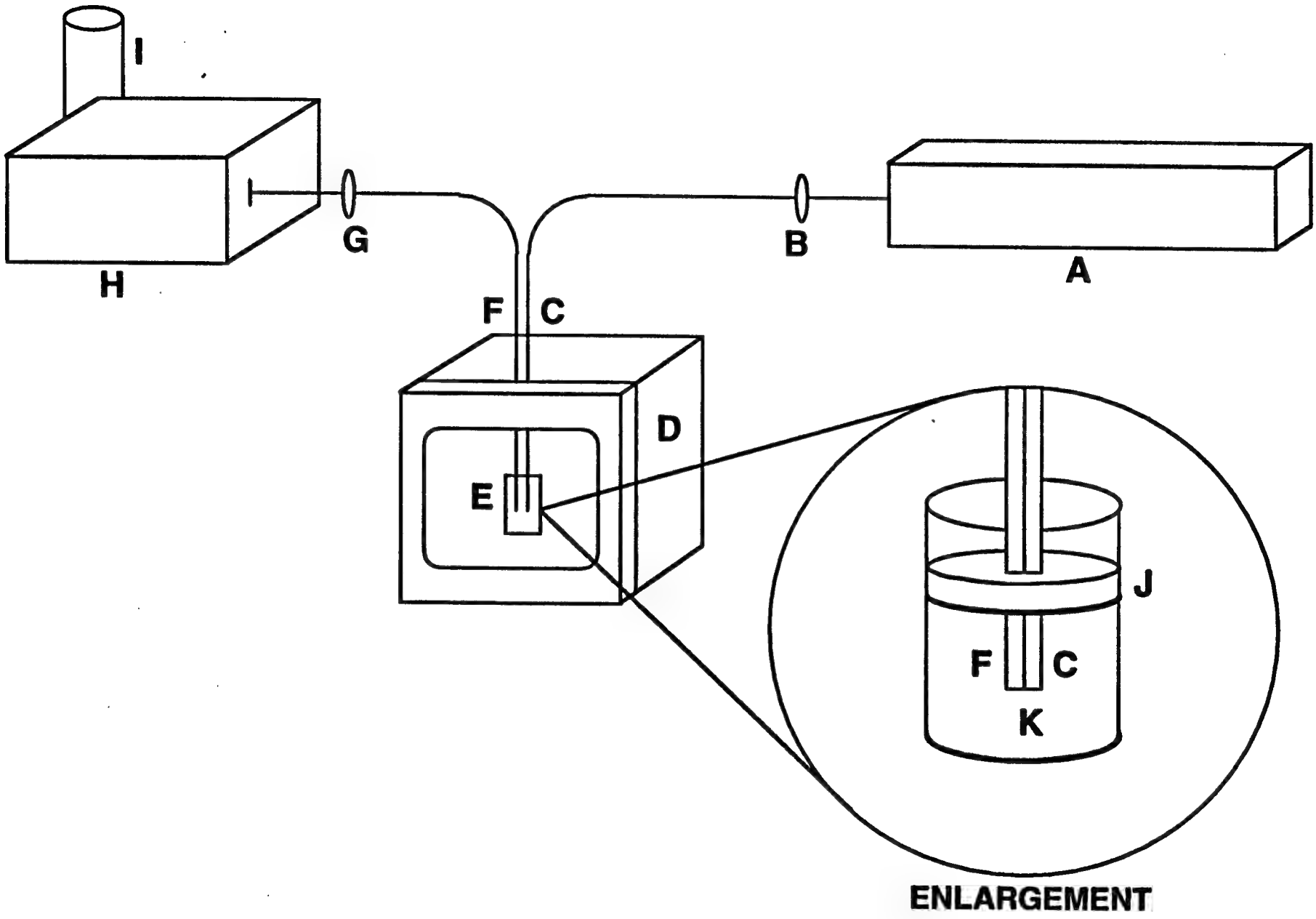
I
H
G
B
A
F
C
D
E
J
F
C
K
ENLARGEMENT

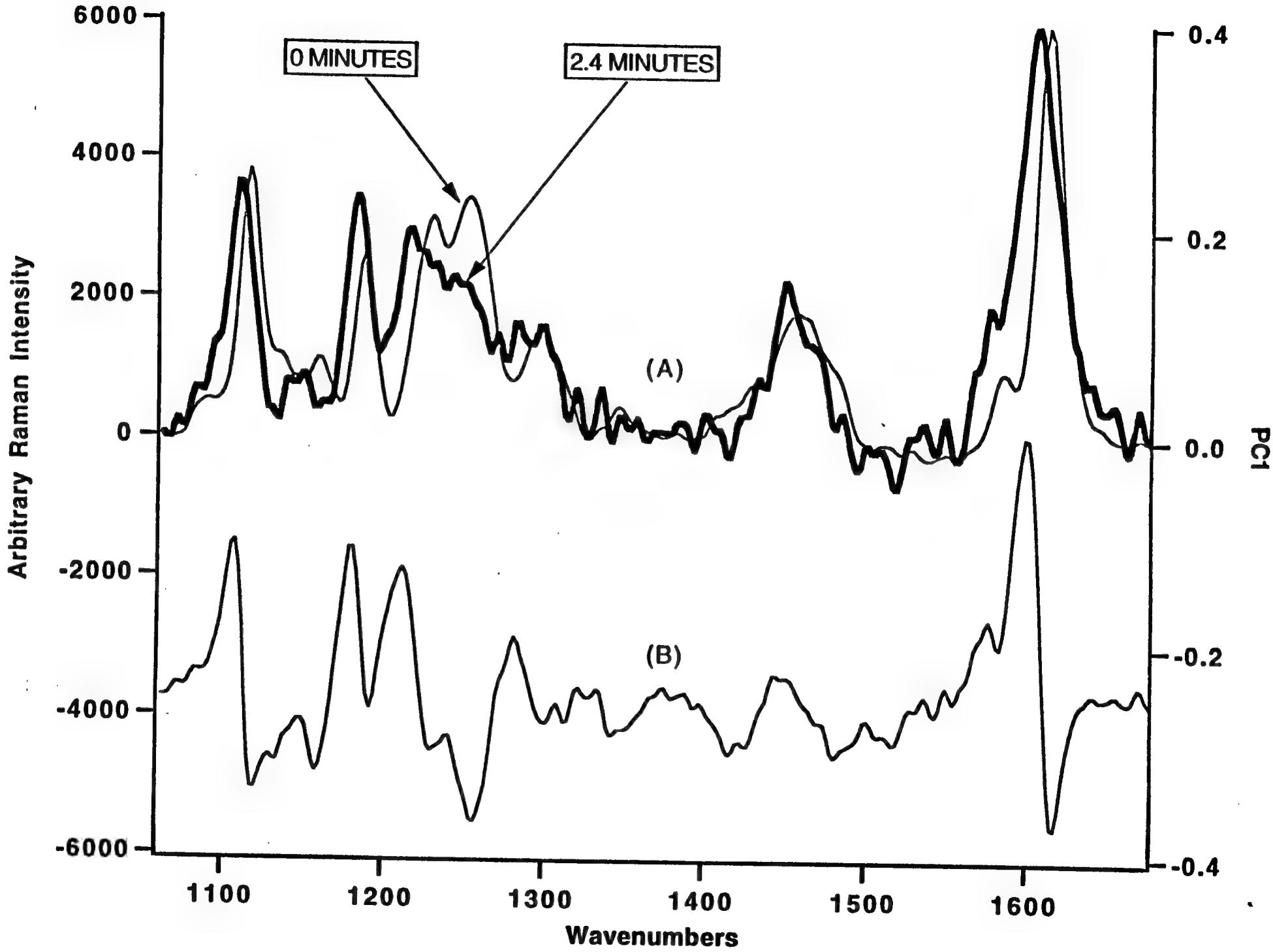
6000
4000
2000
0
-2000
-4000
-6000
Arbitrary Raman Intensity
0 MINUTES
2.4 MINUTES
(A)
(B)
0.4
0.2
0.0
-0.2
-0.4
PC1
1100
1200
1300
1400
1500
1600
Wavenumbers

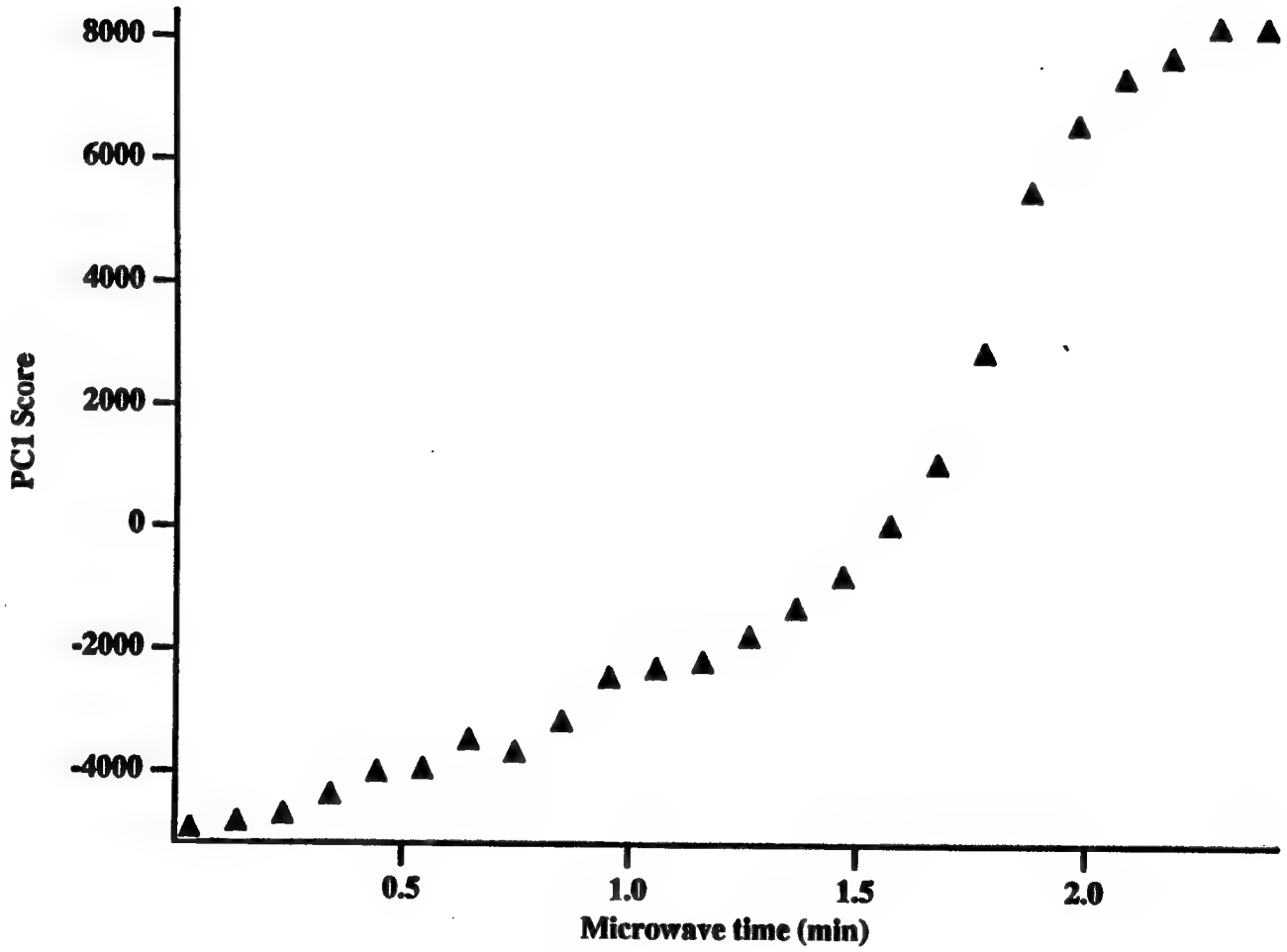
8000
6000
4000
2000
0
-2000
-4000
PC1 Score
0.5
1.0
1.5
2.0
Microwave time (min)

APPENDIX V - Nanofabrication of Organic Materials and Structures

Nanofabrication of Organic Materials and Structures

J. D. Noll, C. M. Stellman, P. G. Van Patten, and M. L. Myrick*
University of South Carolina, Department of Chemistry and Biochemistry, Columbia, SC 29208

Abstract

Organic materials have certain advantages over solid state materials for nanoscale electronics due to electro-migration and the breakdown of bulk properties inherent in semiconductor devices. This report will demonstrate a method in ordering organic materials at the nanometer scale. Highly ordered pyrolytic graphite (HOPG) step defects are used as templates to initiate polymer growth and enable two-dimensional control of the growth of the organic material. Other methods, such as molecular layer depostition, enable nanometer growth of organic material but allow only one dimensional control of the polymer growth and are more complicated procedures.

Organic materials have certain advantages over solid state materials for nanometer scale electronics because of electro-migration and the breakdown of bulk properties inherent in semiconductor devices. Organic materials also have a rich literature of synthetic chemistry, exhibit stability toward oxidation due to highly covalent bonding, and provide physical and chemical flexibility.

Langmuir-Blodgett film growth and molecular layer deposition (MLD) have been demonstrated for growing two dimensional polymer films for nanoscale applications.[1,2] These techniques give only one dimensional control of polymer growth and are constrained by the types of organic materials that can be used.

In the present report, defects on a highly ordered pyrolytic graphite (HOPG) monochromator have been used as templates for the attachment of organic material. HOPG step defects are nearly unique in nature. They may be as small as a single atomic layer in depth while having lengths of several micrometers. This physical characteristic makes them ideal structures upon which to synthesize conducting wires and other organic superstructures. The basal plane of HOPG is unreactive, but reactive sites exist at these step or ledge defects.[3] Our approach has been to chemically modify these reactive edges to introduce chemical functional groups, which may then be further modified for the construction of desired polymers.

To demonstrate the construction of a polymer at a nanoscale template, a test polymer formed from pyromellitic dianhydride

(PMDA) and 4,4'-diaminodiphenyl ether (DDE) was used. These reagents form an alternating copolymer as shown in Figure 1.

To attach this polymer to graphite ledge defects, chemical derivitization of the ledges with organic amine (-NH_2) functional groups to serve as chemical anchor points was attempted. This was done with the 3 step process as shown in Figure 2.

After this manipulation, DDE and PMDA were sequentially added in doses to the ledge. After 10 steps, the growing polymer was end capped with DDE, and then the tag molecule, fluorescamine (Molecular Probes, Inc.), was added. This tag becomes fluorescent when it reacts with an amine and is specific for the presence of this group. Amine groups were only introduced on the HOPG surface by the derivatization and polymerization process described above.

After sample treatment, the monochromator was placed under a microscope, and the image was focused onto a charge-coupled device (Santa Barbara Instrument Group) with a sample magnification of 400x. Figure 3(a) shows the monochromator illuminated with a filtered 488 nm line of an argon ion laser (Coherent, model Innova 305). Figure 3(b) shows the monochromator imaged through a holographic notch filter (Kaiser) used to reject 488 nm light but pass long wavelength fluorescence. In Figure 3a, light spots were scattering centers such as dust particles and other irregularities. Ledges were observed in this image only faintly. In Figure 3b, image intensity was much less than that of Figure 3(a) because no 488 nm light was observed; in the absence of fluorescamine, this image was dark. The absence of any of the bright spots from scattering centers seen in Figure 3a

confirmed the complete rejection of the laser excitation source. The new feature observed in this image was the thin arc of fluorescence which, on comparison with Figure 3a, occurred at a step defect. The width of this line corresponds to the best optical resolution of the microscope used to acquire the image.[4]

This observation confirmed the successful preparation of a polymer at a nanometer-scale template on HOPG. Preliminary scanning tunneling microscopy (STM) following derivitization confirmed the presence of a "disordered" material decorating the HOPG ledges. In addition, reproduction of this experiment without HNO_3/H_2SO_4 ledge oxidation or any other manipulation showed no attachment of polymers. Curiously, the polymer attachment occurred even if no reduction by HCl/SnCl was employed. Apparently oxidation of the ledges was sufficient to produce anchor points for polymer attachment.

In the future, cross-linking of polymers to form self-supporting structures that can be chemically or physically removed from their template may provide direct access to nanometer-scale "wires", etc. Further investigations are continuing, including STM studies to obtain further information on the morphologies of structures so constructed.

References

1) T. Yoshimura, S. Tatsuura, W. Sotoyama, *Appl. Phys. Lett.* 59 (1991) 482.

2) M. Ringger, H. R. Hidber, R. Schlogl, P. Oelhafen, H. J. Guntherodt, *Appl. Phys. Lett.* 46 (1985) 832.

3) J. D. Noll, J. B. Cooper, M. L. Myrick, *J. Vac. Sci. Tech. B.* 11 (1993) 2006.

4) C. M. Stellman, J. D. Noll, J. E. Reddic, M. L. Myrick, M. Submitted to *Rev. Sci. Instru.* (1994).

Acknowledgments

MLM and JDN thank Dr. Norbert Bikales and the National Science Foundation for support of the work. MLM and CMS thank Dr. Edward Chen and the Army Research Office for support.

Figure 1: The copolymerization of pyromellitic dianhydride (PMDA) and 4,4'-diaminodiphenyl ether (DDE) is demonstrated.

Figure 2: The derivatization reaction first attempted on the step defect of HOPG.

Figure 3: (a) is an image of the HOPG ledge after the attachment of the PMDA, DDE, and fluorescamine illuminated with a 488 nm line of an argon laser centered on a 488 nm bandpass filter to remove plasma emission. (b) is the same HOPG ledge but imaged through a holographic filter used to reject 488 nm light.

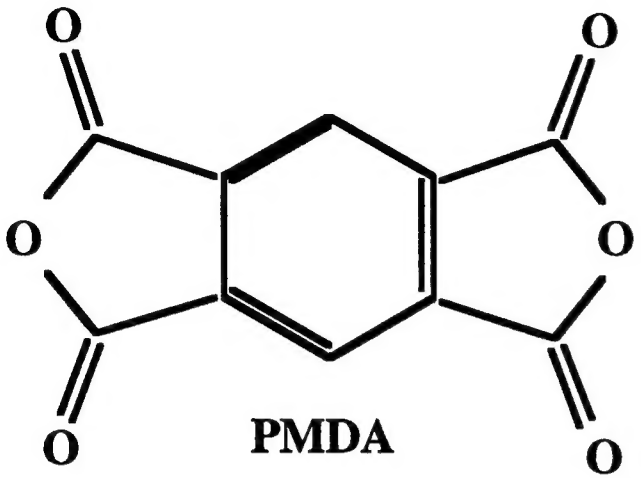

PMDA

+

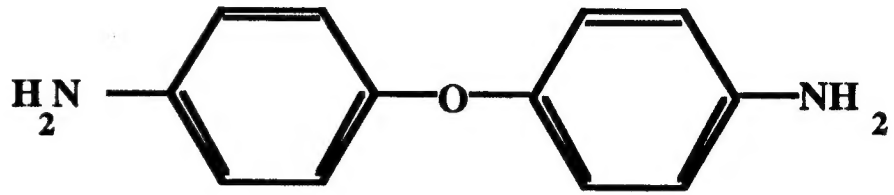

DDE

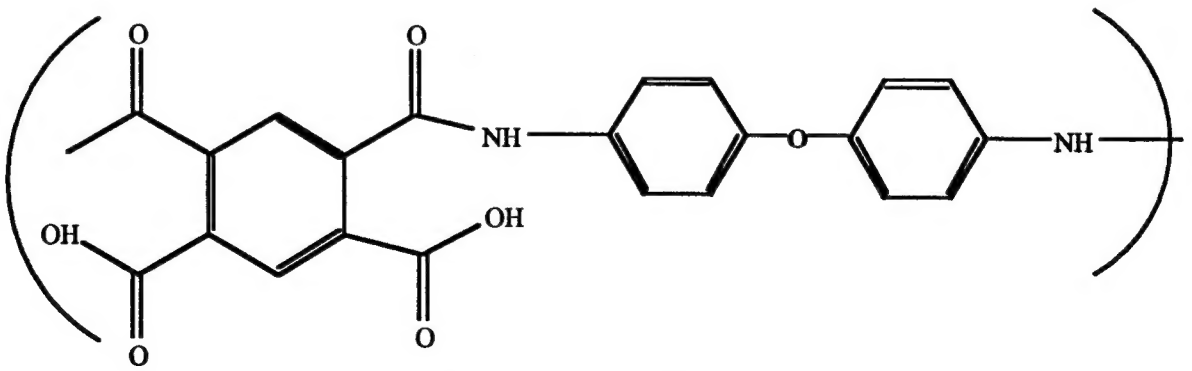

Repeating Unit

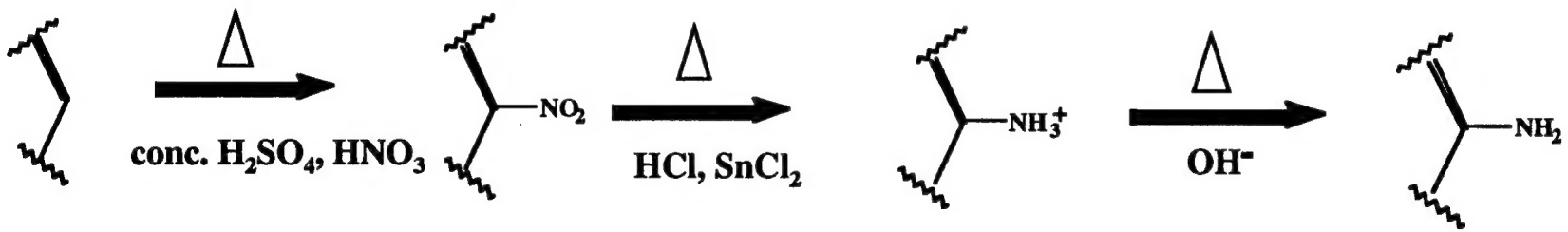
Δ
conc. H_2SO_4, HNO_3
NO_2
Δ
HCl, $SnCl_2$
NH_3^+
Δ
OH^-
NH_2

(a)

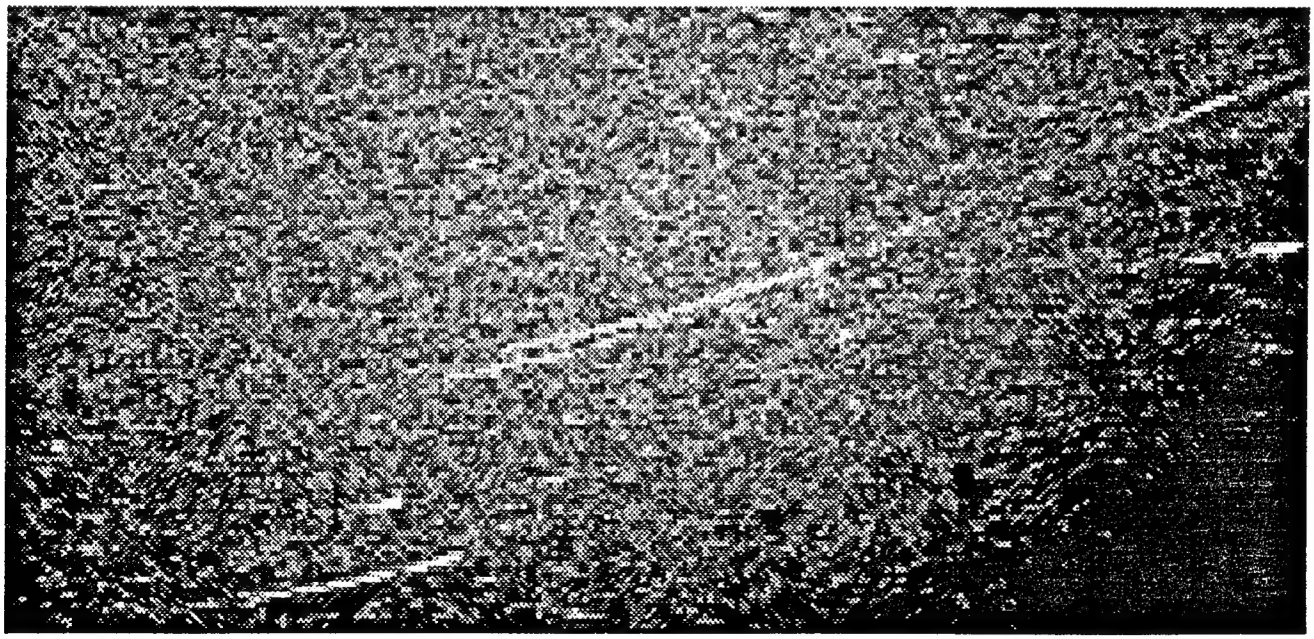

(b)